AD NUMBER

AD890668

LIMITATION CHANGES

TO:

Approved for public release; distribution is unlimited.

FROM:

Distribution authorized to U.S. Gov't. agencies only; Test and Evaluation; 01 NOV 1971. Other requests shall be referred to Air Force Weapons Laboratory, Attn: DEZ, Kirland AFB, NM 87117.

AUTHORITY

AFWL ltr, 19 May 1972

AFWL-TR-
70-113,
Vol IV

MULTIPLE-WHEEL HEAVY GEAR LOAD PAVEMENT TESTS

Volume IV

Analysis of Behavior Under Traffic

G. M. Hammitt II R. L. Hutchinson
J. L. Rice

U. S. Army Engineer Waterways Experiment Station

TECHNICAL REPORT NO. AFWL-TR-70-113, Vol IV

November 1971

AIR FORCE WEAPONS LABORATORY
Air Force Systems Command
Kirtland Air Force Base
New Mexico

DISCLAIMER NOTICE

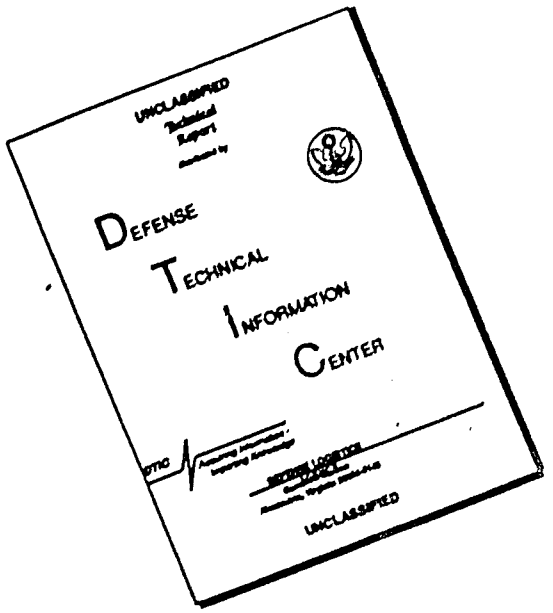

THIS DOCUMENT IS BEST QUALITY AVAILABLE. THE COPY FURNISHED TO DTIC CONTAINED A SIGNIFICANT NUMBER OF PAGES WHICH DO NOT REPRODUCE LEGIBLY.

AIR FORCE WEAPONS LABORATORY
Air Force Systems Command
Kirtland Air Force Base
New Mexico 87117

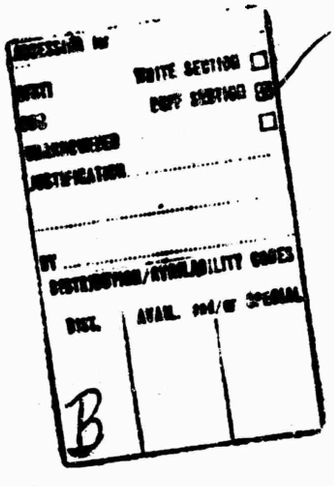

MULTIPLE-WHEEL HEAVY GEAR LOAD PAVEMENT TESTS

Volume IV

Analysis of Behavior Under Traffic

G. M. Hammitt II R. L. Hutchinson

J. L. Rice

U. S. Army Engineer Waterways Experiment Station

TECHNICAL REPORT NO. AFWL-TR-70-113, Vol IV

FOREWORD

This report was prepared by the U. S. Army Engineer Waterways Experiment Station, Vicksburg, Mississippi, under MIPR 68-7. The research was jointly sponsored by the U. S. Air Force under Program Element 64708F, Project 5224, Task 04; the U. S. Army under Task 02, Work Unit 002; and the Federal Aviation Administration under Engineering Requirement FAA-ER-450-034a.

Inclusive dates of research were 1 January 1968 through 1 August 1971. The report was submitted 20 September 1971 by the Air Force Weapons Laboratory Project Officer, Mr. L. M. Womack (DEZ)

The investigation reported herein was conducted under the overall supervision of Messrs. W. J. Turnbull (retired), J. P. Sale, A. A. Maxwell (deceased), and R. G. Ahlvin, Soils Divison, WES. Other Soils Division personnel actively engaged in this study were Messrs. D. N. Brown, H. R. Austin, H. H. Ulery, Jr., D. M. Ladd, R. H. Ledbetter, D. L. Cooksey, and G. M. Hammitt II, and Dr. O. O. Thompson.

Personnel of Construction Engineering Research Laboratory actively engaged in the investigation were Messrs. J. J. Healy, R. L. Hutchinson, J. L. Rice, F. W. Kearney, and J. B. Gambill.

Prime authors of the flexible and rigid pavement portions of the report were Mr. Hammitt and Messrs. Hutchinson and Rice, respectively. Dr. Thompson and Mr. Brown prepared the traffic study portion of the report. Coordination between WES and CERL in preparation of the report was by Mr. Ulery.

This technical report has been reviewed and is approved.

L. M. Womack

L. M. WOMACK
Project Officer

Clarence E. Teske

CLARENCE E. TESKE
Lt Colonel USAF
Chief, Aerospace Facilities Branch

William B. Liddicoet

WILLIAM B. LIDDICOET
Colonel USAF
Chief, Civil Engineering Research Division

ABSTRACT

(Distribution Limitation Statement B)

Flexible and rigid pavement test sections were constructed and tested to obtain data to validate present criteria, to establish modifications to present criteria, or to develop new criteria for the evaluation and design of airfield pavements to be subjected to multiple-wheel heavy gear loads (MWHGL). The basic CBR design method was expanded and modified to obtain a method of design for flexible pavements subject to traffic by MWHGL. The recommended method reflects a reduction of existing U. S. Army Corps of Engineers (CE) thickness requirements that is especially significant for multiple-wheel assemblies in the higher operational level. Current CE evaluation and design methods for rigid pavements are based on stress in the concrete pavement as calculated from the Westergaard analysis; extrapolations to the existing criteria were found to be valid for MWHCL assemblies insofar as pavement thicknesses were concerned. Results of traffic testing of the rigid pavement indicate that current jointing recommendations allowing keyed construction joints may be unconservative when MWHGL assemblies will be trafficking a pavement resting on a low-strength subgrade.

CONTENTS

ILLUSTRATIONS

ILLUSTRATIONS (Continued)

ILLUSTRATIONS (Continued)

TABLES

CONVERSION FACTORS, BRITISH TO METRIC UNITS OF MEASUREMENT

British units of measurement used in this report can be converted to metric units as follows:

Multiply	By	To Obtain
inches	2.54	centimeters
feet	0.3048	meters
square inches	6.4516	square centimeters
square feet	0.092903	square meters
pounds	0.45359237	kilograms
kips	453.59237	kilograms
pounds per square inch	0.070307	kilograms per square centimeter
pounds per cubic inch	27.67984	grams per cubic centimeter
pounds per cubic foot	16.0185	kilograms per cubic meter
inch-pounds	0.011521	meter-kilograms
miles per hour	1.609344	kilometers per hour

SECTION I

INTRODUCTION

1. PURPOSE

The purpose of this investigation was to validate present criteria, to establish modifications to present criteria, or to develop new criteria for the evaluation and design of both flexible and rigid airfield pavements to be subjected to multiple-wheel heavy gear loads (MWHGL). MWHGL as used in this report denotes aircraft with gross loads exceeding 600 kips.[1]

2. BACKGROUND

The multiple-wheel gears of large new aircraft (such as the C-5A and Boeing 747) may impose loads on pavements that are radically different from those previously encountered. Extensions to the existing criteria for pavement evaluation and design are necessary to evaluate the effects of these loads. Data are also required to determine the relative destructive effects of new and proposed aircraft on pavement performance. The Army, Air Force, and Federal Aviation Administration (FAA) jointly sponsored this investigation. The investigation was conducted by the U. S. Army Engineer Waterways Experiment Station (WES), Vicksburg, Miss. Overall supervision of the tests and all details pertaining to the flexible pavement portion of the tests were provided by WES. The rigid pavement testing was directed by the U. S. Army Construction Engineering Research Laboratory, Champaign, Ill.

3. SCOPE

This investigation was accomplished by constructing and testing a specially designed test section consisting of both flexible and rigid pavements as described herein. Testing consisted of instrumentation measurements of deflection, strain, and stress resulting from applied static and dynamic (slowly moving) loads; nondestructive vibratory testing to determine wave velocity and stiffness; and traffic testing with multiple- and single-wheel gear assemblies. This report presents a summary of the investigation of various theoretical concepts of pavement behavior with advantages and limitations of each concept. Following a discussion of all these concepts, a review of the development of

---

[1] A table of factors for converting British units of measurement to metric units is presented on page vii.

the current U. S. Army Corps of Engineers (CE) methods of design for rigid and flexible pavements is presented. Then, the analysis of data from the test section with resulting criteria is given. Data used in the analysis and criteria development were selected from Volumes II and III of this series.

The MWHGL study represented such an extensive effort that the report of the study was divided into the following volumes:

I - Basic Report (background, summary of entire study, conclusions, and recommendations)

II - Design, Construction, and Behavior Under Traffic

III - Presentation and Initial Analysis of Stress-Strain-Deflection and Vibratory Measurements

A. Instrumentation

B. Data and Analysis

IV - Analysis of Behavior Under Traffic

SECTION II

INVESTIGATION OF CONCEPTS OF PAVEMENT BEHAVIOR

1. FLEXIBLE PAVEMENT

One purpose of the MWHGL tests at the WES was to determine the behavior of conventionally constructed flexible pavements subjected to heavy multiple-wheel aircraft loadings. The study was to provide design and evaluation criteria for airfield pavements for very large aircraft.

The analysis was to provide the best flexible pavement design and evaluation criteria presently possible. Within the past several years, many different theories and computer-oriented concepts have been under study for use in flexible pavement design. Reviews of the most prominent of these for possible application to flexible pavement design are presented herein in synopsis form. Coincidentally, the existing semiempirical concepts were investigated and reviewed for the purpose of possible design usage.

Any pavement behavior system must involve a behavior system and a set of parameters to cause the behavior to be similar to that of the prototype being represented. Since these two components of a system act as independent variables, two different systems can yield identical numerical answers. Therefore, any philosophically correct behavior concept can, through suitable adjustment of these two components, be made to produce the desired output. The problem area in design formulation revolves around the validity of the behavior concept when translated to a different system of different inputs and unknown output. The problem of translation exists in a solely theoretical or empirical system (or some combination of both) as applied to the prediction of the complicated structural behavior of flexible pavements.

Recent concepts, theories, and computer programs were examined in detail to determine their applicability to the MWHGL flexible pavement test sections. All applications were made using data from the MWHGL static-load instrumentation tests. Each program in its present form was studied to evaluate the soundness of theory, correctness of mathematics and boundary conditions, and compatibility of computer programs with the WES computer system. The following is a brief discussion of this work.

a. Layered System - Shell Laboratories

A computer program for design was developed by the Shell Laboratory to

calculate stresses, strains, and displacements for a multilayered, three-dimensional, elastic, homogeneous, isotropic media (reference 1). The basic theory was derived from Boussinesq's and Burmister's concepts on one- and two-layer elastic systems (reference 2). A perfectly rough interface condition was assumed to exist between layers, with the lower layer providing continuous support to the layer above it. The basic study has been expanded from this background to include any number of layers and loads. For adaptation for use in the MWHGL analysis, changes were made in certain phases of the program. The maximum number of loads was increased from 10 to 30, and the number of terms in the Bessel functions was altered to afford the accuracy desired. The program computed all orthogonal values of stresses, strains, and deflections, as well as principal values and directions of total stresses and strains, strain energy, and strain energy of distortion. The preliminary investigation indicated an applicability of a program for layered systems under normal surface loads to the flexible pavement portion of this test.

Initial computer output from this program reflected good agreement between two computed values of deflection for a multiple-wheel gear in comparison with measured data. A typical input statement and format are shown in figure 1, and a typical output statement is given in figure 2. A comparative plot of computed and measured (from Volume III) values of vertical stress versus depth for 15,000- and 30,000-lb static loadings is shown in figure 3. This computer program is relatively large, but can be reduced greatly by reducing the number of layers or less greatly by decreasing the number of loads. Trial computations were made with various material properties as input values in an attempt to duplicate the measured values. Although this could be accomplished for one set of loading conditions, the results could not then be translated to other loading conditions for duplication of field results. Also, the method used two values of limiting strain, one at the bottom of the surface course and one at the top of the subgrade, and accounts for the effects of traffic repetitions on the pavement structure through selection of suitable strain values.

The Shell multilayer program results were compared with instrumented readings of stress, deflection, and strain. In item 4, the computed surface elastic deflection for center-line 12-wheel 30,000-lb loading was 0.226 in., and the equivalent instrumentation measurement was 0.272 in.; at the 6-in. depth, the computed deflection was 0.226 in., and the equivalent value

SYSTEM NUMBER 1

LAYER NUMBER	BASE CONDITION	ELASTICITY	POISSON RATIO	THICKNESS	MODULAR RATIO
1	ROUGH	0.2500E 05	0.3000E 00	0.3000E 01	0.6000E 01
2	ROUGH	0.1500E 06	0.3000E 00	0.6000E 01	0.4643E 00
3	ROUGH	0.7500E 05	0.4000E 00	0.2400E 02	0.8000E-01
4	ROUGH	0.6000E 04	0.4000E 00	0.2100E 02	0.5000E 00
5	ROUGH	0.3000E 04	0.4000E 00	0.3600E 02	0.2000E 01
6	ROUGH	0.6000E 04	0.4000E 00	0.5400E 02	0.1000E 01
7		0.6000E 04	0.4000E 00		

LOAD NUMBER	NORMAL STRESS	RADIUS OF LOADED AREA	X-LOAD	Y-LOAD
1	0.291E 02	0.1780E 02	0.2370E 02	0.
2	0.291E 02	0.1780E 02	0.3400E 03	0.
3	0.107E 03	0.9430E 01	0.1585E 03	0.2760E 03
4	0.107E 03	0.9430E 01	0.2065E 03	0.2760E 03
5	0.107E 03	0.9430E 01	0.1215E 03	0.3410E 03
6	0.107E 03	0.9430E 01	0.1555E 03	0.3410E 03
7	0.107E 03	0.9430E 01	0.2085E 03	0.3410E 03
8	0.107E 03	0.9430E 01	0.2425E 03	0.3410E 03
9	0.107E 03	0.9430E 01	0.1585E 03	0.4960E 03
10	0.107E 03	0.9430E 01	0.2065E 03	0.4960E 03
11	0.245E 02	0.1690E 02	0.	0.5130E 03
12	0.245E 02	0.1690E 02	0.3640E 03	0.5130E 03
13	0.107E 03	0.9430E 01	0.1215E 03	0.5610E 03
14	0.107E 03	0.9430E 01	0.1555E 03	0.5610E 03
15	0.107E 03	0.9430E 01	0.2085E 03	0.5610E 03
16	0.107E 03	0.9430E 01	0.2425E 03	0.5610E 03

Figure 1. Typical Computer Input Statement and Format for Shell Multilayer Program

```
POSITION NUMBER    2
LAYER NUMBER       2
X-COORDINATE OF POSITION IS     0.1d20E 03
Y-COORDINATE OF POSITION IS     0.3410E 03
Z-COORDINATE OF POSITION IS     0.6v00E 01

LOAD LOAD    DISTANCE     XESTRN      RASTRN      TLSTRN      SHSTRN      XESTRS      RASTRS      TLSTRS      SHSTRS      XEDISP      RADISP
NUM  RADIUS  RADIUS
 1  17.8000 375.9520  0.524E-07  0.392E-06 -0.511E-06  0.843E-08  0.279E-03 -0.395E-01 -0.648E-01  0.973E-03  0.334E-02 -0.192E-03
 2  17.8000 375.8258  0.524E-07  0.393E-06 -0.512E-06  0.84PE-08  0.291E-03 -0.396E-01 -0.648E-01  0.978E-03  0.334E-02 -0.192E-03
 3   9.4300  69.1177  0.801E-05  0.110E-04 -0.300E-04 -0.556E-05 -0.282E-01  0.318E 00 -0.442E 01 -0.641E 00  0.239E-01 -0.208E-02
 4   9.4300  69.4640  0.787E-05  0.111E-04 -0.298E-04 -0.549E-05 -0.280E-01  0.349E 00 -0.434E 01 -0.634E 00  0.229E-01 -0.207E-02
 5   9.4300  60.5000  0.121E-04  0.695E-05 -0.356E-04 -0.754E-05 -0.330E-01 -0.630E 00 -0.554E 02 -0.870E 00  0.292E-01 -0.216E-02
 6   9.4300  20.5000  0.479E-04 -0.482E-04 -0.651E-04 -0.227E-04 -0.129E 00 -0.112E 02 -0.132E 02 -0.202E 01  0.365E-01 -0.172E-02
 7   9.4300  20.5000  0.479E-04 -0.482E-04 -0.651E-04 -0.227E-04 -0.129E 00 -0.112E 02 -0.132E 02 -0.202E 01  0.365E-01 -0.172E-02
 8   9.4300  60.5000  0.121E-04  0.695E-05 -0.356E-04 -0.754E-05 -0.330E-01 -0.630E 00 -0.554E 01 -0.870E 00  0.292E-01 -0.216E-02
 9   9.4300 156.7713 -0.198E-05  0.102E-04 -0.568E-05  0.184E-06 -0.597E-02  0.140E 01 -0.435E 00  0.120E-01  0.953E-02 -0.869E-03
10   9.4300 156.9243 -0.197E-05  0.102E-04 -0.566E-05  0.185E-06 -0.589E-02  0.140E 01 -0.431E 00  0.121E-01  0.951E-02 -0.869E-03
11  16.9000 259.4157 -0.423E-06  0.198E-05 -0.101E-05  0.120E-06 -0.129E-02  0.276E 00 -0.688E-01  0.138E-01  0.383E-02 -0.252E-03
12  16.9000 256.4157 -0.423E-06  0.198E-05 -0.101E-05  0.120E-06 -0.129E-02  0.276E 00 -0.688E-01  0.138E-01  0.383E-02 -0.252E-03
13   9.4300 228.1672 -0.857E-06  0.382E-05 -0.182E-05  0.211E-06 -0.222E-04  0.540E 00 -0.111E 00  0.244E-01  0.582E-02 -0.415E-03
14   9.4300 221.5903 -0.958E-06  0.423E-05 -0.199E-05  0.224E-06 -0.831E-04  0.598E 00 -0.119E 00  0.258E-01  0.603E-02 -0.441E-03
15   9.4300 221.5903 -0.958E-06  0.423E-05 -0.199E-05  0.224E-06 -0.831E-04  0.598E 00 -0.119E 00  0.258E-01  0.603E-02 -0.441E-03
16   9.4300 228.1672 -0.857E-06  0.382E-05 -0.182E-05  0.211E-06 -0.222E-04  0.540E 00 -0.111E 00  0.244E-01  0.582E-02 -0.415E-03

                          XX          YY          ZZ          XY          XZ          YZ          UX          UY          UZ
TOTAL STRESS    -0.324E 02  -0.328E 02  -0.394E 00  -0.134E 01   0.543E-02  -0.353E-01
TOTAL STRAIN    -0.149E-03  -0.153E-03   0.128E-03  -0.116E-04   0.471E-07  -0.306E-06
TOTAL DISPLACEMENT                                                                      0.302E-04  -0.459E-03   0.226E 00

PRINCIPAL VALUES AND DIRECTIONS OF TOTAL STRESSES AND STRAINS
                NORMAL      NORMAL      SHEAR       SHEAR          X           Y           Z
                STRESS      STRAIN      STRESS      STRAIN     COMPONENT   COMPONENT   COMPONENT
MAXIMUM     -0.339E 00   0.126E-03                              0.000      -0.041       0.999
MINIMAX     -0.324E 02  -0.149E-03                              0.997      -0.073      -0.003
MINIMUM     -0.328E 02  -0.154E-03                              0.073       0.996       0.041
MAXIMUM                                  0.162E 02   0.141E-03   0.052       0.676       0.736
MINIMUM                                 -0.162E 02  -0.141E-03  -0.052      -0.734       0.678
              STRAIN ENERGY 0.491566E-02
STRAIN ENERGY OF DISTORTION 0.300679E-02
```

Figure 2. Typical Computer Output Statement for Shell Multilayer Program

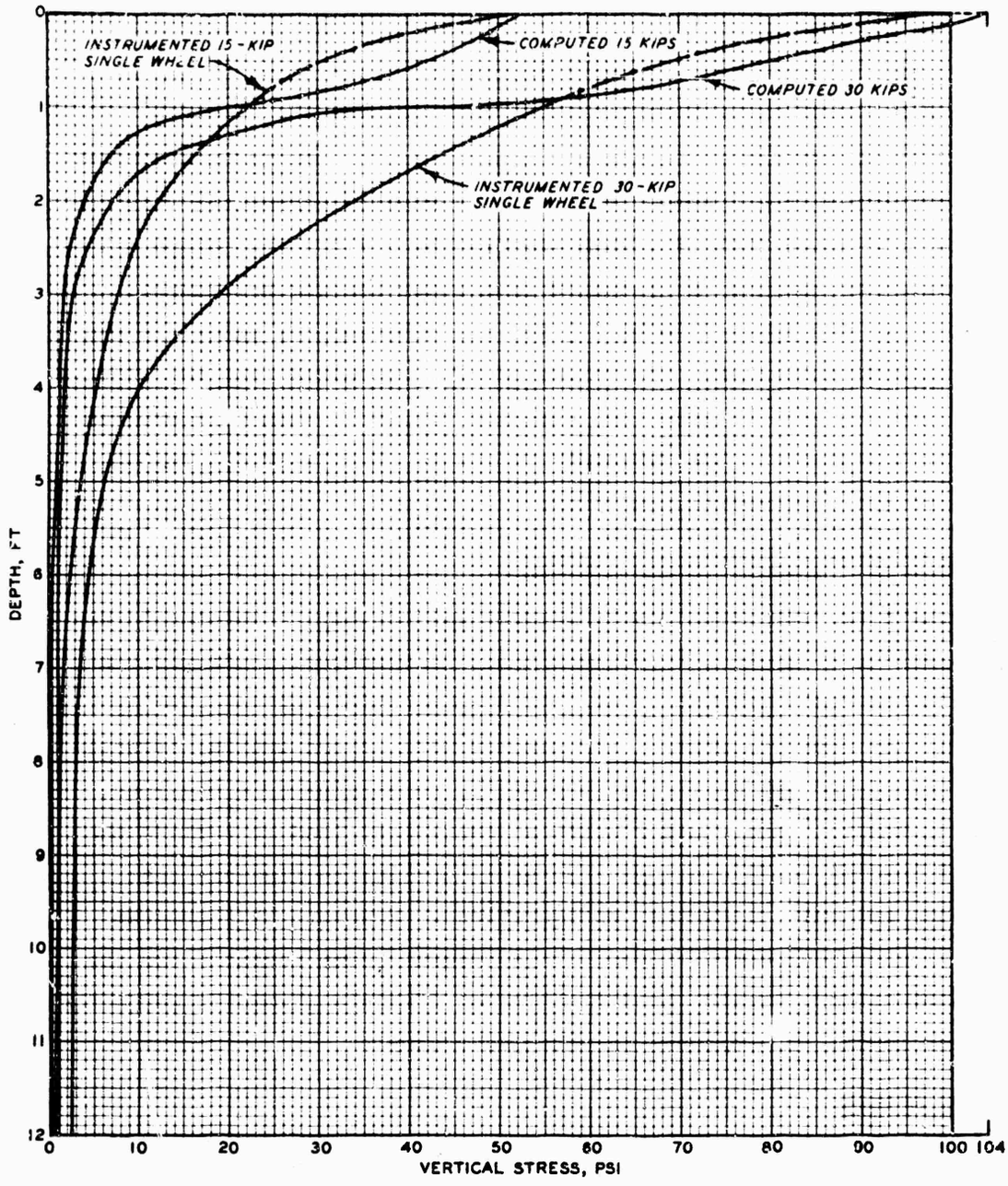

Figure 3. Computed and Measured Values of Vertical Stress Versus Depth for Single-Wheel Load

interpolated from instrumentation measurements was 0.266 in. These computed values were based on 16 loaded areas (12 load wheels plus 4 load cart outrigger wheels) and 7 layers. The Young's modulus of elasticity E values were determined for each layer by multiplying the measured CBR values by 1500 to arrive at E values in pounds per square inch. This is an empirical relationship developed from dynamic triaxial test results correlated with CBR data. It should be noted that E , when measured by a vibratory method, is higher than secant or tangent E obtained from other testing procedures. Poisson's ratio ν was assumed to be 0.3 for the cohesionless materials and 0.4 for the cohesive materials. The values of E determined from the vibratory testing were not used because they were not available when this program was run. In most instances, the vibratory values of E , later determined, were higher than the above-mentioned values.

b. Layered System - Chevron Oil Company

A computer program developed by Chevron Oil Company (reference 3) was based on an elastic, N-layered, two-dimensional, homogeneous, isotropic concept similar to the Shell program. Deflection computations agreed closely with results of the Shell program. Only limited work beyond initial investigation was accomplished, primarily because of the constraint of a one-load, two-dimensional input. This would require an equivalent load to replace the multiple-wheel loading configurations. No applicability to flexible test sections existed for multiple-wheel configurations. However, this program was used for single-wheel computations. This program seems feasible for the determination of stress, strain, or deflection on flexible pavements subjected to single-wheel loads. The program is relatively short.

c. Energy Method

The energy method of analysis, as applied to beams and bars, was studied to determine its applicability to this project. Energy is the ability to do work and is measured by the amount of work a body is capable of doing in changing from some given condition to some standard condition. In a defined system, the external work can be equal to the change in internal energy of the pavement structure, or the sum of energies applied to the system is equal to the energy used plus the energy transferred outside, if equilibrium-stability exists. This internal energy can be computed using the principle of minimum potential energy and related to the external work done

by applied loadings. This principle of minimum potential energy states that if a system is in equilibrium both internally and externally and if a very small change in displacement is imposed, then the external work done by the loads must equal the change in strain energy δU, where δ symbolizes a small change and U is strain energy. The strain energy (area under force-displacement plot) versus depth was computed (figure 4) by the Shell multilayer program and used in conjunction with the energy method.

The principle is stated in terms of displacements or strains and applied loads on deformable bodies (references 4-7). The external work W equals

$$\frac{1}{2} \Sigma U^T K_i U = U \tag{1}$$

where

U^T = U transposed

K_i = stiffness matrix derived from energy methods

Also

$$X_i = \frac{\partial U}{\partial u} = K_i u \tag{2}$$

where

X_i = reactions

u = displacements

Furthermore, the stiffness matrix K is defined as $K_{ij} = \partial^2 u/(\partial u_i \, \partial u_j)$, which expresses a force induced by a unit displacement. For the linear case, this matrix is composed of constants.

A nonlinear relationship may be considered and the relationship between force F and change of length x is as follows, for example:

$$\left.\begin{aligned} F &= kx + ax^3 \\ F &= kx - ax^3 \end{aligned}\right\} \tag{3}$$

where

k and a = constants

When $a = 0$, this matrix would be composed of first-order values.

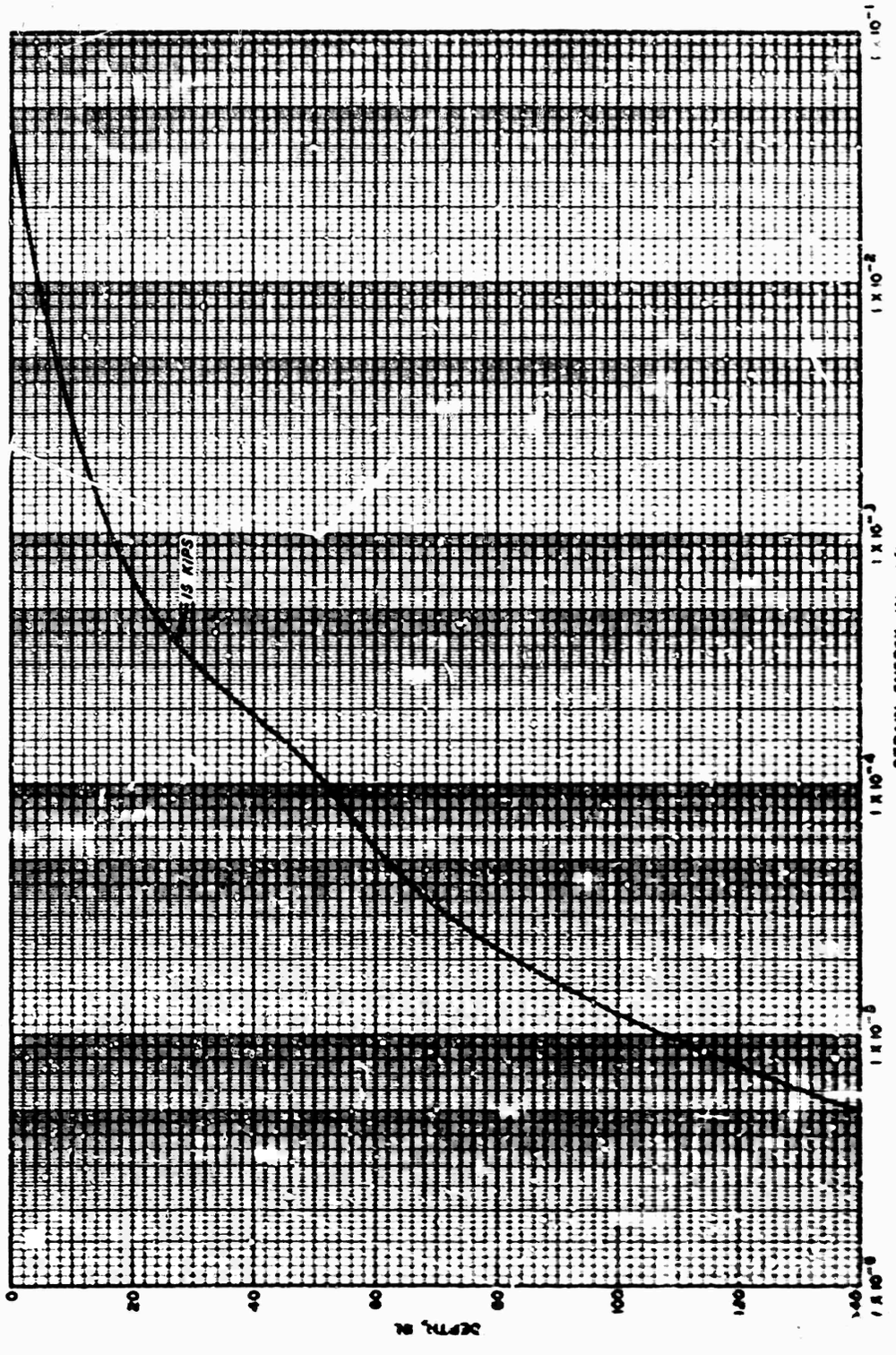

Figure 4. Typical Plot of Strain-Energy Versus Depth. Item 4, 15,000-lb Single-Wheel Static Load

Other terms ΔV in the system are the work items resulting from applied loads or potential energy of applied loads. A typical strain-energy versus depth plot for item 4, MWHGL test section, 15,000-lb single-wheel load is shown in figure 4. The concept of virtual work, i.e.,

$$\Delta(U + V) = \Delta(U - W) = 0 \tag{4}$$

was reviewed and considered applicable, but no adaption was made to this test section because of time constraints and limitations imposed in developing the nonlinear constitutive equations. Another area of difficulty revolves around the fact that the input energy level per stress repetition can be quite different from that in seemingly similar situations. The application of this method to the analysis was questionable based on the type of support assumed and on the lack of sufficient data to describe the stiffness matrix of the structure, but in principle the method seems applicable for analysis. No computer program was available for this method at the time of the study.

d. Stiffness Method - Structural Analysis (References 8-10)

This method is incorporated into the finite difference and finite element methods as applied to pavement structures and is shown in detail for basic explanation.

A plane truss or frame may be considered to be composed of members (elements) connected at the joints (nodes). The force components and moments, such as X_i , Y_i , M_i , acting at all the nodes constitute the generalized force vector X . The deflection components and rotations, such as u_i , v_i , θ_i , at all the joints constitute the displacement column vector $\{u\}$. Therefore

$$\{X\} = \{Y_1, Y_1, M_1, X_2, Y_2, M_2, \ldots, X_i, Y_i, M_i\} \tag{5}$$

$$\{u\} = \{u_1, v_1, \theta_1, u_2, v_2, \theta_2, \ldots, u_i, v_i, \theta_i\} \tag{6}$$

The forces and displacements are related through functions depending upon the geometric and material properties of the elements of the structure. In the stiffness method of matrix structural analysis, the relationship between forces and displacements at the nodes may be expressed as:

$$\{X\} = [K]\{u\} \tag{7}$$

In $\{X\} = [K]\{u\}$, K is shown as the stiffness matrix. The element K_{ij} of the stiffness matrix is the force along i corresponding to unit displacement along j . The concept of the stiffness matrix may be discussed in relation to springs.

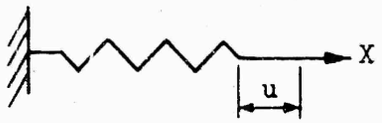

X = ku , where k is the stiffness of the spring

(1) Stiffness matrix for an element.

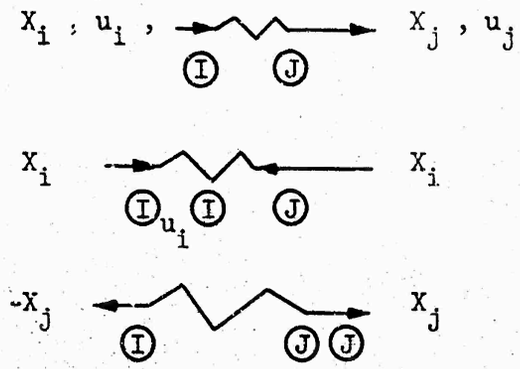

$$\{X\} = \begin{Bmatrix} X_i \\ X_j \end{Bmatrix} , \quad \{u\} = \begin{Bmatrix} u_i \\ u_j \end{Bmatrix}$$

Consider a spring IJ with J fixed. Force at J due to u_i alone, $(u_j = 0)$, $X_i = ku_i$, and $X_j = -X_i = -ku_i$. Due to u_j alone, $(u_i = 0)$, $X_j = ku_j$, and $X_i = -X_j = -ku_j$.
The stiffness relation between $\{X\}$ and $\{u\}$ may be written as

$$\begin{Bmatrix} X_i \\ X_j \end{Bmatrix} = \begin{bmatrix} k & -k \\ -k & k \end{bmatrix} \begin{Bmatrix} u_i \\ u_j \end{Bmatrix} \tag{8}$$

The stiffness matrix for the spring element is, therefore

$$[K] = \begin{bmatrix} k & -k \\ -k & k \end{bmatrix} \tag{9}$$

where

k = the stiffness constant of the spring

(2) Stiffness matrix for an assemblage. For an assemblage of two

springs with stiffness constants k_a and k_b

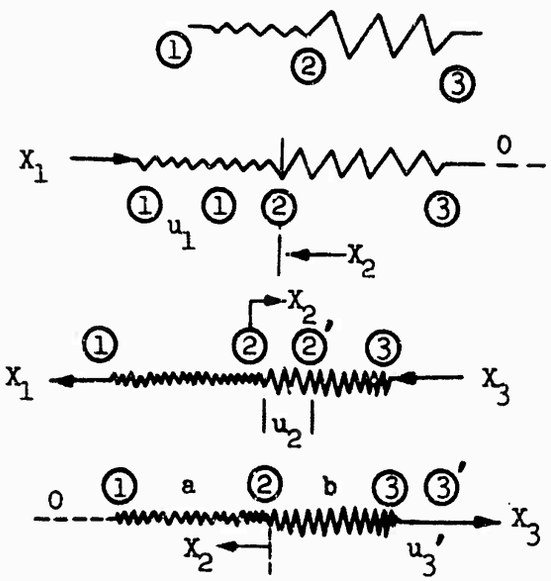

Due to u_1 alone,

$X_1 = k_a u_1$, $X_2 = -k_a u_1$, $X_3 = 0$

Due to u_2 alone,

$X_1 = -k_a u_2$, $X_2 = k_a u_2 + k_b u_2$, $X_3 = -k_b u_2$

Due to u_3 alone,

$X_1 = 0$, $X_2 = -k_b u_3$, $X_3 = k_b u_3$

Stiffness relation for the spring assemblage is

$$\begin{Bmatrix} X_1 \\ X_2 \\ X_3 \end{Bmatrix} = \begin{bmatrix} k_a & -k_a & 0 \\ -k_a & (k_a + k_b) & -k_b \\ 0 & -k_b & k_b \end{bmatrix} \begin{Bmatrix} u_1 \\ u_2 \\ u_3 \end{Bmatrix} \tag{10}$$

The stiffness matrix for the assemblage may itself be assembled from the stiffness matrices for the individual elements, expanding each of them to conform to the order and composition of the total stiffness matrix. Thus, for the spring a , the element stiffness matrix is

$$[K]_{12} = \begin{bmatrix} k_a & -k_a \\ -k_a & k_a \end{bmatrix} = \begin{bmatrix} k_a & -k_a & 0 \\ -k_a & k_a & 0 \\ 0 & 0 & 0 \end{bmatrix}_{(3\times3)} \tag{11}$$

Similarly, the stiffness matrix for the spring b , is

$$[K]_{23} = \begin{bmatrix} k_b & -k_b \\ -k_b & k_b \end{bmatrix} = \begin{bmatrix} 0 & 0 & 0 \\ 0 & k_b & -k_b \\ 0 & -k_b & k_b \end{bmatrix}_{(3\times3)} \tag{12}$$

Superposing the two expanded matrices gives the stiffness matrix of the assemblage:

$$[K] = [K]_{12} + [K]_{23} = \begin{bmatrix} k_a & -k_a & 0 \\ -k_a & (k_a + k_b) & -k_b \\ 0 & -k_b & 0 \end{bmatrix} \tag{13}$$

as before.

For a long chain of elements, the superposition of the element stiffness matrices leads to a banded matrix as indicated below.

$[K] =$ 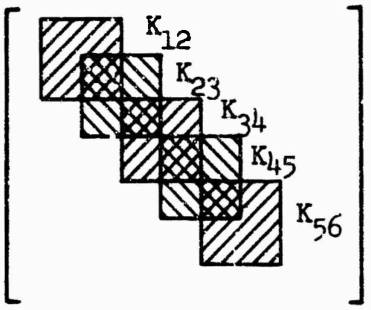

The stiffness matrix is also symmetric with $K_{ij} = K_{ji}$, in accordance with the law of reciprocal deflections (Maxwell's law).

(Deflection at i due to a unit force at j is equal to the deflection at j due to a unit force at i.)

In the stiffness method, the nodal displacements due to a set of specified forces are generally the primary unknowns. But $X = Ku$ for the entire assemblage cannot be inverted at this stage because the total K matrix is singular. Physically, the situation corresponds to rigid body motion, which must first be prevented by prescribing support (boundary) constraints before a solution is possible.

The displacements u are separated into the prescribed set u_α and the unknown set u_β. The force components may be correspondingly divided; X will then be the reactions at the prescribed displacements, and X_β will be the specified load components along the unknown displacements u_β. The partitioning of the K matrix along the same lines leads to the following:

$$\left[\begin{array}{c} X_\alpha \\ \hline X_\beta \end{array}\right] = \left[\begin{array}{c|c} K_{\alpha\alpha} & K_{\alpha\beta} \\ \hline K_{\beta\alpha} & K_{\beta\beta} \end{array}\right] \left[\begin{array}{c} u_\alpha \\ \hline u_\beta \end{array}\right] \tag{14}$$

This represents the two matrix equations, and

$$\begin{aligned} \{X_\alpha\} &= [K_{\alpha\alpha}]\{u_\alpha\} + [K_{\alpha\beta}]\{u_\beta\} \\ \{X_\beta\} &= [K_{\beta\alpha}]\{u_\alpha\} + [K_{\beta\beta}]\{u_\beta\} \end{aligned} \qquad (15)$$

Known Known Unknown

From the latter, the unknown displacements $\{u_\beta\}$ for the prescribed displacements $\{u_\alpha\}$ and forces $\{X_\beta\}$ may be determined. Once $\{u_\beta\}$ is known, the unknown forces $\{X_\alpha\}$ at the constraints can be calculated. (The solution technique described is only symbolic, as the prescribed displacements $\{u_\alpha\}$ may be introduced into the matrix equation $X = Ku$ without partitioning.)

The stiffness method of matrix analysis corresponds to the classical method of slope deflection for (indeterminate) beams and frames in which the moment at one end of a member is expressed as a function of the rotations at both ends and the relative deflection. The stiffness method is also known as the displacement method. (The other important method of matrix structural analysis is the flexibility method or force method.)

e. Finite difference Method

The finite difference method is the representation of the derivative in discrete form (reference 11). In general, the n^{th} difference is defined as

$$\Delta^n y_k = \Delta^{n-1} y_{k+1} - \Delta^{n-1} y_k \qquad (16)$$

where

$\Delta^n = n^{th}$ difference

y_k = the mate of a finite set of arguments x_k

This method is developed from the definition of the derivative as the limit, as distance approaches zero, of the difference between two values divided by the distance between them. For points spaced relatively close together, a continuous function can be represented by values taken at discrete points. In this method, it is assumed that the behavior at each grid point represents the behavior in the region surrounding the point. Region differential equations represent the behavior at a point in the field. By representing the derivatives as finite differences and substituting these expressions in the field equations, a system of differential equations is converted to a system of linear difference equations.

The nature of finite difference schemes requires that four properties of the solution be investigated. These four properties are convergence,

consistency, stability, and error. The scheme must be so formulated that the error growth with each step is tolerable. This method, similar to finite elements analysis, produces solutions with discretization and rounding error. A proper balance must be made between the use of large numbers of points or elements with corresponding high roundoff error, and small numbers of points or elements and a correspondingly high discretization error.

The finite difference method is a type of numerical technique that deals with a means of numerical approximation of field equations. The similarity of the technique to finite element analysis precluded any further investigation of this method.

f. Finite Element Method

The term "finite element method of analysis" refers to a method of solving boundary value problems in which the distribution of stress and strain throughout a solid mass under the influence of either internal or external loadings is desired (reference 12). The method generally has been applied only to two-dimensional masses: in soil mechanics, plane stress or plane strain. (Three-dimensional solutions are not generally available for use.) In two-dimensional problems, the mass is divided into elements composed of plane figures, such as triangles. The elements are connected to each other at the vertexes or nodes, thus forming an interconnected assemblage of finite elements equivalent in shape and area to the mass. Although the elements are connected only at the node points, an additional restriction is placed on the displacement field which requires that boundaries between adjacent elements are in continuous contact during deformation.

The initial assumption made in the finite element method is the character of the displacement field. In a computer program used at WES, it is assumed that the displacements are linear functions of the coordinate system. The assumption that the displacement field is linear will lead to a unique strain associated with each triangular element, i.e., a straight line in the undeformed element remains straight after deformation. The displacements within each element can be evaluated in terms of the local coordinates of each element; thus, if the element were to approach an infinitesimal size, the displacements in the assemblage of discrete elements would approach the idealization of the continuum.

The nodal displacements are found by a procedure often used in structural mechanics. That is, the force on a member is equal to the displacement

times the stiffness of the element. The stiffness is the force causing a unit displacement of the element, and the stiffness matrix for the entire assemblage of elements is formed by relating the position of the nodal points and the stress-strain relations of the elements under investigation. Briefly, displacements are described in terms of the local coordinates of each element, and the strain within each element is computed from the displacements of the node points and the size of the elements. Stress is expressed as a function of strain, and the force on the nodes of the element is a function of stress. Thus, by proper mathematical manipulation, an equation of the type $F = kd$ can be written for each element in which the stiffness k is a function of the element coordinates and the stress-strain relation, and the displacement d can be resolved into its x and y components. Since each (triangular) element has three node points and two reactions, the equation $F = kd$ can be thought of as representing six linear equations. Also, since each element is connected to its neighbor at the node points, the solutions for the nodal displacement in one element must be compatible with the solutions for its neighbors. Thus, a total stiffness matrix K can be formed by adding all of the individual stiffnesses k, resulting in a system of simultaneous linear equations of size $2n$, where n is the number of nodal points. A solution to these equations is obtained by specifying either forces or displacements at the boundary and solving for the displacements at each node. As mentioned previously, when the nodal displacements are known, the average strain and stress in each element can be computed. The basic equation for finite element analysis relates virtual work to virtual strain energy as follows (references 8 and 13):

$$\int_V [B]^T [D]\{\epsilon_o\}\, dv + \int_V [N]^T \{g\}\, dv + \int_S [N]^T \{p\}\, ds + \{X\} = \left(\int_V [B]^T [D][B]\, dv\right)\{u\} \qquad (17)$$

or

$$\{X_o + X_g + X_p + X\} = [K]^e \{u\}$$

where

$\{X_o\} = \int_V [B]^T [D]\{\epsilon_o\}\, dv$, equivalent forces for initial strains

$\{X_g\} = \int_V [N]^T \{g\}\, dv$, equivalent forces for body force effect

$\{X_p\} = \int_S [N]^T \{p\}\, ds$, equivalent forces for surface traction

$\{X\}$ = vector of actual concentrated nodal forces

$[K]^e = \int_V [B]^T [D] [B]\, dv$, stiffness matrix for the element

$\{u\}$ = vector of nodal displacements

$[N]$ = function of coordinates matrix

$[B]$ = function of stress-strain relation matrix

$[D]$ = elasticity matrix

$\{\epsilon_o\}$ = initial strain matrix

$\{g\}$ = body forces matrix

$\{t\}$ = surface traction matrix

Other element shapes may be used.

A typical flexible pavement structure was analyzed using quadrilateral finite elements (references 14 and 15), and the results were compared with Burmister's solution for a three-layered problem. This comparison is shown in figures 5 and 6.

Computer programs exist for the two-dimensional case and can be almost unlimited in size, depending on accuracy desired and the number of simultaneous equations. Each equation would normally contain six coefficients, each of which must be evaluated on the basis of the geometry and stress-strain relation of the stressed mass. Most computer codes are derived from an elastic-stress analysis written by Professor E. L. Wilson, University of California (reference 16).

The axisymmetric finite element program results were compared with the instrumentation data. This comparison indicated an almost duplicate pattern as the layered system analysis for a vertical normal stress versus depth plot. The calculated stress did not attenuate as rapidly as measurements and had a different shape. The deflection basins indicate a close agreement in both the finite element analysis and the elastic half-space analysis. However, the curve shapes from both of these analyses differed from the instrumented deflection curves.

The limitations of two-dimensional loading and pavement response, the requirement for measurable values of E and ν , the neglect of stress

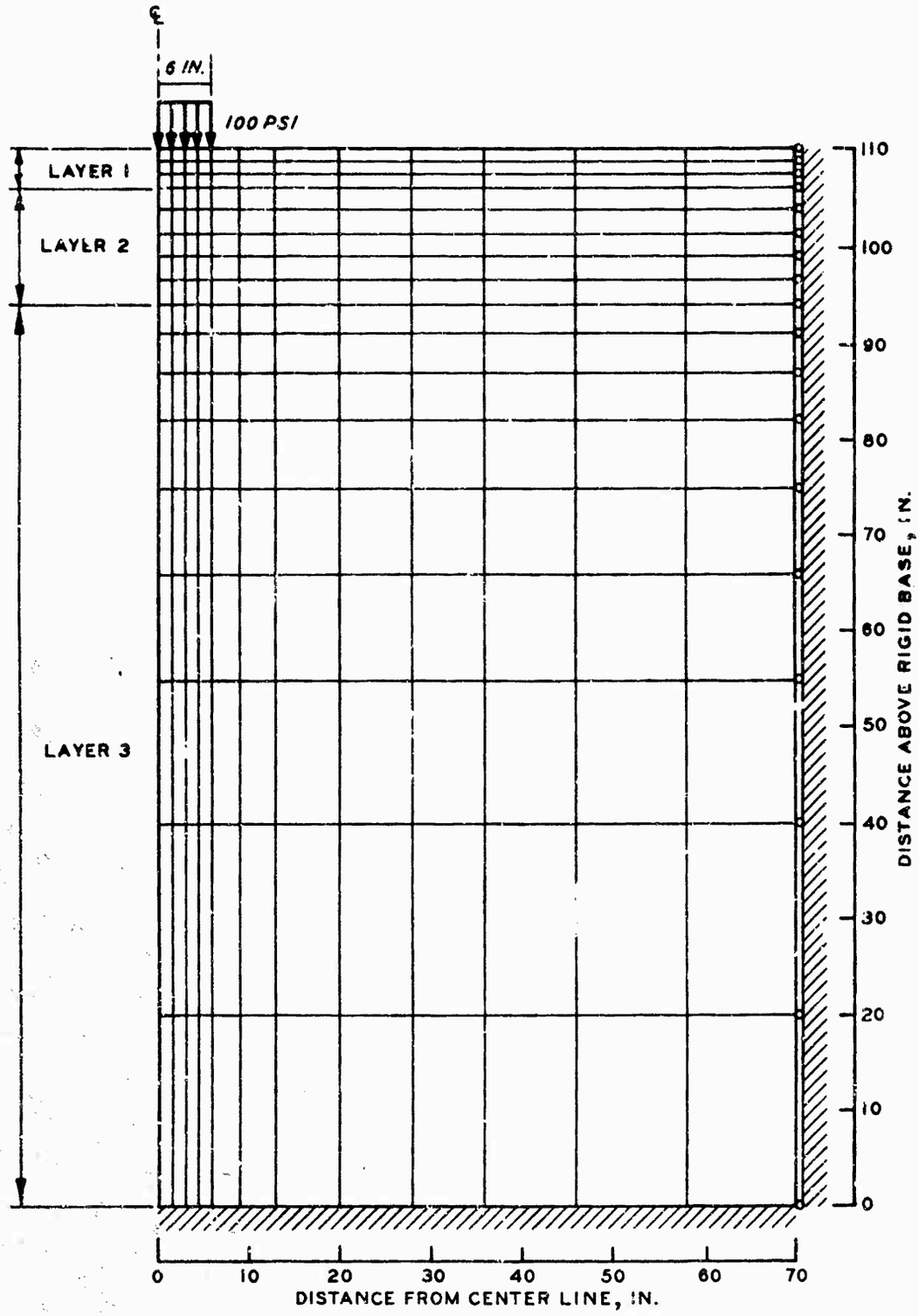

Figure 5. Finite Element Configuration Used for Analysis of Layered System (Reference 15)

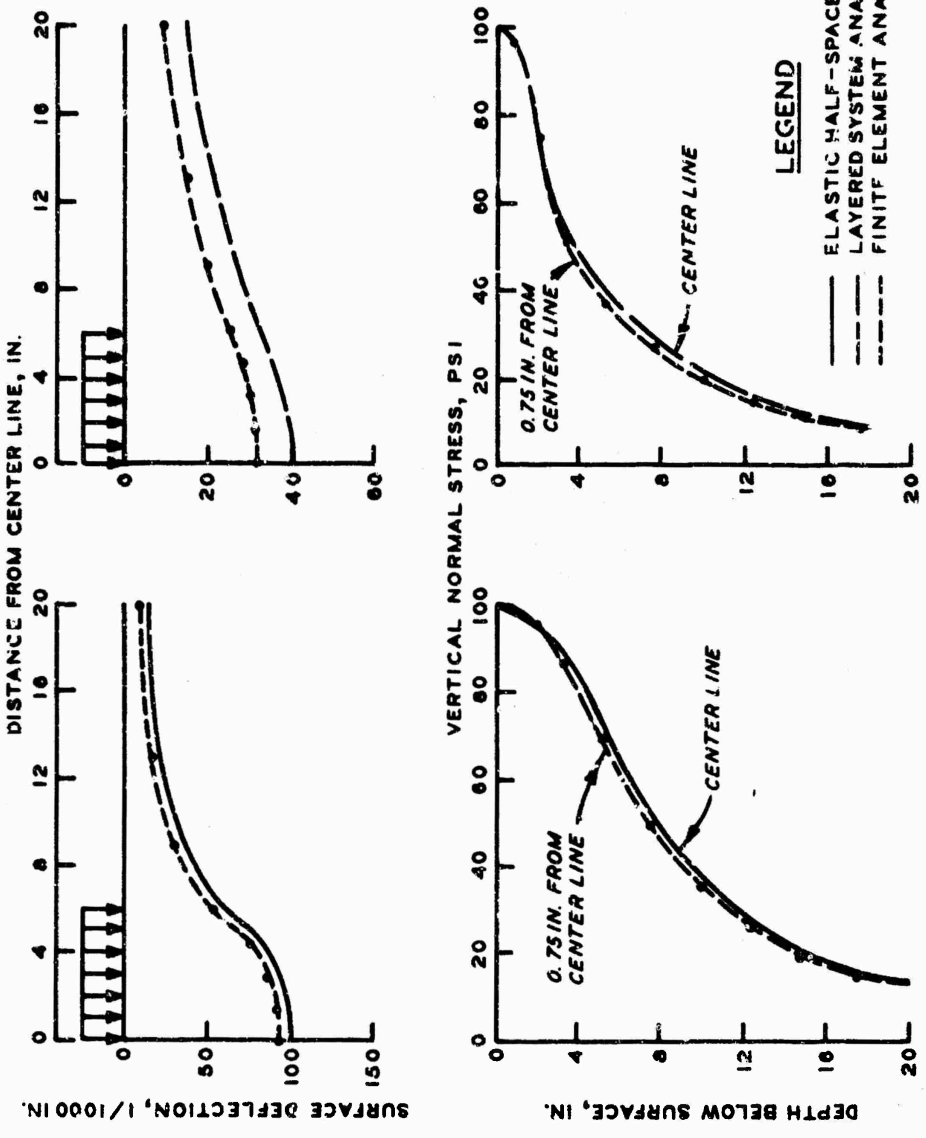

Figure 6. Comparison of Deflections and Stresses Derived by Finite Element, Elastic Half-Space, and Layered System Analyses for a Surface Load of 100 psi (Reference 14)

repetitions, and the difficulty in accurately describing the constitutive equations all limited the use of the finite element program in accomplishing the objective of this study. The finite element program results agree closely with the elastic half-space analysis results as shown in figure 6. However, the field instrumentation readings do not agree with either of these analyses. This is discussed in detail in Volume III.

The three-dimensional program eliminates the two-dimensional loading-response limitation but is still in the development stage. The program is mammoth in size and the band-width increase in the three-dimensional program will greatly increase computational effort. The limitation of adequately describing the construction material characteristics will still exist in the bug-free three-dimensional program.

g. Mechanistic Models

Mechanistic models consist of mechanical components, such as springs (representing elasticity), dashpots (representing viscous behavior), and Coulomb dampers (representing plasticity). Various combinations of these components have been used to represent pavement structures. One such model was developed at Purdue University (reference 17). Basically, the theory used for the mechanistic model in the Purdue study was derived from a translation of a Russian book by V. Z. Vlasov and N. M. Leont'ev (reference 18). An infinite beam resting on an elastic foundation was used to represent a landing mat-soil structure.

A limited investigation of this study indicated that a more general form of the solution was available for use in studying flexible pavements. A performance prediction portion of the Purdue study was developed for a Vlasov and Leont'ev model with an infinite beam and a hyperbolic stress distribution. A limitation of this program was the restriction of two-dimensional analysis treating single- or multiple-wheel loads that act only on a two-dimensional loading plane. An advantage, however, was the ability to account for a nonsymmetric loading condition. The first model in this study, which was based on elastic theory, was shown to be capable of duplicating a given loading system. It is noteworthy that the model behavior was extremely sensitive to the magnitude of the subgrade modulus k, which was found to decrease with traffic. However, this decrease in k may be influenced by the effect of construction technique.

The second mechanistic model developed at Purdue was capable of

simulating actual loading sequences and could also provide a means of estimating residual deformations of a surface. This process involved an iterative method of duplicating the loaded-deflection basins from actual measured input data. This model handles an asymmetric load that can treat a viscoelastic model, which predicts a response to a simulation of actual sequence of traffic loads. This model is a two-layer system with the surfacing layer elastic and the subgrade layer viscoelastic. A computer program for determining deflection of two layers was available but was not used in conjunction with this project. The program is relatively small.

h. Viscoelastic Models

(1) General. Freudenthal and Lorsch (reference 19) were among the first investigators to employ a linear viscoelastic analysis to infinite beams. In their study, the soil support was replaced by a series of Kelvin, Maxwell, or Standard linear solid elements. For each of these elements, the authors were able to develop relationships for the deflection of an infinite beam subjected to time-invariant concentrated and uniform loads. Other investigators have continued similar work, and development has continued through the work of Barksdale (reference 20). Barksdale developed one creep compliance response for an asphalt mixture and another for a clay subgrade in his analysis of a viscoelastic-layered pavement system. A limitation of using viscoelastic models is the difficulty in assigning representative numerical values to the parameters for even the simplest mode.

(2) WES study. A viscoelastic, multilayered, half-space system under stationary and moving axisymmetric loads has been analyzed in another study (reference 21). Solutions have been computed for normal stress, radial stress, tangential stress, shear stress, vertical deflection, and radial displacement at any point within the half-space. This viscoelastic solution was based on the elastic-viscoelastic correspondence principle and was obtained by applying the Laplace transformation to replace the time variable with a transformed variable. The time dependency was changed to an associated elastic problem. This program has not been written for computer usage and therefore was not used in conjunction with this project.

i. Discontinuous Orthotropic Plates and Pavement Slabs

The theory involved in this University of Texas computer program (reference 22) primarily consists of a recursion solution of a system of

beams resting on an elastic subgrade represented by a system of springs. The model consists of discrete elastic beams connected at their nodal points by elastic blocks. Torsion is accounted for by rods connecting midpoints of opposite beams. This model accounts for a two-layer system. One stipulation of the model is the requirement for a specified ratio of slab width to slab length grid system. Applicability of this program to flexible pavement analysis is limited because of the restriction to two layers, requiring a derivation of equivalent relationship for multilayers. The plate analysis assumes that the pavement is a flexural member extending in two dimensions with the significant generalized forces of transverse force and two moments at the joint. The computer program is available and is relatively large in capacity.

j. Equivalent Thickness Theory

In the Odemark equivalent thickness theory (reference 25), the upper layer of thickness is replaced by an equivalent thickness of the lower material according to a relation with thickness of layer E (modulus of elasticity) and ν (Poisson's ratio). The specific equations follow the Boussinesq solution and are purely elastic. In the Odemark method, the stresses and displacements are evaluated by considering the pavement layers to behave as a slab resting on the subgrade soil. The deformation moduli are determined by plate load tests. The design criterion used is to limit the maximum curvature of the deflected pavement surface. Results derived from the equivalent layer theory agree closely with those from Burmister (reference 2), assuming the same E and ν parameters. Computer programs exist for the application of this theory, but the programs were not used in this project due to the questionableness of layer equivalency.

k. Elastic Plate on Dense-Liquid Bottom Layer

Application of the Westergaard theory (reference 24) to flexible pavement design has been investigated only for the case of a vertical deflection immediately under the center of a uniformly loaded circular area for two layers. Both layers were assumed to be homogeneous and isotropic and of infinite horizontal extent. When applying the Westergaard theory, it is assumed that the bottom layer material is a dense liquid. Westergaard analyzed the system of an elastic plate on a dense-liquid subgrade using mathematical series expansion. The usefulness of this theory is limited by the basic

assumptions and is also limited to two layers; therefore, it was eliminated from further study in flexible pavement design.

l. Elastic Plate on Elastic Solid Subgrade

Hogg and Holl (references 25 and 26, respectively) independently analyzed an elastic plate on an elastic solid subgrade by expressing the subgrade reaction as a Fourier-Bessel transform. The solution is valid only for a symmetrical loading. Also, the determination of stresses, strains, deflections, and subgrade reactions may be computed only under the center line of the applied load. The solution of the elastic layered system does not have some of the restrictions inherent in the plate theory. This work is limited to use in a two-layered system. Finally, essentially the same information obtained by this solution can be obtained from Burmister's solution of the elastic layered system. Therefore, this theory was not considered further.

m. Barenberg Shear Layer

Though it is common practice to use an elastic layered system analysis for pavement structures composed of granular materials, the application of such an analysis is obviously not valid. Tensile stresses are developed at the bottom of a layer supported by a weaker layer. Since the E-values of most granular materials are greater than the E-values for subgrades, tensile stresses will develop and the equilibrium assumed in setting up basic equations for the system will be violated. Barenberg's approach (reference 27) was to examine conditions for a continuously supported shear layer that has no flexural resistance. The development of a critical shear layer may occur when the resistance to shear, usually provided by the subgrade, is lost. No computer program was available for the Barenberg shear layer concept, but the approach seems applicable to certain conditions which develop in flexible pavement structures.

n. Peattie Method

The Peattie method, which is still in the process of development, uses two design criteria (reference 28). The vertical stresses on the subgrade, as well as the radial tensile strain in the surfacing layer, are kept within certain allowable limits. The deformation moduli of pavement layers are determined in the field by vibrational techniques. This method is

essentially a part of the multilayered elastic method and is not a separate procedure.

o. Single-Layer Elastic Theory Program

The one-layer program that assumes a pavement is elastic, homogeneous, isotropic, weightless, and of semi-infinite extent has been programmed for the WES computer system. This program, which was derived from Boussinesq's work (reference 13), may be modified to allow the deflection to reach zero at any predetermined distance from the loaded area. The assumptions are circular load, one layer, uniform load distribution, and no lateral surface stresses.

With proper assumption of Poisson's ratio and modulus of elasticity, the program can closely duplicate measured deflection data at any given point. Also, the change in the program to allow an offset cutoff in deflection values can be used to describe the equivalent single-wheel load causing the deflection.

A plot of maximum elastic deflection versus depth is shown in figure 7. This plot shows a comparison of measured data with predictions derived from the single-layer elastic theory program. The measured data represented static-load test, 30,000-lb-per-wheel, 12-wheel assembly, item 3. The Young's modulus of elasticity E was determined by inverse computations using the measured deflection at the surface. The findings from other studies (reference 29) also indicate that the stress distribution at normal temperatures in conventionally constructed flexible pavements follows relatively closely the pattern predicted by the elastic theory.

The measured vertical stress profile with depth was different from the elastic single-layer case, and an attempt was made to duplicate these measurements by changing the concentration factor n. The value of the concentration factor (reference 30) parameter n depends on the properties of the soil mass. For $n = 3$, in the following relation,

$$\sigma_Z = \frac{nP}{2\pi Z^2} \cos^{n+2} B \qquad (18)$$

where

σ_Z = vertical stress
n = concentration factor
P = load
Z = depth
B = smallest angle with vertical ordinate and component of force in direction of radius vector

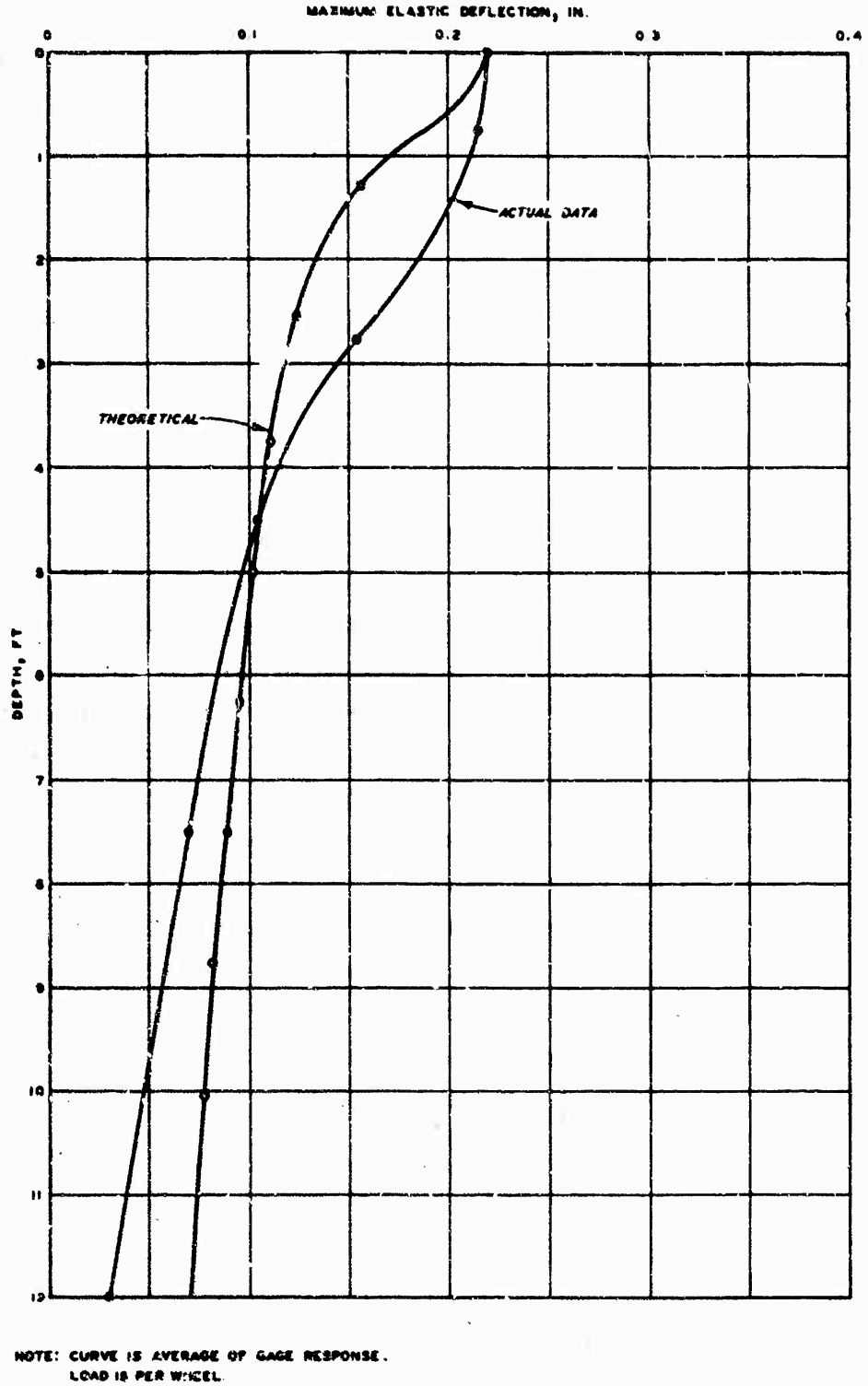

Figure 7. Comparison of Predicted Maximum Elastic Deflection with Maximum Elastic Deflections Measured During Static Loading of Item 3 Using 360,000-lb 12-Wheel Assembly

The vertical stress component is the same as that obtained by Boussinesq for a semi-infinite body satisfying the assumptions of the theory of elasticity. Using this concept, the instrumented vertical normal stress basin at a depth of 2.75 ft under a 12-wheel static load was duplicated using an $n = 6.5$ value. The same procedure was attempted using deflection measurements, but this could not be accomplished in a simple manner because the equations of compatibility (reference 13) could not be satisfied.

p. Discussion

The preceding brief summaries represent a major portion of the theoretical treatment afforded the background analysis of this project. Other methods, such as Laplace transformations, Canadian method, and Navy method, were reviewed for possible usage but have not been reported.

The previously discussed theories allow a better understanding of the behavior of continuous soil media from a simplified viewpoint. In the absence of knowledge for a specific condition, these theories all contribute to a general enlightenment regarding soil structure behavior. There are many limitations and constraints imposed by each of these concepts, coupled with advantages. There is no such thing as an exact theory to explain an aspect of the physical world. All scientific knowledge is fundamentally empirical and is based on observed physical behavior. A theory may be used to explain or predict physical behavior within the present limitations of knowledge or ability to observe. A precise mathematical derivation of a theory often deludes the observer into believing that his theory is exact, but this is not true as observational powers are limited by precision of available measuring equipment (reference 31). The MWHGL test represents controlled experimentation necessary to accomplish specific objectives. The following limitations would hinder a purely theoretical treatment for the MWHGL project.

(1) The theories are based on a static loading condition and thus do not account for the detrimental effect of repetitive design loadings or for the effect of mixed loadings on the performance of the structure.

(2) Most concepts are an extension of classical structural material analysis in which material properties are reasonably exact quantities. For this analysis, the determinations of two typical input parameters, Young's modulus of elasticity E and Poisson's ratio ν, are at best an estimate for different soils. The determination of whether E is in tension or compression may not have a significant effect on the behavior of the pavement

layer under load, but becomes quite important when evaluating stresses in layers based on strain values.

(3) Body forces (motion, inertia) are generally ignored because they are higher order terms in comparison with forces distributed over the surface of the body (surface forces). They may or may not have an effect on the pavement structure, which is known to exhibit certain degrees of deterioration even in the absence of applied loading.

(4) Layers must be composed of isotropic, homogeneous materials for which Hooke's linear law may be applied to linear systems. Also, the upper layers must be weightless and infinite in extent in the horizontal direction, but must be of finite thickness.

(5) Certain boundary conditions must be imposed to identify the specific problem. Type of support and conditions at the layer interfaces must be specified. Normally, the top layer must be free of normal and shearing stresses outside the loaded area; in the lower layer, the displacement and stress must approach zero as the depth approaches infinity. Similarly, it is necessary that the layers be in continuous contact with each other.

(6) Results from each program depend on the constitutive equations that have been developed for the particular material. At present, there are no realistic constitutive equations for the materials employed in construction of flexible pavements or to describe their property changes.

(7) Variations of vertical subgrade stress occur with variations in pavement temperature, subgrade moisture, and vehicle speed, and as a result of deep frost action. The change in the moisture content in the subgrade is accompanied by a change in the rheologic properties of the soil. No program handles these changing conditions caused by environmental effects or those related to previous stress history.

(8) The time and space locations of loadings are almost random because of the manner in which an aircraft operates. Also, the distribution of load repetitions is difficult to define for aircraft prior to actual operation. This random transfer of coordinate system complicates the assumptions required of these programs and presents another problem area in the mathematical expression of this loading (for example, point loading or uniformly distributed loads).

(9) Numerous arbitrary failure criteria presently employed are difficult to incorporate into a generalized theory. Most theories seemingly refuse to operate as a preselected failure criterion is approached. A limiting

quantity of stress, strain, deflection, or other parameter is currently not established as an acceptable unique value of failure. The assumption that the system obeys Eulerian conditions regardless of the stress level is questionable.

(10) Any representation of the soil structure as a series of springs, dashpots, dense liquids, etc., is limited by this representation and by the assumption that the system is not altered by changes in the system. The main disadvantage of this type of simulation is the difficulty in assigning parameter values that correlate with various actual conditions, such as quality of materials from a viewpoint other than strength, i.e., drainage, intended use of structure, etc.

The above limitations, coupled with the inability to apply any one theoretical concept to the total problem of the design and evaluation of flexible pavement airfields, led to the review of the present Corps of Engineers CBR method and investigation to determine its adaptability to the analysis of this test section.

2. RIGID PAVEMENT

A wide variety of algorithms are currently available to predict pavement response to loads. These solution methods are generally applicable only to static or quasi-static loads. The basic differences among the solution methods lie in the assumptions of subgrade and pavement structure characteristics. The analysis methods usually applied to rigid pavement structures involve the assumption of either a dense-liquid subgrade or an elastic solid subgrade together with an assumption of one or several elastic layers (plates) over the subgrade. Considerable work has been done in computerizing these solutions. Of particular interest has been the use of finite element techniques to more accurately describe the structure and to provide for more realistic boundary conditions. The computerized solutions including the finite element procedures are, nevertheless, subject to the same assumptions listed above; i.e., elastic behavior is assumed for all components and/or subgrade behavior is characterized by a dense liquid, and the loads are static. The algorithms generally applicable to rigid pavements are discussed in the following paragraphs. (Details already given in the flexible pavement discussions are not repeated here.)

a. Elastic Plate on Dense-Liquid Bottom Layer

This method is commonly referred to as the Westergaard analysis (reference 32). The pavement slab is assumed to be an elastic, homogeneous, isotropic, uniform plate supported by a dense liquid of infinite depth. The subgrade is represented by a series of independent linear springs that react in direct proportion to the slab deflection at the point. The slabs are assumed to cover a semi-infinite half-space. Application of the Westergaard analysis to rigid pavement design is given in Section IV.2.

b. Elastic Plate on Elastic Solid Subgrade

In this method, the pavement slab is assumed to be an elastic, homogeneous, isotropic, uniform plate supported by an elastic solid of variable thickness (references 25 and 26). The elastic solid is characterized by a rigidity factor that is a function of the modulus of elasticity and Poisson's ratio of the subgrade material. One advantage of this method is that the subgrade materials are not independent, i.e., a deformation occurring at one point influences adjacent points to some degree. One disadvantage of this analysis method is defining the input parameters for the elastic solid.

c. Layered Systems (References 1-3)

In this type of analysis, the pavement structure is assumed to be composed of a variable number of elastic layers resting on an elastic solid. The analysis has the advantage of being capable of solving problems of composite pavements and of examining conditions in a wide variety of locations in the pavement structure. One disadvantage is defining the pseudo-elastic constants for the various layers based on standard testing procedures in which the appropriate boundary conditions are not reasonably approximated.

d. Discontinuous Orthotropic Plates and Pavement Slabs

This method was developed by the University of Texas and is a finite element approach to the problem (reference 22). Slabs are represented by a grid of beams connected by elastic blocks and torsional springs all supported by vertical springs. The output presents the deflections, bending moments, and twisting moments at all nodal points in the slab. The output describes conditions in the slab only; no information is produced on the subgrade conditions. The solution, if programmed with sufficient nodal points, tends to yield the same results as the Westergaard method. The finite elements

representation allows more freedom in describing boundary conditions, such as cracks, discontinuous subgrade support, nonuniform thickness, etc.

SECTION III

REVIEW OF CURRENT CE METHODS

1. DEVELOPMENT OF CBR METHOD OF DESIGN OF FLEXIBLE PAVEMENTS (REFERENCE 33)

During 1928 and 1929, the California Division of Highways made an intensive investigation of pavement failures throughout California. Areas that had failed were investigated to determine the local drainage conditions and other factors affecting the stability of the pavement. A test method was sought that would be satisfactory for establishing the density that should be achieved in the construction of subgrades as well as the shear strength that was required to support the anticipated traffic. A quick, simple test was sought that could be used to evaluate the quality of subgrade, subbase, and base course materials. Static-load field tests were unsuccessful, mainly because of the influence of the elastic and plastic deformation of the material beneath the load and also because saturated conditions were not considered.

A California bearing ratio (CBR) test was devised that determined the resistance of a specimen to lateral displacement (reference 34), thus measuring the combined influence of cohesion and internal friction. Samples were first thoroughly consolidated to the density obtainable under good construction methods or to approximately the density ultimately produced by traffic in good subgrade materials. A plot of total thickness versus CBR values resulting from this study is shown in figure 8. Curve A was developed on a basis of experience available in 1929 and was believed to be adequate for average traffic conditions. Curve B represents values derived from the original survey.

During the early 1940's the responsibility for the design and the construction of military airfields was assigned to the Corps of Engineers, U. S. Army. Later the Corps was delegated the same function pertaining to civil airfields required for military occupancy. After deliberation and investigation, the principles used by the California Highway Department, known as the CBR method, were adopted tentatively for the design of flexible pavements. Among the reasons for adoption were: (a) The CBR method had been correlated to the service behavior of flexible pavements and construction methods and had been used successfully by the State of California for a number of years. Two other states were known to have methods of a similar nature that had been successful; (b) It could be adapted for immediate use in airfield pavement design; (c) It was thought to be as reasonable and as sound as any of the other methods

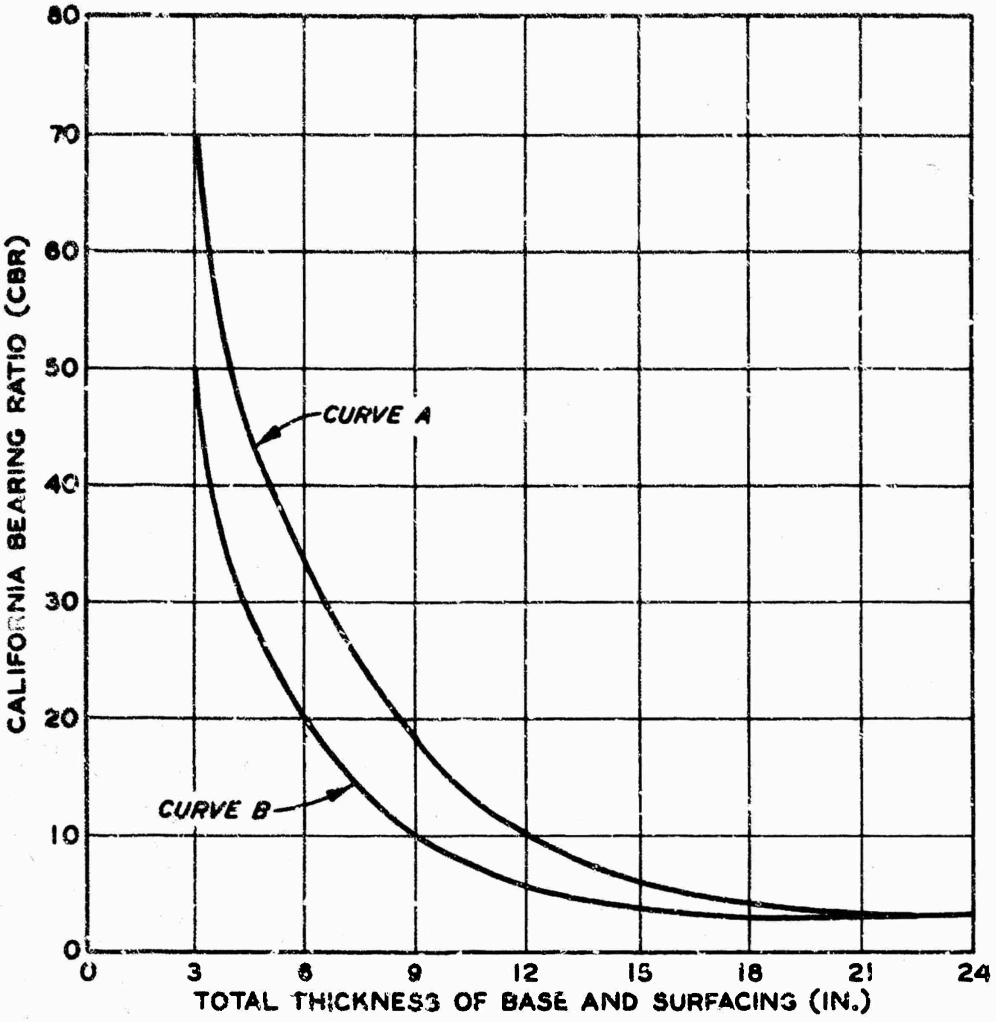

Figure 8. Original California Pavement Design Curves Relating Total Pavement Thickness to the CBR Value of the Subgrade (Reference 35)

investigated; (d) The subgrade strength value could be determined either in the laboratory or in the field with simple portable equipment. Testing could be done on samples of soil in the condition representative of the foundation moisture state under most pavements.

To evaluate figure 8 curves in terms of aircraft traffic, the relationship among (a) relative weights of loaded vehicles, (b) characteristics of airplane and automobile tires, and (c) lateral distribution of traffic were considered. On the basis of these factors and recognizing the need for verification tests, curve A, figure 8, was assumed to represent a 12,000-lb aircraft wheel load, and curve B, a 7000-lb aircraft wheel load. Service behavior records of adequate pavements had indicated that it was necessary for elastic deformation to govern pavement performance over an extensive period of use. Accordingly, the Office, Chief of Engineers (OCE), decided to develop empirical curves by extrapolating the original data on the basis of the elastic theory. Since all bearing tests (even those such as the CBR test conducted on confined specimens) are essentially shear tests and since shear deformation must be eliminated in a satisfactory pavement, shear stresses were used as a guide in making the extrapolation.

A review of airplane tire data indicated that a uniform tire pressure of 60 psi could be selected for the entire group of planes in use. Wheel loads of 25,000, 40,000, and 70,000 lb were selected to cover the range of existing and future heavy aircraft loads. Contact areas were computed from wheel loads and tire pressures. Circular areas were used for ease of computation and also because the shear stresses in the base course and subgrade did not vary materially when elliptical areas were used. Shear stresses were computed, as shown in figure 9, by use of stress tables (reference 36). The thicknesses of base course and pavement corresponding to bearing ratios of 3, 5, 7, and 10 were located on the stress curve for the 12,000-lb load curve, and the stresses corresponding to these thicknesses were noted. On the basis that these stresses should not be exceeded for other wheel loads in order to retain a uniform standard of design, the stress values were located on the curves for the 25,000-, 40,000-, and 70,000-lb wheel loads (figure 9). (The values indicated by the curve in figure 8 for the 12,000-lb wheel load were comparable to the California values for medium heavy highway traffic.) The thicknesses corresponding to these stresses were transferred to the graph of thickness versus bearing ratio, and the curves similar to those shown in figure 10 were drawn.

The preliminary design curves obtained by extrapolation were developed at

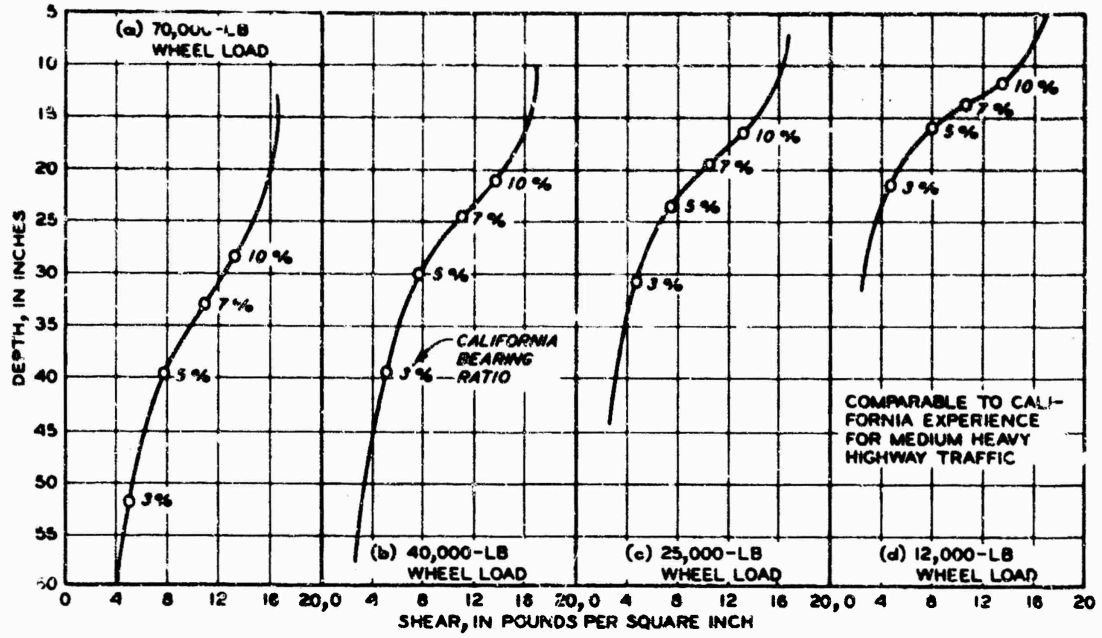

Figure 9. Extrapolation of Highway Pavement Thicknesses by Elastic Theory (Tire Pressure, 60 psi). From Reference 37

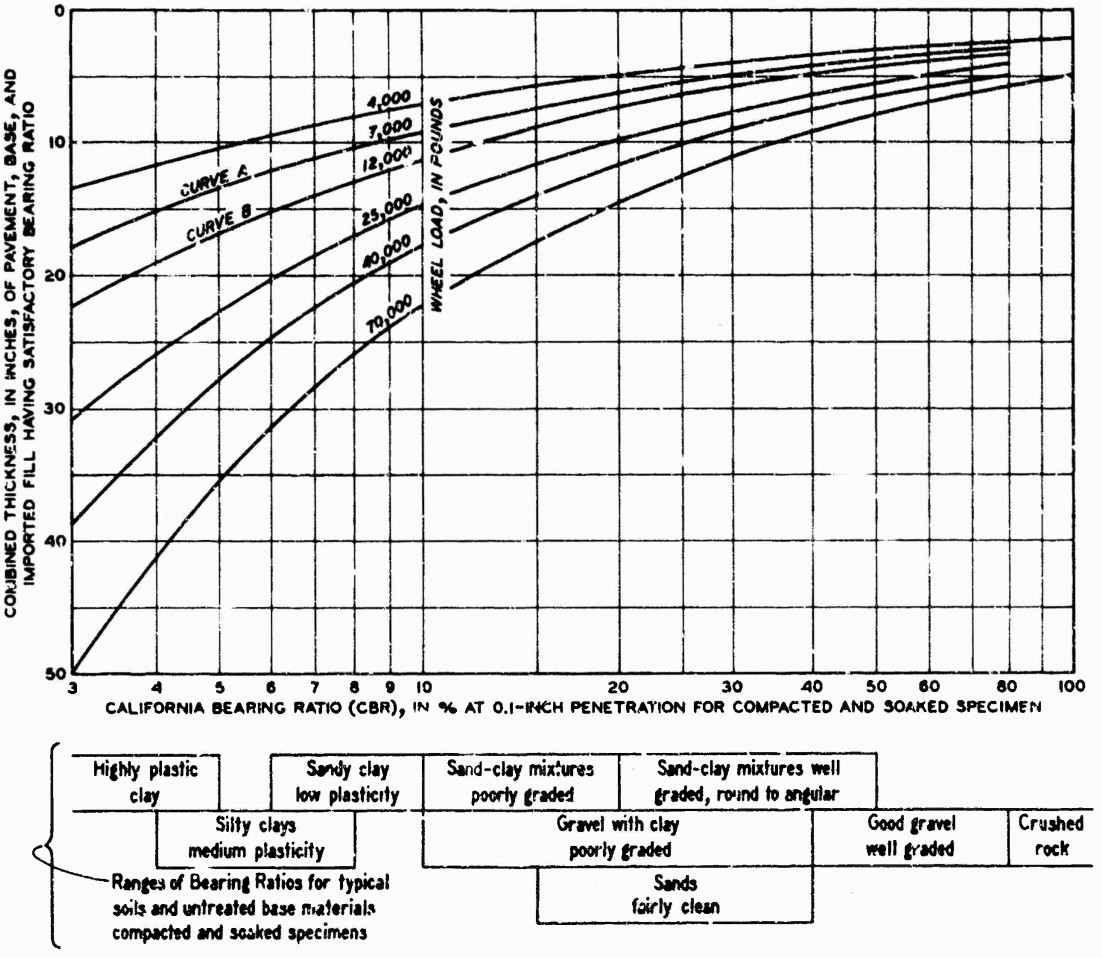

Figure 10. Tentative Design of Foundation for Flexible Pavements (Reference 37)

the meeting of consultants held in February 1942 in Washington, D. C., which included T. A. Middlebrooks and others from OCE; O. J. Porter, who developed the California method for design and evaluation of highway pavements; and Professor Arthur Casagrande of Harvard University. The consultants each made independent calculations to extrapolate the basic curves. Those of Mr. Porter were based on an allowable deformation for the various loads, whereas those of Professor Casagrande were based on the relationships between the relative size of the loaded areas. The three sets of computations (OCE, Porter, Casagrande) were in substantial agreement when the data were reviewed by the group. It was decided that the average thicknesses shown by the three extrapolations were reasonable for the low CBR values; however, the majority agreed that the less conservative values should be chosen for higher CBR values. Figure 10 expresses the best judgment of the engineers and consultants. This later became capacity operational criteria.

Test sections and evaluation of field performance continued, and in April 1949, a relationship for the effect of less-than-capacity operations was offered (reference 38). Also, the term "cycles required to produce one coverage," defined as $\frac{200}{NW}$, where N = number of main wheels and W = tire width in inches, was introduced. Full-scale, multi-item tests were conducted through 1955 (references 38-46).

In 1958, an analysis of all available service-behavior data from test sections and prototype airfields (reference 39) indicated that the CBR design criteria for single-wheel loads could be expressed in the two basic parameters $\frac{t}{\sqrt{A}}$ and $\frac{CBR}{Pe}$ (reference 47). These parameters could be reduced to a single plotted curve that separated service-behavior data with regard to failures and non-failures, but without regard to repetitions. The relationship for the capacity-operational level is shown in figure 11 and is expressed mathematically as

$$t = \sqrt{\frac{P}{8.1\ (CBR)} - \frac{A}{\pi}} \qquad (19)$$

where

t = design thickness, in.

P = single-wheel load, lb

CBR = measurement of supporting layer strength

A = measured tire contact area, sq in.

In 1959, the effects of less-than-capacity design repetitions and

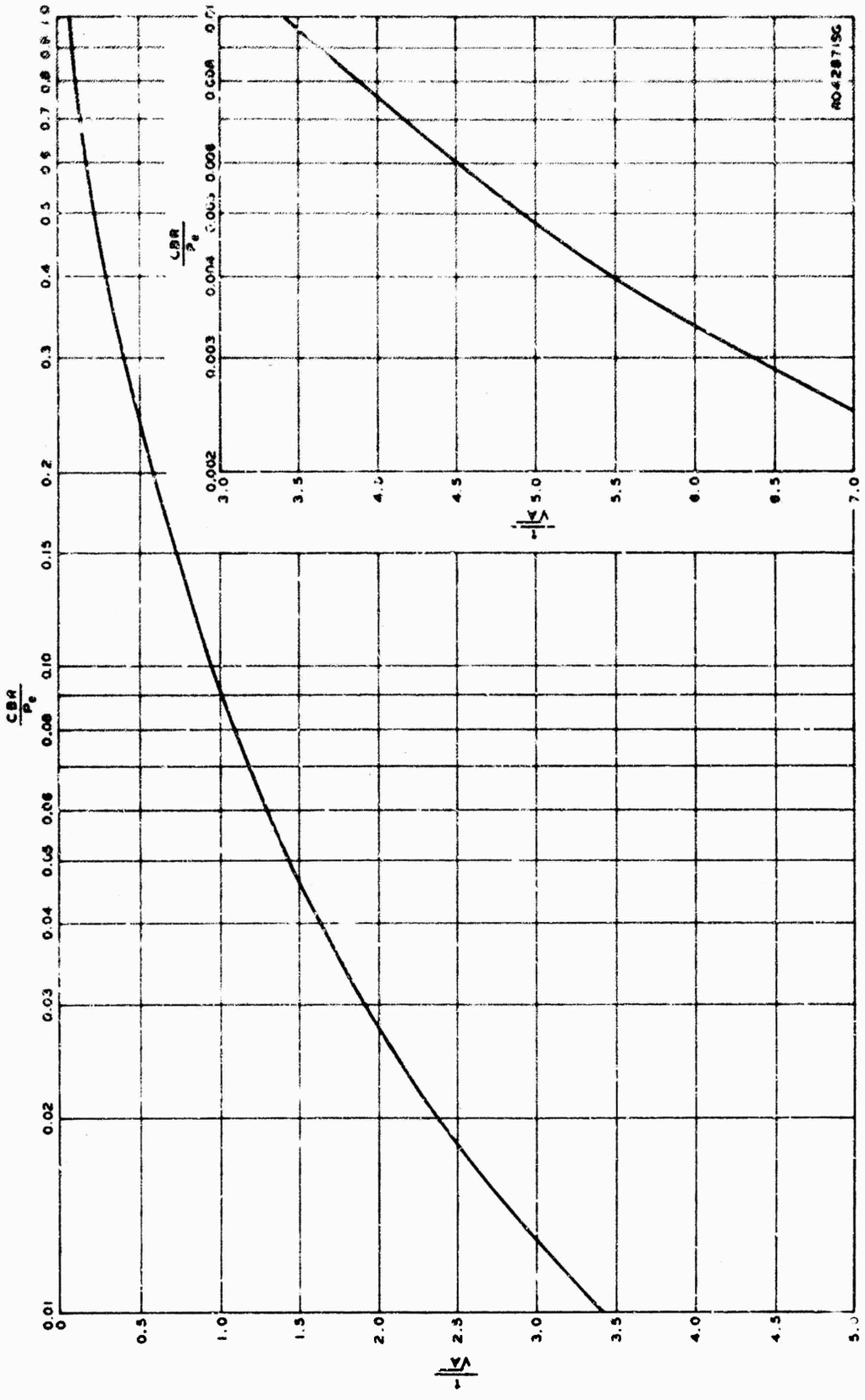

Figure 11. Relationship of Basic Parameters for the Capacity-Operational Level

multiwheel configurations were combined into a single relation that is essentially a combination of all developed CBR design criteria resulting from CE research (reference 48). The equation for relating flexible pavement design in the lower CBR regions (approximately <15 CBR) is

$$t = f\sqrt{\frac{ESWL}{8.1(CBR)} - \frac{A}{\pi}} \qquad (20)$$

where

t = design thickness, in.

f = percent of design thickness (0.23 log C + 0.15)

ESWL = equivalent single-wheel load (load on a single tire that produces the same vertical deflection on the supporting medium as that particular multiple-wheel assembly with the same single-wheel tire contact area)

C = coverage (sufficient wheel passes to cover every point of a traffic lane once)

CBR = measure of supporting layer's strength

A = measured contact area of loaded tire, sq in.

This formulation represents the required thickness to prevent excessive deflection of underlying pavement layers resulting from repetitions of load.

Construction control procedures are thoroughly treated in appropriate CE specifications and are a part of the design that accompanies these thickness requirements. These controls are intended to ensure that a pavement is not subject to differential settlement of materials in the underlying layers or lateral displacement of the subgrade resulting from water absorption. The influence of mixed aircraft traffic, climatic effects, and aircraft lift and speed, etc., are also automatically incorporated in this method. The judgment of the design engineer as to intended use of facility and distribution of traffic, channelized-nonchannelized traffic, etc., are also incorporated in the CE design concept.

This is the current CE procedure for the design of each layer in a flexible pavement structure. Concurrently, each layer must be compacted sufficiently to prevent detrimental consolidation, as shown in reference 49, and the wear- and weather-resistant surface must be designed so as not to be displaced by traffic (reference 50).

This brief background investigation indicated that the CBR method was both reasonable and sound and had been successfully correlated with service behavior. It was decided that the CBR method offered the best available means of

providing design and evaluation criteria and would best reflect the finding of the MWHGL test section. This method also represents the best experimentation and semiempirical technique of analyzing pavements with consideration of theoretical, materials testing, and construction control aspects. The next phase involved adapting the present CBR method of behavior prediction to the specific results of traffic from the test section.

2. DEVELOPMENT OF CURRENT RIGID PAVEMENT DESIGN PROCEDURE

a. Plain Concrete

The development of a design procedure for any structure to resist load requires that the most likely mode of failure be determined for the weakest nonredundant element comprising the structure. The mode of failure assumed by the current CE design method for a rigid pavement subjected to repeated rolling loads is that a crack is initiated at the bottom of the slab due to flexural action and migrates upward through the slab under continued traffic. Repeated application of traffic results in further cracking of the slab in the same manner until the slab is cracked into many pieces. This action continues until the integrity of the slab is destroyed to the point where it cannot effectively distribute load through beam action and excessive permanent deformations occur because of excessive shear forces in the foundation materials. As the slab deteriorates, deflections due to load increase, causing a working of the concrete at the cracks. This working results in spalling and faulting at the cracks and joints, which produces a rough riding surface with debris formed by the spalling of the concrete. The formation of the crack at the bottom of the slab is assumed to be a function of the magnitude of the stress and the fatigue effects of the repeated loading. The rapidity at which the crack, once initiated, migrates through the slab is found to be a function of the foundation strength and number of load repetitions. This mode of failure has been observed in both operational and experimental pavements. It is recognized that failures of the materials supporting the concrete slab, such as pumping, frost action, swelling, shrinkage, etc., can precipitate cracks in the pavement slab; current design procedures attempt to prevent these effects through the proper design and construction of the supporting medium. In general, a pavement slab will fail in flexure before sufficient distress, such as shear failure, can be generated in the supporting medium. Only under exceptional conditions are cracks initiated in the surface of the slab and migrate downward due to traffic.

Current CE evaluation and design methods are based on stress in the concrete pavement as calculated from the Westergaard analysis (reference 32). Westergaard assumed the slab to be an elastic, homogeneous, isotropic uniform plate supported on a dense liquid. The plate was either infinite in horizontal extent or semi-infinite (one free edge) in horizontal extent. Calculations and numerous tests have indicated that the stresses produced by loading near a free or jointed edge are equal to or greater than stresses produced by loading in the interior of a slab. Thus the edge-loading assumption was adopted as the basis for the CE design method. In practice, some means of load transfer is provided in the joints between individual slabs or the edges of the slab are thickened to resist the higher edge stresses. Load-transfer mechanisms commonly used are keys, dowels, or aggregate interlock that develops from the crack through the concrete thickness, such as at the weakened-plane (dummy groove) joints. Laboratory model tests and prototype aircraft loading tests in the field have been employed to determine the amount of load that can be transferred from the loaded slab to the adjacent unloaded slab through the load-transfer mechanism. Under normal conditions, it has been found that the load transfer can vary from a maximum of nearly 50 percent to a minimum of 25 percent. The minimum value of 25 percent has been selected for use in the CE criteria, and when computing the stress due to a load tangent to a joint having a load-transfer mechanism, the applied load is reduced by 25 percent. This value varies depending upon such factors as the joint opening, subgrade strength, warping and curling within the slabs, degree of distress in the slabs, and condition of the load-transfer device constructed in the pavement; however, longtime performance studies have indicated that 25 percent is a reasonable value.

Westergaard's equation for calculating free-edge stress is as follows:

$$\sigma_e = \frac{3(1+\mu)P}{\pi(3+\mu)h^2}\left[\ln\frac{Eh^3}{100k\left(\frac{a+b}{2}\right)^4} + 1.84 - \frac{4}{3}\mu + (1+\mu)\frac{a-b}{a+b} + 2(1-\mu)\frac{ab}{(a+b^2)} + 1.18\,(1+2\mu)\frac{b}{\ell}\right] \qquad (21)$$

where

σ_e = free-edge stress due to single wheel tangent to edge, psi

μ = Poisson's ratio of slab material

P = load, lb

h = thickness of slab, in.

E = modulus of elasticity of slab materials, psi

k = modulus of subgrade reaction $lb/in.^2/in.$

a,b = semimajor and semiminor axes, respectively, of elliptical contact area, in.

ℓ = radius of relative stiffness of slab and subgrade, in., where

$$\ell = \sqrt[4]{\frac{Eh^3}{12(1 - \mu^2)k}}$$

For multiple-wheel gears, the equations developed by Westergaard become rather complex. A graphical solution of these equations in the form of influence charts was developed by Pickett and Ray (reference 51). Current CE practice utilizes results found from these influence charts for multiple-wheel assemblies. The calculated values are again adjusted to account for load transfer across joints.

Fatigue or repeated load effects are accounted for in the design method by establishing an allowable flexural stress for a specified number of load repetitions based on design factor DF-versus-traffic volume relationships. The design factor is defined as the ratio of concrete flexural strength to the maximum edge stress as calculated by use of equation 21, with allowances given for load transfer across joints.

From the results of full-scale accelerated traffic tests utilizing single-wheel gear loadings ranging from 25,000 to 150,000 lb, twin-wheel gear loadings ranging from 60,000 to 100,000 lb, and twin-tandem-wheel gear loadings ranging from 150,000 to 325,000 lb, DF-versus-traffic volume relationships have been developed for three separate conditions of failure in plain concrete pavements. These failure conditions have been designated as "initial," "shattered slab," and "complete." The DF-versus-traffic volume for each of these failure conditions is shown in figures 12 through 14. In these figures, the traffic volume has been expressed in terms of coverages, a coverage being defined as when each point in the selected traffic area width has been subjected to a maximum stress repetition by the gear in question. Since the aircraft gears are composed of a variety of combinations of wheels, wheel sizes, wheel spacings, and arrangements of the wheels and gears, it is obvious that the traffic volume (number of aircraft passes) represented by any one coverage level is variable, depending upon the aircraft gear configuration. Thus to convert from coverages to aircraft passes or vice versa requires the

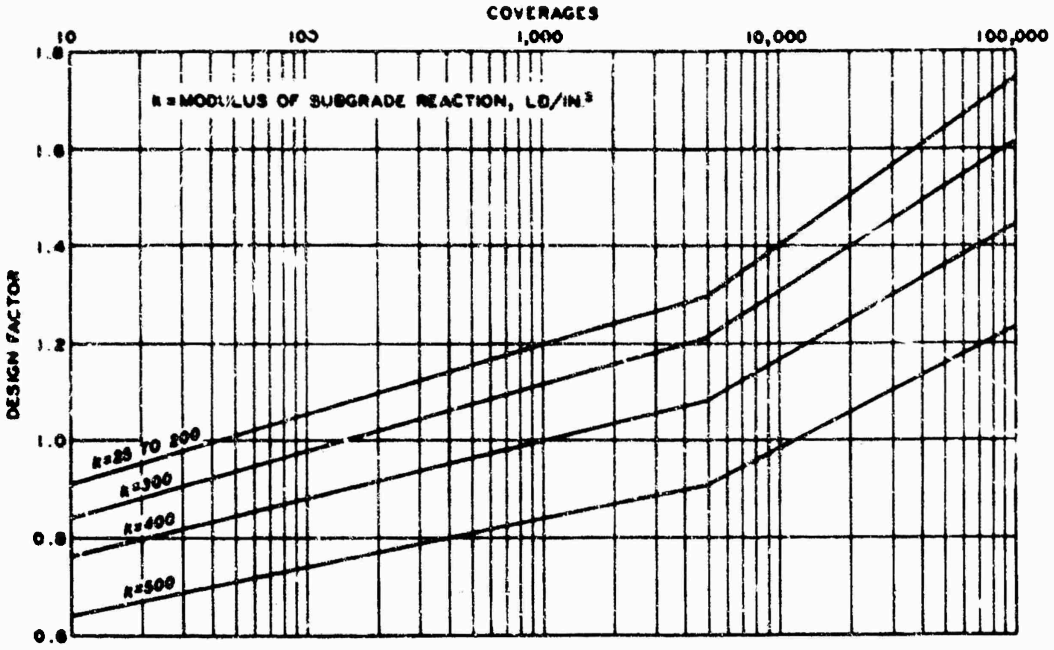

Figure 12. Design Factor Versus Coverages for Initial Failure Condition. Pass per Coverage Ratios for 12-Wheel and Twin-Tandem Assemblies = 1.34 and 3.30, Respectively

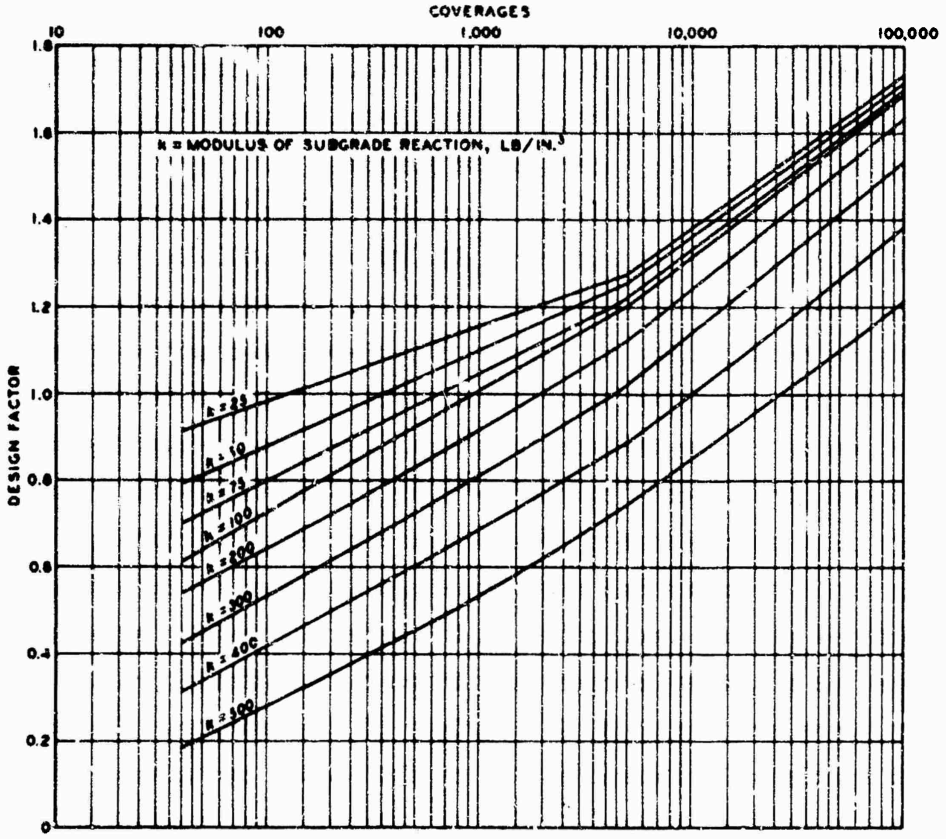

Figure 13. Design Factor Versus Coverages for Shattered-Slab Failure Condition. Pass per Coverage Ratios for 12-Wheel and Twin-Tandem Assemblies = 1.34 and 3.30, Respectively

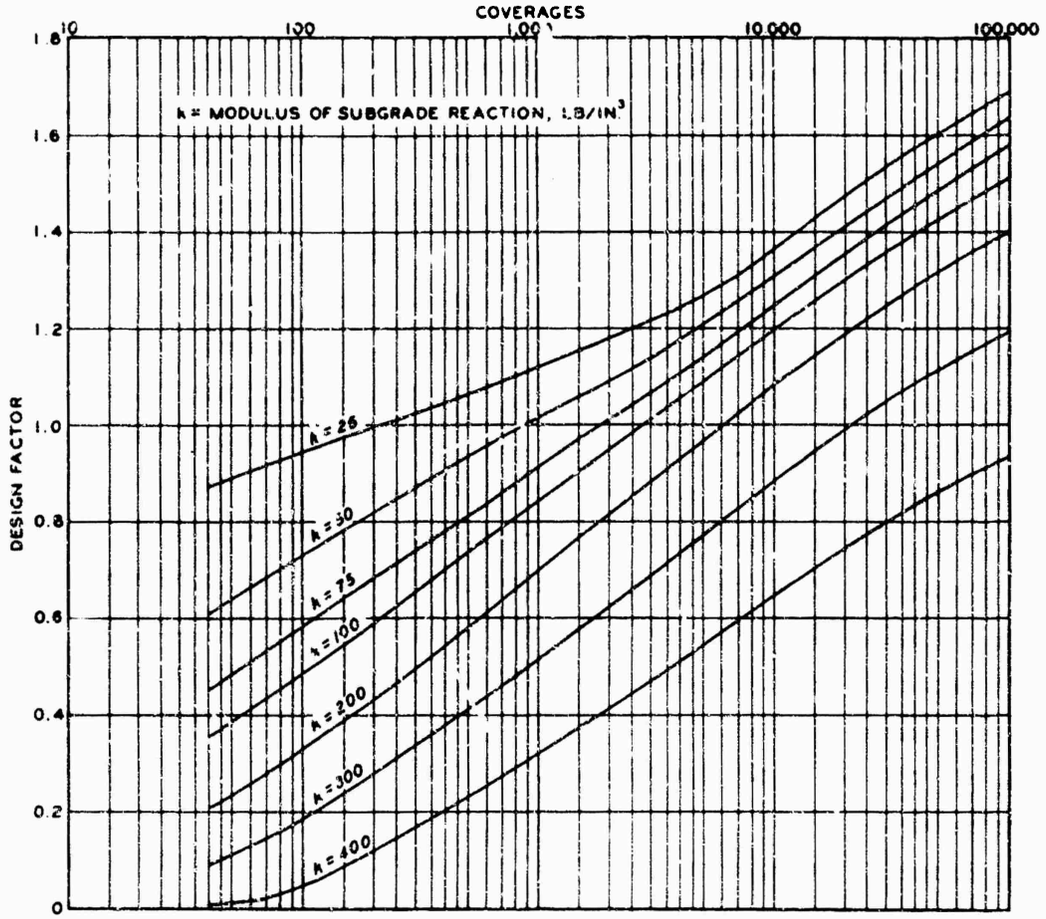

Figure 14. Design Factor Versus Coverages for Complete Failure Condition. Pass per Coverage Ratios for 12-Wheel and Twin-Tandem Assemblies = 1.34 and 3.30, Respectively

determination of a pass per coverage (p/c) ratio that is constant for any one aircraft. The development of the p/c ratio is illustrated in Section IV 1c(2) of this report. In this section, the development of the p/c ratio is specifically for flexible pavements wherein a coverage is defined as sufficient contiguous wheel passes that every point in a traffic lane has been touched one time by a moving wheel. The p/c ratio is the same for both types of pavements for single wheels, for multiple wheels where the wheels are arranged abreast, and for multiple wheels where the wheels are arranged in tandem when the tandem spacing is sufficiently large to result in separate maximum stresses in the concrete under each tandem wheel. However, when the tandem spacing is small, only one maximum stress occurs in rigid pavements for each pass of the gear, while in flexible pavement, the pavement is subjected to two moving wheel passes. For these situations, the p/c ratio for rigid pavements is two times the p/c ratio for flexible pavements. Figures 15 and 16 show strain profiles in the concrete as the 12-wheel and twin-tandem-wheel gears pass over an instrumented point in the pavement. For the 12-wheel gear, it can be seen that there are four excursions; however, only two are maximum. Thus for rigid pavements, a pass of the 12-wheel gear produces two maximum stresses, while for flexible pavements, a point on the pavement is subjected to four wheel passes. For the twin-tandem gear, it can be seen that there are two strain excursions of almost equal magnitude with very little relaxation between the wheels. Thus for one pass of this gear, there is only one maximum stress repetition in rigid pavements, while in flexible pavements, there are two wheel passes. Therefore, for both the 12-wheel and twin-tandem-wheel gears used, the p/c ratio for rigid pavements is twice the p/c ratio for flexible pavements.

Figure 12 represents the DF-versus-traffic volume relation used for CE plain concrete pavement design criteria. The initial failure condition represented is the point at which the crack, which originates at the bottom of the slab and migrates upward to the surface, commences to spall and ravel, which produces debris on the surface. This failure is more a functional failure than a structural failure since the pavement slab will continue to support the loaded aircraft after the initial failure condition has been reached. Test data result in a family of curves depending upon the modulus of subgrade reaction; however, the range of the DF's for subgrade moduli from 25 to 200 lb/in.^{3} is small and for practical purposes is represented by a single curve.

Figure 13 represents the DF-versus-traffic volume relation for a

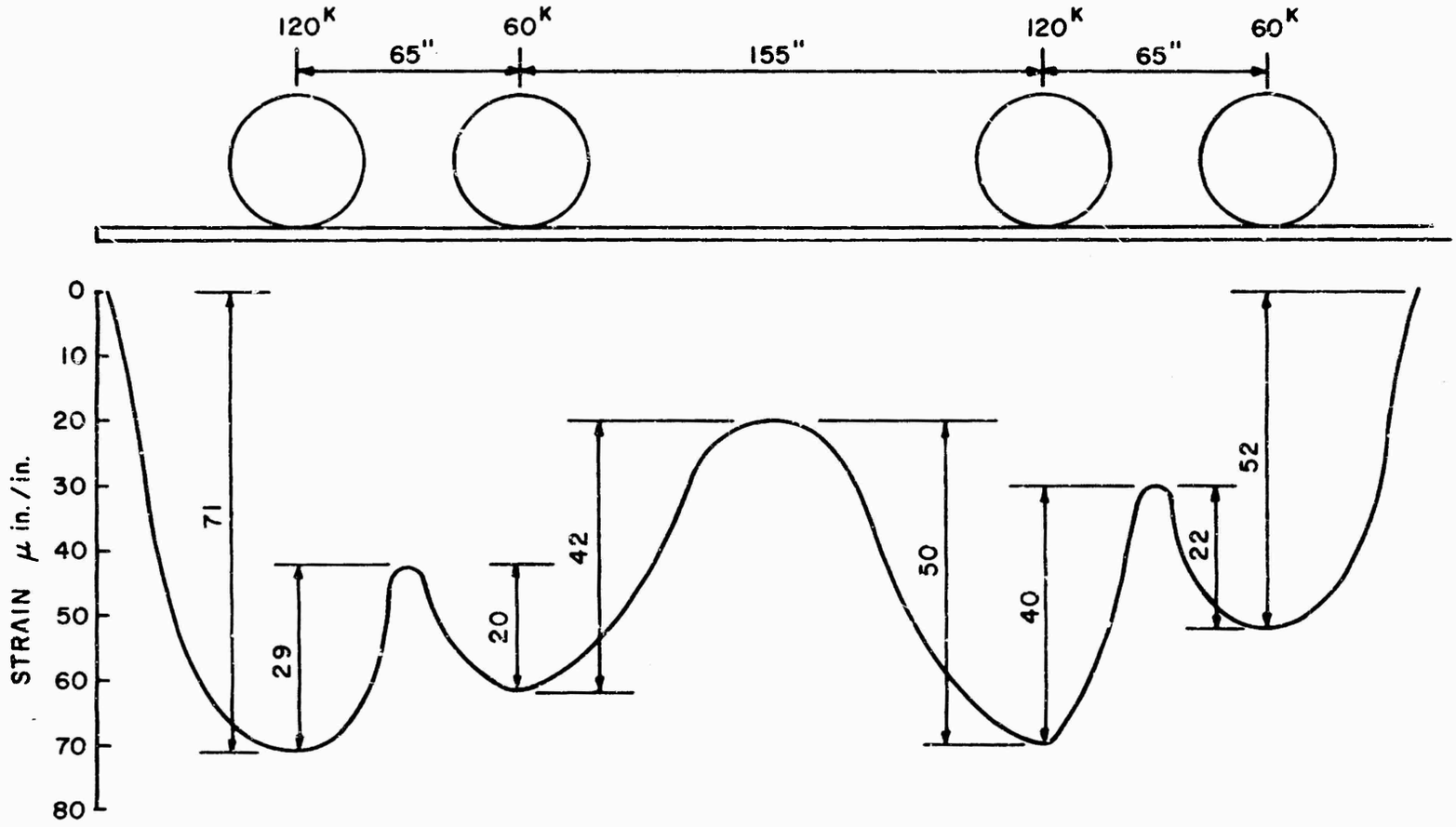

Figure 15. Typical Strain Trace Under 12-Wheel Traffic Showing Strain Profile for One Pass (Gage 2 SCL, Test Item 2, Surface Strain Gage, Longitudinal Direction, Gear on Traffic Line 2, Outside Wheel of Gear Is Passing Gage at a Distance of 16 in., Concrete Thickness = 12.1 in., Subgrade Modulus = 78 lb/in.^{3}, and Concrete Flexural Strength = 800 psi)

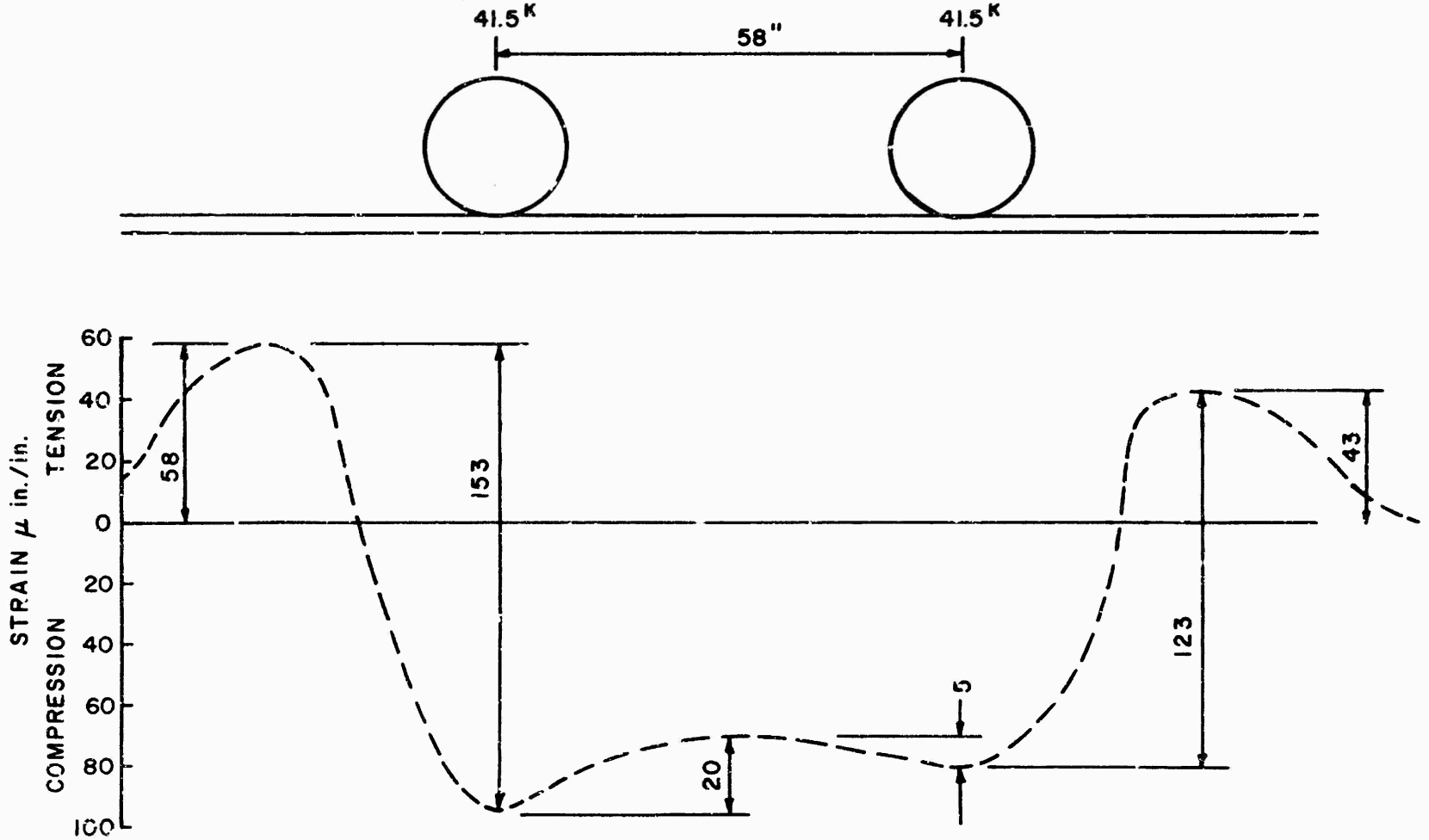

Figure 16. Typical Strain Profile Under Twin-Tandem Assembly (Gage 2 NSCL, Test Item 2, Surface Strain Gage, Longitudinal Direction, Gear on Traffic Line 3, Concrete Thickness = 11.3 in., Subgrade Modulus = 111 lb/in.^{3}, and Concrete Flexural Strength = 700 psi)

failure condition designated as shattered slab (sometimes referred to as three or four cracks per slab). This relation is used primarily for rigid pavement evaluation for operational conditions where greater structural deterioration can be tolerated to accommodate overloading.

Figure 14 represents the DF-versus-traffic volume relation for a failure condition designated as complete. The curves represent a condition wherein the concrete has been cracked into pieces of about 20 to 25 sq ft in area. Test data show that shortly after this condition has been achieved, shear failures and excessive deformations begin to occur and danger of a punching shear-type failure is imminent. This relationship forms the basis for the CE nonrigid overlay design criteria. That is, when a nonrigid overlay is used, the base pavement is allowed to crack during traffic to about the condition represented by this figure.

b. Nonrigid Overlay

Current CE nonrigid overlay thickness requirements for strengthening existing rigid pavements are completely empirical, having been developed from full-scale accelerated traffic tests. Several test tracks have been constructed and traffic tested to failure wherein the load, gear configuration, thickness of existing rigid pavement, and thickness and types of nonrigid overlay pavement have been varied. From these tests, it has been found that when the nonrigid overlay materials are of high quality and are well constructed traffic can be safely applied until the rigid base pavement has broken into pieces of about 20 to 25 sq ft in area. Some reflection cracking in the nonrigid overlay induced by the movement at joints and cracks in the base pavement may be experienced which creates minor maintenance requirements; however, the system is structurally safe and will provide a relatively smooth operating surface until the base pavement has deteriorated to the above-described condition. Continued traffic beyond this point will result in further cracking and deterioration of the base pavement and eventually excessive deflections, faulting, and even punching shear-type failure. From traffic test results, it was determined that the required thickness of nonrigid overlay could be related to the deficiency in plain concrete thickness that would be required to carry the load and volume of traffic. The required thickness of nonrigid overlay can be expressed as 2.5 times the difference between the existing rigid pavement thickness and the thickness of plain concrete pavement that would be required for the loading and traffic volume based upon the complete

failure concept. This relation is expressed as follows:

$$t = 2.5(Fh_d - Ch_b) \tag{22}$$

where

t = required thickness of nonrigid overlay, in.

F = factor expressing the percentage reduction in required plain concrete thickness from the initial to the complete failure condition. This factor is dependent upon both subgrade modulus and volume of traffic.

h_d = required thickness of plain concrete for initial failure condition.

C = factor dependent upon the structural condition of the existing rigid pavement prior to overlay. $C = 1.0$ when the existing slabs have only initial cracking and 0.75 when existing slabs have two or more cracks.

SECTION IV

ANALYSIS OF MWHGL DATA

1. FLEXIBLE PAVEMENT

a. Comparison with Existing Criteria

The analysis of the MWHGL test section data was based on the as-constructed values shown in table 1, the traffic test data shown in table 2, and the vertical deflection measurements obtained from instrumentation in items 3 and 4. Tables 1 and 2 are from Volume II.

A plan layout is shown in figure 17. The test section was designed based on medium-load pavement design, consisting of a design loading of 100 kips, twin wheels spaced 37 in. center-to-center, and a contact area of 267 sq in. Items 1, 2, 3, 4, and 5 were designed for 8, 40, 200, 200, and 1000 coverages, respectively, based on a subgrade of 4 CBR. The reason for this design stemmed from the requirement to determine if a medium-load pavement was adequate for operation of C-5A aircraft. The existing design equation,

$$t \rightarrow (0.23 \log C + 0.15)\sqrt{\frac{ESWL}{8.1\ CBR} - \frac{A}{\pi}} \qquad (23)$$

was used to predict (see equation 20) thickness requirements for the above coverage levels. The equivalent single-wheel load (ESWL) for the 12-wheel gear was determined using the single-layer elastic theory with a 20-radii cut-off modification incorporated (see figure 18). This modification adjusts the deflection based on a subtraction of the prescribed constant deflection factor at the desired offset, 20 radii. The ESWL's for other wheel gear configurations were computed using the single-layer elastic theory with no cutoff modification (i.e., 20-radii cutoff for C-5A and single-layer no cutoff for Boeing 747). These two methods of determining ESWL represented design procedure at the time that the test section was designed.

The as-constructed subgrade CBR varied. The as-constructed thicknesses were the same as design thicknesses except in item 5. Therefore, the design was adjusted, based on the as-constructed values (table 1). Using the design equation and as-constructed values of CBR and thickness, the design coverages became 9, 79, 206, 248, and 810 for items 1, 2, 3, 4, and 5, respectively. A comparison of existing criteria with the performance of the MWHGL test section is shown in table 3.

Table 1

As-Constructed Thickness, CBR, Water Content, and Density Data for Flexible Pavement Test Section

Test Item	Material	Station	Elev ft	Layer Thickness* ft	Layer Thickness* in.	Total Thickness in.** Design	Total Thickness in.** Actual	CBR	Water Content %	Dry Density, pcf In Place (A)	Dry Density, pcf CE 55† (B)	Percent CE 55 Density (A/B)
West maneuver area	Cr stone base	3+90	194.05	0.90	10.8	12	13	34	1.4	135.2	140	97
	Subgrade							11	19.0	105.8	106	100
1	Cr stone	3+30	193.97	0.30	3.6	15	15	51	1.9	136.6	140	98
	Subbase		193.37	0.89	10.7			13	5.0	124.1	126	98
	Subgrade (CH)		192.48					3.0	33.2	86.0	85	101
	(CH)		191.64					3.7	31.8	86.0	88	98
	(CH)		190.79					3.4	32.5	84.3	87	96
	(CL)		189.82					2.2	23.8	97.0	97	100
	(CL)		188.88					4.0	23.5	98.9	97	102
2	Cr stone	2+70	193.42	0.60	7.2	24	24	81	1.8	141.3	140	101
	Subbase		192.82	1.26	15.1			12	5.0	129.4	126	103
	Subgrade (CH)		191.56					4.5	30.9	88.6	89	100
	(CH)		190.44					3.6	33.4	82.9	85	98
	(CH)		189.70					3.4	33.9	87.6	84	103
	(CL)		188.45					3.6	24.8	97.3	95	102
	(CL)		187.56					3.8	21.4	92.0	101	92
3	Cr stone	2+10	193.15	0.69	8.1	33	33	61	2.0	142.2	140	102
	Subbase		192.46	2.0	24.0			13	3.4	121.6	126	96
	Subgrade (CH)		190.46					3.4	30.9	87.6	89	99
	(CH)		189.55					2.4	32.5	85.4	86	99
	(CH)		188.54					3.3	34.8	84.0	83	101
	(CL)		187.74					4.5	20.9	102.8	102	101
	(CL)		186.59					3.7	20.6	101.9	102	100
	(CL)		185.61					3.9	23.0	99.7	98	101
	(CL)		184.81					1.8	22.1	99.0	100	99
	(CL)		184.00					1.1	23.2	98.6	98	101
	(CL)		182.69					1.9	21.7	98.1	99	99
	(CL)		181.78					2.2	22.2	96.7	99	98
4	Cr stone	1+50	192.84	0.65	7.8	33	33	72	1.4	142.0	140	101
	Subbase		192.19	1.93	23.2			15	3.0	130.4	126	103
	Subgrade (CH)											
	4-CBR design		190.26					3.5	30.2	89.3	89	100
			189.43					3.1	33.4	84.4	85	99
			188.65					3.3	33.0	84.2	85	99
	2-CBR design		187.69			54	53	2.7	36.7	79.9	80	100
			186.75					3.0	33.2	83.2	85	98
	(CL)		185.68					[illegible]	24.0	97.3	96	101
	(CL)		184.71					1.4	22.4	98.4	99	99
5	Cr stone	0+90	192.50	0.64	7.7	42	41	6[illegible]	1.0	140.6	140	100
	Subbase		191.86	2.64	31.7			15	2.7	131.9	126	104
	Subgrade (CH)		189.22					4.0	31.8	87.5	88	100
	(CH)		188.13					2.7	34.1	83.5	84	100
	(CH)		187.29					3.1	31.5	84.1	88	96
	(CL)		186.19					2.7	23.5	98.1	98	100
	(CL)		185.23					2.0	[illegible].6	98.6	99	100
East maneuver area	Cr stone	0+30	192.80	0.63	7.5	33	32	41	1.[illegible]	138.9	140	99
	Subbase		191.57	1.91	23.0			16	2.9	126.5	126	100
	Subgrade (CL)		189.66					8	20.5	103.4	103	100

* Layer thicknesses measured at test pit locations.

** Total actual thicknesses derived from cross sections taken during construction at the top of each pavement element.

† Laboratory densities shown in this column are the CE 55 maximum densities at optimum water content for the crushed-stone base and the gravelly sand subbase material and the CE 55 density corresponding to the field in-place water contents for the subgrade material.

Table 2

Summary of After-Traffic Water Content, Density, and CBR Data for Flexible Pavement Test Section

Lane	Assembly	Test Item	Pit No.	Sta	Location	Material	Elev ft	Layer Thickness ft	Layer Thickness in.	Total Thickness in. Design	Total Thickness in. Actual	Traffic Cov	CBR	Water Content %	Dry Density pcf In Place (A)	Dry Density pcf CE 55 (B)	Percent CE 55 Density (A/B)
1	360 kip 12 wheel	1	1	3+45	Inside traffic lane	Asphaltic conc	193.83	0.28	3.36	15	15.36	8	-	-	-	-	-
						Cr stone base	193.55	0.42	5.04				8	1.9	137.1	140	98*
						Subbase	193.13	0.58	6.96				4.3	3.8	134.5	126	107*
						Subgrade (CH)	192.55						2.7	32.7	88.5	87	102**
						(CH)	191.50						4.2	31.1	86.2	89	97
						(CH)	190.50						3.8	32.7	84.3	87	97
						(CL)	189.50						3.6	20.5	102.2	103	99
					Outside traffic lane	Asphaltic conc	193.76	0.28	3.36	15	15.48		-	-	-	-	-
						Cr stone base	193.48	0.56	6.72				36	2.0	136.9	140	98*
						Subbase	192.92	0.45	5.40				21	6.5	133.8	126	106*
						Subgrade (CH)	192.47						3.4	30.3	88.5	90	98**
						(CH)	191.50						5	31.1	86.5	89	97
						(CH)	190.50						4.8	30.8	86.4	90	97
		1	2	3+05	Inside traffic lane	Asphaltic conc	193.68	0.39	4.68	15	14.10	12	-	-	-	-	-
						Cr stone base	193.29	0.44	4.26				11	1.4	132.5	140	95*
						Subbase	192.94	0.43	5.16				4.2	3.6	128.0	126	102*
						Subgrade (CH)	192.51						2.8	30.9	87.4	90	97*
					Outside traffic lane	Asphaltic conc	193.62	0.25	3.00	15	14.40		-	-	-	-	-
						Cr stone base	193.37	0.59	6.24				58	0.9	141.1	140	101*
						Subbase	192.85	0.43	5.16				7	3.2	126.5	126	100*
						Subgrade (CH)	192.42						3.1	32.2	85.6	87	98**
		2	3	2+70	Inside traffic lane	Asphaltic conc	193.39	0.35	4.20	24	23.64	200	-	-	-	-	-
						Cr stone base	193.04	0.49	5.88				79	1.0	140.3	140	100*
						Subbase	192.55	1.13	13.56				15	3.8	130.7	126	104*
						Subgrade (CH)	191.42						4	31.3	87.5	89	98*
						(CH)	190.48						6	30.8	87.7	90	97
						(CH)	189.48						6	31.7	85.7	89	96
						(CL)	188.28						4.5	20.8	101.6	102	100
					Outside traffic lane	Asphaltic conc	193.43	0.30	3.60	24	24.72		-	-	-	-	-
						Cr stone base	193.13	0.50	6.00				67	1.1	141.0	140	101*
						Subbase	192.63	1.26	15.12				20	3.0	128.1	126	102*
						Subgrade (CH)	191.37						5	30.6	88.5	90	98**
						(CH)	190.35						7	30.8	86.9	90	97
						(CH)	189.35						4.0	34.1	82.4	84	98
		3	4	2+30	Inside traffic lane	Asphaltic conc	193.16	0.33	3.96	33	31.32	2342	-	-	-	-	-
						Cr stone base	192.83	0.42	5.04				103	0.6	139.8	140	100*
						Subbase	192.41	1.86	22.32				23	2.5	129.2	126	103*
						Subgrade (CH)	190.55						4.3	32.4	86.7	87	100**
						(CH)	189.56						5	32.6	84.8	87	98
						(CH)	188.56						3.6	32.4	83.0	87	95
						(CL)	187.85						3.5	22.1	98.4	100	98

Table 2 (cont'd)

			Outside traffic lane	Asphaltic conc	193.32	0.32	3.84	33	34.44		-	-	-	-	-
				Cr stone base	193.00	0.56	6.72				92	1.1	141.7	140	101*
				Subbase	192.44	1.99	23.88				32	1.9	129.4	126	103*
				Subgrade (CH)	190.45						3.9	32.1	85.8	88	97**
				(CH)	189.35						6	31.7	85.7	85	96
				(CH)	188.35						3.8	33.4	83.0	85	98
				(CL)	187.45						3.7	22.1	101.4	100	101
	5	1+90	Inside traffic lane	Asphaltic conc	192.98	0.37	4.44	33	33.36	2342	-	-	-	-	-
				Cr stone base	192.61	0.37	4.44				86	1.1	143.9	140	103*
				Subbase	192.24	2.04	24.48				27	2.3	137.6	126	109*
				Subgrade (CH)	190.20						4.9	31.5	86.0	89	97**
				(CH)	189.20						5	31.9	85.0	88	97
				(CH)	188.20						2.5	36.4	79.7	80	100
				(CL)	187.38						6	21.7	100.2	101	99
				(CL)	186.38						5	19.6	101.6	105	97
4	6	1+36	Inside traffic lane	Asphaltic conc	192.72	0.37	4.44	33	32.40	2351	-	-	-	-	-
				Cr stone base	192.35	0.32	3.84				60	0.9	143.0	140	102*
				Subbase	192.03	2.01	24.12				38	3.4	130.1	126	103*
				Subgrade (CH)	190.02						4.5	31.4	87.0	89	98**
				(CH)	189.04						2.7	33.9	84.8	85	100
				(CH)	187.54						2.2	34.7	83.1	84	99
				(CH)	186.54						4.2	33.9	82.5	85	97
				(CH)	185.54						2.5	33.7	82.3	85	97
				(CL)	185.45						3.0	22.3	99.0	100	99
				(CL)	184.52						3.3	22.3	100.3	100	100
				(CL)	183.52							21.8			
				(CL)	182.52							21.0			
				(CL)	181.52							20.1			
				(CL)	180.72							20.9			
			Outside traffic lane	Asphaltic conc	192.76	0.35	4.20	33	33.36		-	-	-	-	-
				Cr stone base	192.41	0.49	5.88				65	1.7	146.0	140	104*
				Subbase	191.92	1.94	23.28				31	3.0	130.8	126	104*
				Subgrade (CH)	189.98						4.7	31.3	86.2	89	97**
				(CH)	188.97						3.7	32.3	85.5	87	98
				(CH)	187.47						2.5	35.9	81.2	81	100
				(CH)	186.47						2.0	33.3	83.9	86	98
5	7	0+90	Inside traffic lane	Asphaltic conc	192.37	0.29	3.48	42	41.04	3850	-	-	-	-	-
				Cr stone base	192.08	0.37	4.44				104	1.6	151.0	140	108*
				Subbase	191.71	2.76	33.12				33	2.8	138.6	126	110**
				Subgrade (CH)	188.95						2.0	34.3	85.4	84	102
				(CH)	188.45						3.6	33.5	84.9	85	100
				(CH)	187.95						3.0	37.6	79.3	79	100
			Outside traffic lane	Asphaltic conc	192.45	0.29	3.48	42	41.76		-	-	-	-	-
				Cr stone base	192.16	0.50	6.00				107	1.6	145.6	140	104*
				Subbase	191.66	2.69	32.28				19	3.7	139.7	126	111**
				Subgrade (CH)	188.97						1.5	32.0	86.2	88	98
				(CH)	188.47						3.8	32.0	87.5	88	99
				(CH)	187.97						3.1	32.5	85.1	87	98

Table 2 (cont'd)

3A	30 kip Single wheel	1	8	3+45	Inside traffic lane	Asphaltic conc	194.06	0.35	4.20	15	19.20	120	-	-	-	-	-
						Cr stone base	193.71	0.55	6.60				59	1.0	144.4	140	103*
						Subbase	193.16	0.70	8.40				-	-	-	-	-
						Subgrade (CH)	192.46						3.8	33.4	85.4	86	99**
						(CH)	191.46						3.5	31.6	85.8	89	96
						(CH)	190.46						2.7	34.7	81.7	84	97
2	50 kip Single wheel	2	9	2+90	Inside traffic lane	Asphaltic conc	193.63	0.36	4.32	24	23.52	200	-	-	-	-	-
						Cr stone base	193.27	0.45	5.40				69	2.9	133.0	140	95*
						Subbase	192.82	1.15	13.80				-	-	-	-	-
						Subgrade (CH)	191.67						4.1	33.2	86.0	86	100**
						(CH)	190.67						4.9	31.4	85.8	89	96
2		2	10	2+48	Inside traffic lane	Asphaltic conc	193.20	0.34	4.08	24	24.60	200	-	-	-	-	-
						Cr stone base	192.86	0.32	3.84				60	1.8	140.5	140	100*
						Subbase	192.54	1.39	16.68				-	-	-	-	-
						Subgrade (CH)	191.15						3.5	31.5	87.3	89	98**
						(CH)	190.15						4.3	32.2	85.0	87	98
2A	50 kip Single wheel	2	11	2+50	Inside traffic lane	Asphaltic conc	193.15	0.34	4.08	24	22.20	200	-	-	-	-	-
						Cr stone base	192.81	0.37	4.44				67	1.9	138.1	140	99*
						Subbase	192.44	1.14	13.68				17	-	-	-	-
						Subgrade (CH)	191.30						2.5	30.8	91.8	90	102**
						(CH)	190.30						6	31.6	86.5	89	97
3B	240 kip Twin tandem	3	12	2+10	Inside traffic lane	Asphaltic conc	193.12	0.33	3.96	33	33.00	40	-	-	-	-	-
						Cr stone base	192.79	0.39	4.68				55	1.2	143.2	140	102*
						Subbase	192.40	2.03	24.36				-	-	-	-	-
						Subgrade (CH)	190.37						5.4	30.8	88.0	90	98**
						(CH)	189.37						2.6	34.5	82.8	84	99
					Outside traffic lane	Asphaltic conc.	193.33	0.30	3.60	33	34.20		-	-	-	-	-
						Cr stone base	193.03	0.44	5.28				-	-	-	-	-
						Subbase	192.59	2.11	25.32				-	-	-	-	-
						Subgrade (CH)	190.48						4.2	30.1	88.6	91	97**
						(CH)	189.48						3.4	33.2	84.2	86	98
		4	13	1+50	Inside traffic lane	Asphaltic conc	192.86	0.31	3.72	33	32.16	40	-	-	-	-	-
						Cr stone base	192.55	0.54	6.48				76	1.4	137.7	140	98*
						Subbase	192.01	1.83	21.96				-	-	-	-	-
						Subgrade (CH)	190.18						4.5	31.3	88.2	89	99**
						(CH)	189.18						5.7	33.2	84.8	86	99
					Outside traffic lane	Asphaltic conc	193.08	0.39	4.68	33	32.86		-	-	-	-	-
						Cr stone base	192.69	0.44	5.28				-	-	-	-	-
						Subbase	192.25	1.91	22.92				-	-	-	-	-
						Subgrade (CH)	190.34						6	31.7	86.3	88	98**
						(CH)	189.34						3.2	35.6	83.0	85	100

Table 2 (cont'd)

	5	14	1+05	Inside traffic lane	Asphaltic conc	192.51	0.26	3.12	42	40.21	280	-	-	-	-	-
					Cr stone base	192.25	0.51	6.13				55	1.5	139.5	140	100*
					Subbase	191.74	2.58	30.96				-	-	-	-	-
					Subgrade (CH)	189.16						4.4	33.4	86.5	86	101**
					(CH)	188.16						5.3	30.0	86.4	90	96
				Outside traffic lane	Asphaltic conc	192.85	0.35	4.20	42	42.60		-	-	-	-	-
					Cr stone base	192.50	0.41	4.92				-	-	-	-	-
					Subbase	192.09	2.79	33.48				-	-	-	-	-
					Subgrade (CH)	189.30						4.8	33.5	85.3	86	99**
					(CH)	188.30						4.5	30.7	89.0	90	99
		15	0+75	Inside traffic lane	Asphaltic conc	192.43	0.33	3.95	42	40.88	280	-	-	-	-	-
					Cr stone base	192.10	0.48	5.80				-	-	-	-	-
					Subbase	191.62	2.59	31.13				-	-	-	-	-
					Subgrade (CH)	189.03						4.9	32.0	89.2	88	99**
					(CH)	188.03						3.9	32.7	85.9	87	99
	East maneuver area	16	0+40	Inside traffic lane	Asphaltic conc	192.34	0.31	3.70	33	33.63	120	-	-	-	-	-
					Cr stone base	192.03	0.48	5.73				41	1.3	140.1	140	100*
					Subbase	191.55	2.02	24.20				-	-	-	-	-
					Subgrade (CL)	189.53						8	21.1	103.8	102	102**
					(CL)	188.53						6	22.0	100.7	100	101

* Based on CE 55 maximum density at optimum water content.
** Based on CE 55 maximum density at field in-place water content.

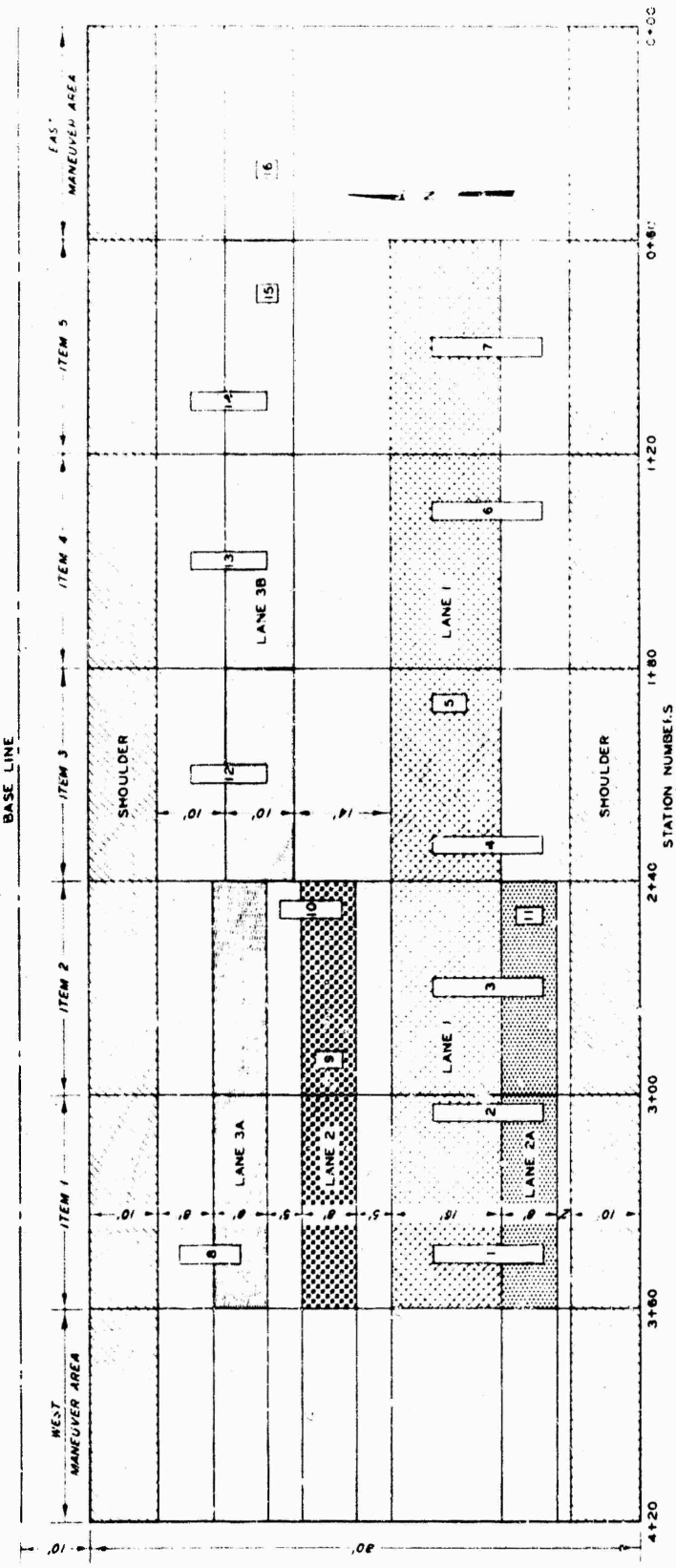

Figure 17. Layout of Flexible Pavement Test Lanes (See table 2 for Identification of Lanes)

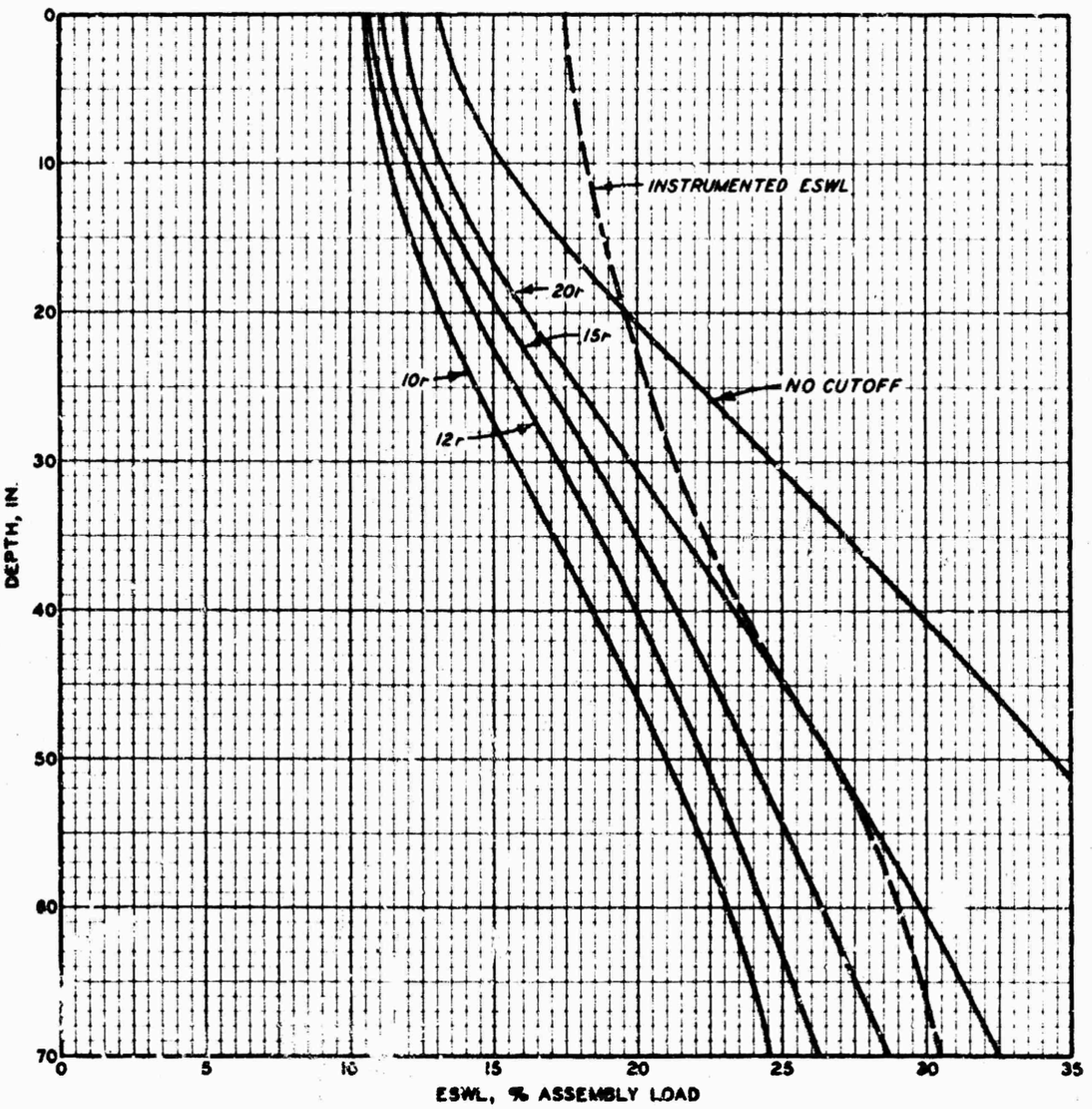

Figure 18. Comparison of Measured and Computed Equivalent Single-Wheel Loads Versus Depth for 12-Wheel Assembly (Data from Volume III, Item 3, Static Load)

Table 3

Comparison of Existing Criteria with Performance of Multiple-Wheel Heavy Gear Load Test Section

Identification	CBR	ESWL* lb	Thickness t, in.		Failure Coverages	
			Actual	Indicated**	Actual	Predicted
Lane 1, item 1	3.7	52,200	15	14.5	8	9
item 2	4.4	63,000	24	25.1	104	79
item 3	3.8	74,900	33	42.6	1500	206
item 4	4.0	74,900	33	41.5	1500	248
item 5	4.0	84,250	41	48.8	3850†	810
Lane 2, item 1	3.7	50,000	15	13.1	6	10
item 2	4.4	50,000	24	24.6	200	170
Lane 3A, item 1	3.7	30,000	15	19.0	120	33
item 2	4.4	30,000	24	20.8	450†	1438
Lane 3B, item 3	3.8	124,800	33	32.6	40	43
item 4	4.0	124,800	33	31.8	40	49
item 5	4.0	144,000	41	47.0	280	113

* Lane 1 ESWL computations made using elastic theory with 20-radii cutoff modification. All other lanes ESWL computed using elastic theory with no modification.

** Thickness indicated by number of coverages at failure.

† Nonfailure.

After testing, the failure coverages were used in the design equation to determine the thicknesses. These values are shown in column 5 of table 3 (Indicated Thickness). A comparison of indicated and actual thicknesses reflects the close agreement between predictions based on the present criteria and the actual behavior of the thinner items at low coverage levels. The agreement is not as good for lane 1, item 5, for which present criteria indicate that 810 coverages (t = 41.0) should have failed the item, but the item actually withstood 3850 coverages (t = 41 in.) without developing a failure. Also in lane 3B, item 5, present criteria indicate a required thickness of 47.0 in. for 280 coverages, but actually 41 in. sufficed. A plot of thickness versus failure coverages for the 12-wheel loading shown in figure 19 shows this divergence at higher coverage levels. Curve A represents actual performance data, and curve B represents design thickness requirements determined by the existing criteria.

b. Equivalent Single-Wheel Load

The computation of ESWL for use in predicting the behavior of the test items with traffic was investigated next. Using the relation

$$t \rightarrow (0.23 \log C + 0.15)\sqrt{\frac{ESWL}{8.1\ CBR} - \frac{A}{\pi}} \tag{23}$$

the ESWL was computed by rearranging the behavior pattern to the following form:

$$ESWL \rightarrow 8.1\ CBR\left(\frac{A}{\pi} + \frac{t^2}{(0.23 \log C + 0.15)^2}\right) \tag{24}$$

The ESWL was then calculated using field data and the present flexible pavement design method. The results of this computation for five coverage levels are shown in table 4. These computations show a decrease in the 12-wheel ESWL beginning at shallow depths as shown in the plot of t versus ESWL for 5000 coverages in figure 20. This curve also shows a discontinuity at shallow depths. The indicated decrease in ESWL with depth is impossible by definition. The ratio of the deflection under a multiple-wheel assembly to the deflection under any single-wheel assembly must approach unity with depth as the deflections under each assembly approach the same value; therefore, the present flexible pavement design equation does not accurately predict ESWL for use in this analysis.

Deflections determined through use of the elastic theory yield values

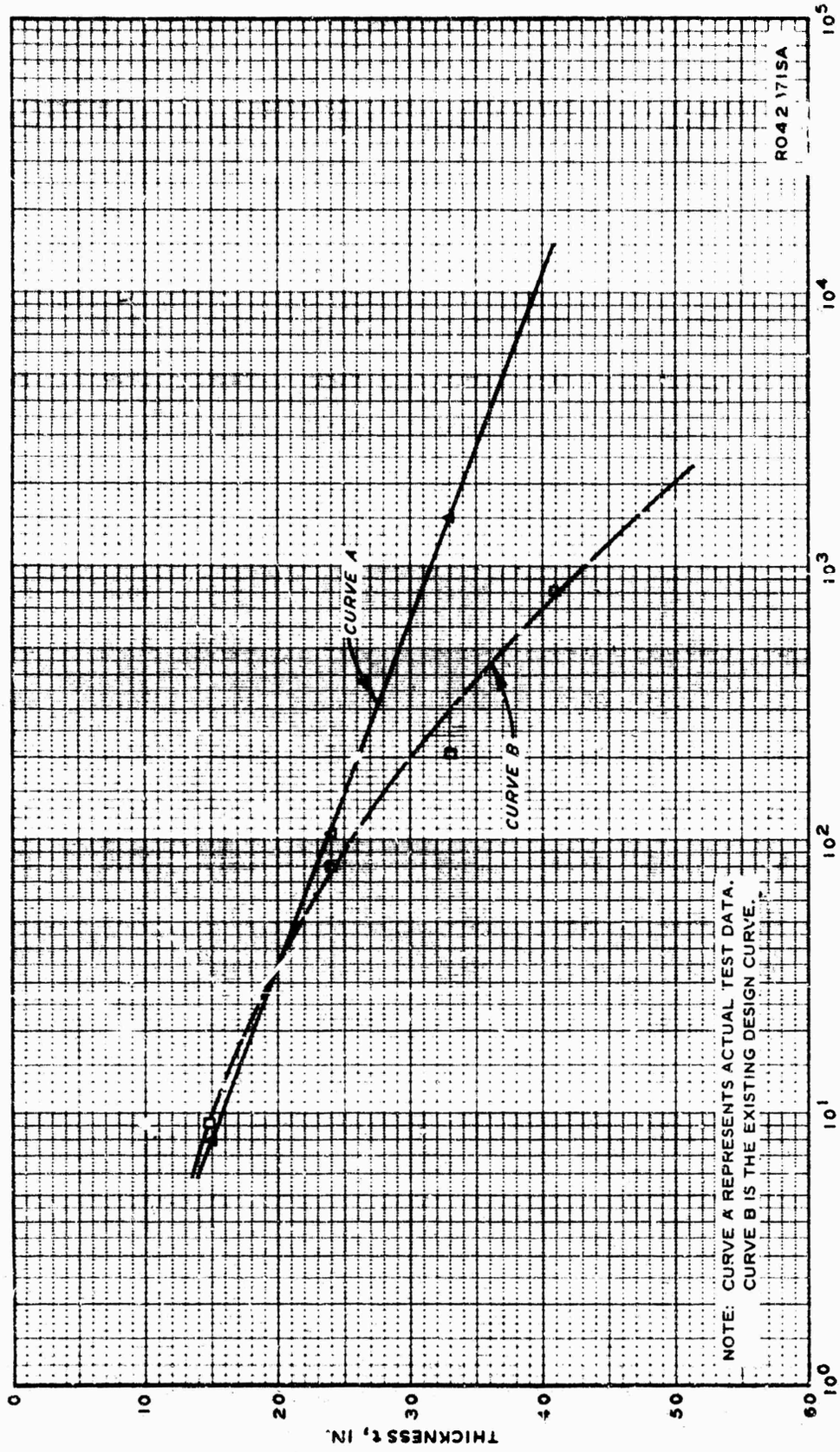

Figure 19. Comparison of Actual Data (Curve A) with Existing Design Curve (Curve B) for Thickness-Failure Coverage Relationship, 12-Wheel Gear

Table 4

Computed ESWL's and Depths

25,000 Coverages		5000 Coverages		1000 Coverages		200 Coverages		40 Coverages	
t in.	ESWL %	t in.	ESWL %	t in.	ESWL %	t in.	ESWL %	t in.	ESWL %
5.8	35.8	5	47.3	5.04	49.5	4.76	51.0	5.2	43.5
7.0	28.2	6	34.1	5.88	35.8	5.44	40.0	6.24	32.2
8.1	24.5	7	28.2	6.72	29.5	6.12	33.0	7.80	25.5
9.3	21.8	8	24.8	7.56	26.0	6.80	29.2	10.4	20.0
10.5	19.8	9	22.2	8.4	23.5	8.16	24.5	13.0	17.6
11.6	18.7	10	20.65	10.08	20.5	10.2	20.2	15.6	16.5
13.9	17.2	12	18.45	12.6	17.8	13.6	17.3	18.2	15.5
17.4	15.8	15	16.75	16.8	16.0	17.0	15.9	20.8	15.0
23.2	14.6	20	15.18	21.0	15.0	20.4	15.1	23.4	14.6
29.0	14.0	25	14.38	25.2	14.4	23.8	14.5	26.0	14.3
34.8	13.4	30	13.88	29.4	14.0	27.2	14.0	28.6	14.0
40.6	13.1	35	13.5	33.6	13.55	30.6	13.8	31.2	13.7
46.4	12.7	40	13.25	37.8	13.3	34.0	13.5	33.8	13.5
		45	12.9	42.0	13.0	37.4	13.3	36.4	13.4
		50	12.5	46.2	12.8	40.8	13.2		
		55	12.25			44.2	12.9		
		60	11.80			47.6	12.7		
		65	11.50						
		70	11.20						

Note: The present flexible pavement equation was used in computations of t and ESWL.

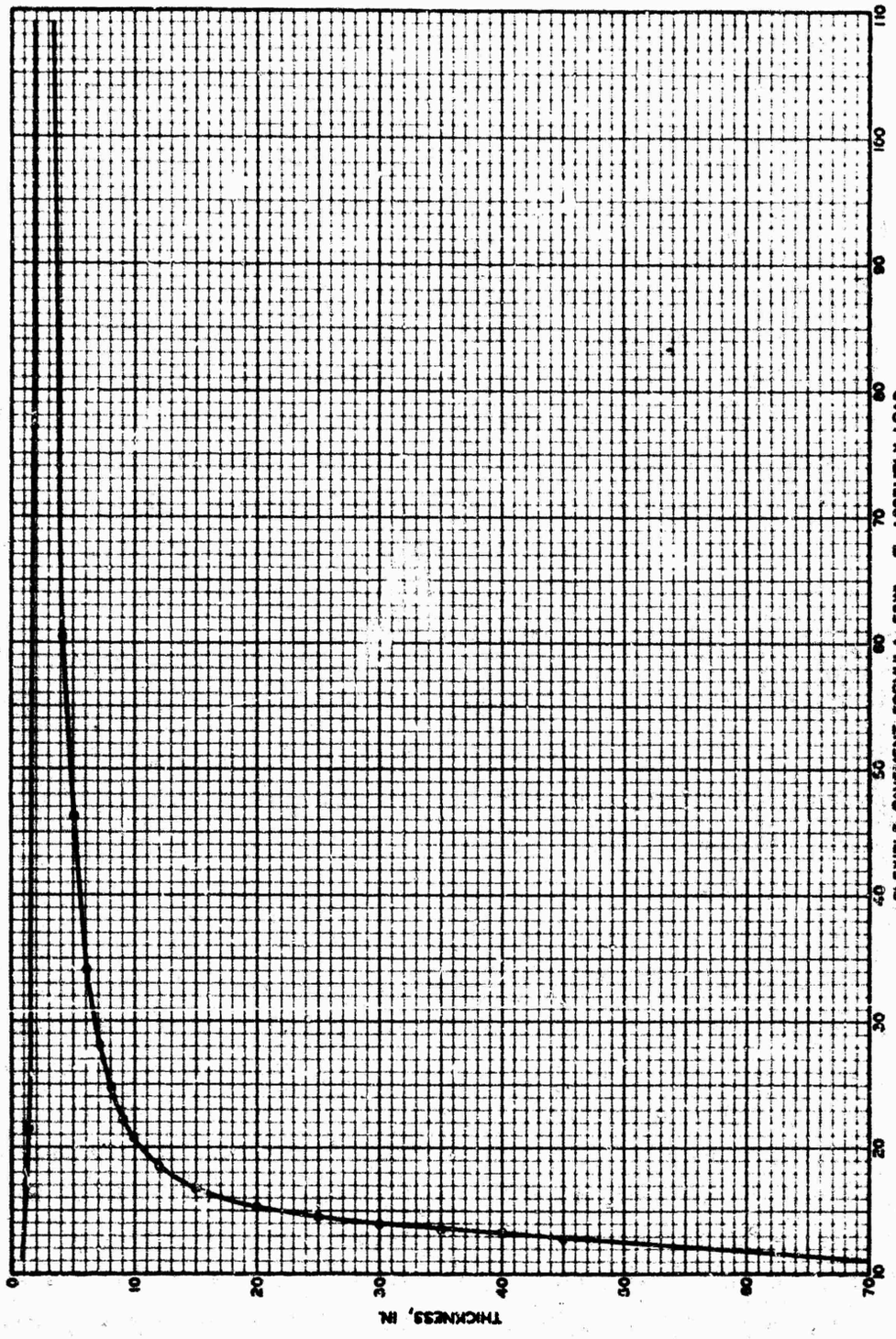

Figure 20. Thickness Versus Equivalent Single-Wheel Load

in an elastic, isotropic, homogeneous half-space under a uniformly distributed circular load, and the computations will always indicate some deflection at any distance from the loaded area. In reality, the deflection basin attenuates to insignificantly small values. In an effort to duplicate the theoretical ESWL that most closely represents the behavioral pattern based on the results of actual performance, different offset distances in radii of negligible effect were assumed, and ESWL's were computed. These ESWL's were computed using modified deflection curves in which the theoretical deflections for the 12-wheel assembly attenuated to zero at the respective radii distances. Figure 18 shows the result of these computations. Past experience has shown the need for this nonaccumulation of small deflections at given offsets from the loaded area. This is especially important when a large number of wheels are involved and is one method of representing field performance with a modified theory. This modification is accomplished by a subtraction of a constant deflection factor with depth at the selected offset distance. The following deflection factor modification constants were used for 10-, 12-, 15-, and 20-radii cutoffs, respectively: 0.0077, 0.0053, 0.0034, and 0.0019. The deflection modification factors were computed as follows:

$$F = \frac{WE}{p_e r} \tag{25}$$

where

F = deflection modification factor
W = vertical deflection, in.
E = elastic modulus, psi
p_e = average contact pressure, psi
r = radius of loaded circular area, in.

A computer grid and coordinate system was selected by an iterative process to select the location of maximum deflections with depth. Migration of deflection with depth is shown in figure 21. The theoretical maximum deflection occurred under the tire at the surface (point A). The maximum deflection actually never reached the centroid of the six wheels (point B) within the depth of 12 ft, but would with increased depth and would, at greater depths, approach the centroid of the 12 wheels (point C). The instrumentation results for vertical deflections with depth for item 3 are shown in figure 22, and the ESWL's were computed from this plot. The ESWL's were determined from figure 22 in the following manner.

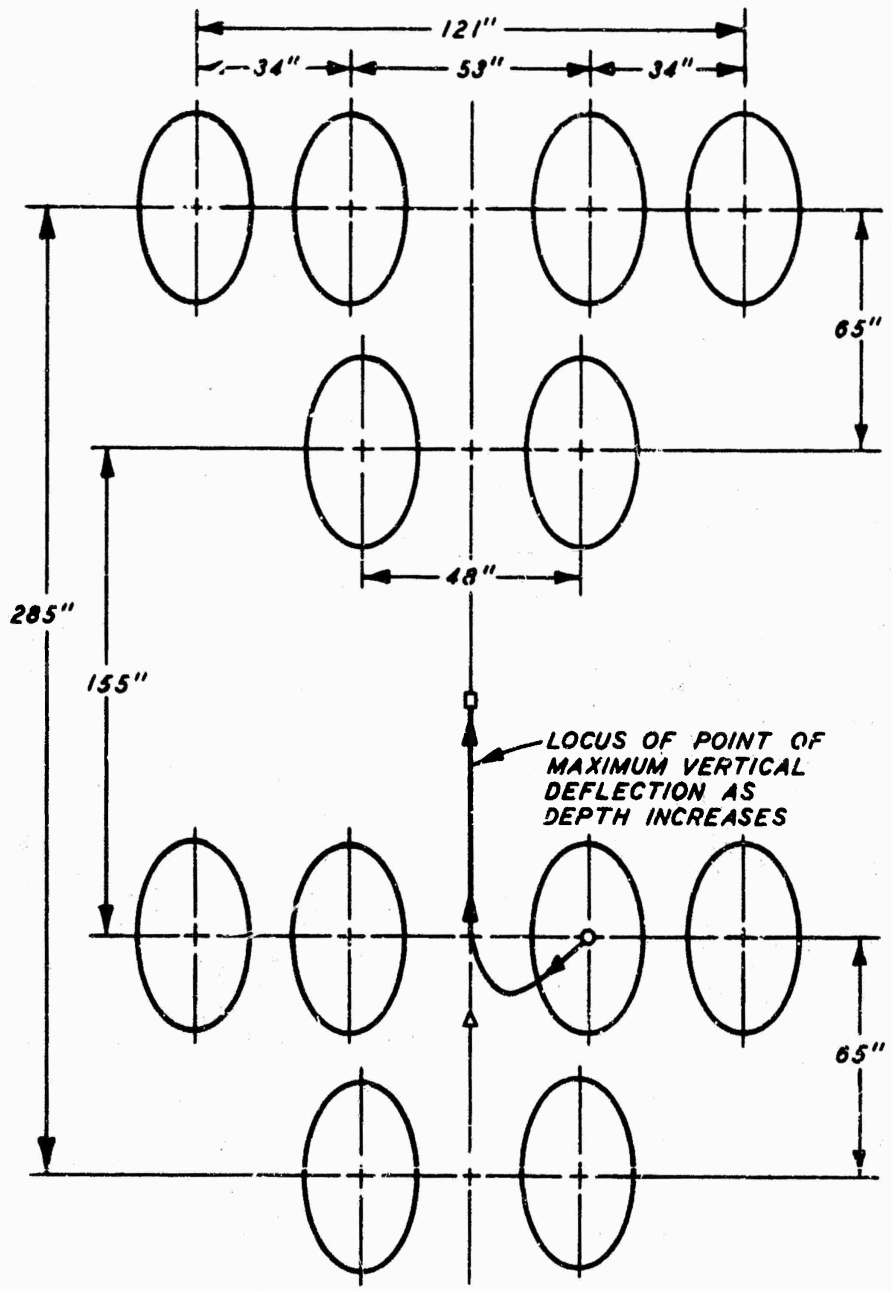

Figure 21. General Flow of Maximum Vertical Deflection with Depth

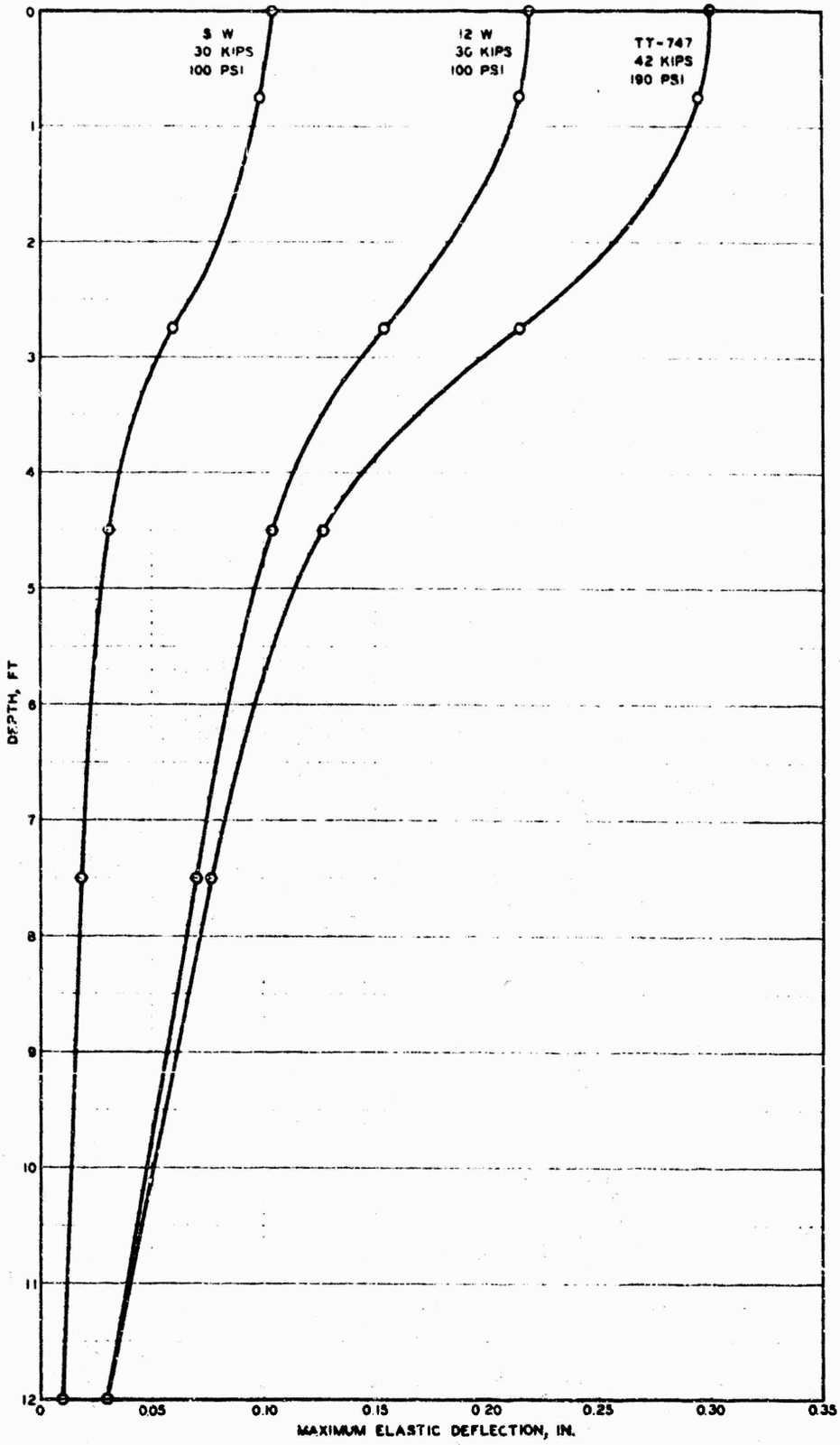

Figure 22. Vertical Deflection Versus Depth (Static Load, Item 3, Volume III-B)

$$\text{ESWL, \% assembly} = \left(\frac{\Delta 12WH \times 30^k}{\Delta SW}\right)\left(\frac{1}{360^k} \times 100\right) \tag{26}$$

For example, at 9-in. depth

$$\text{ESWL, \% assembly} = \frac{0.215}{0.098} \times \frac{30}{360} \times 100 = 18.28\%$$

The ESWL's are shown in figure 18 for comparison of the measured and computed values.

Of the relationships of ESWL with depth shown in figure 18, the 10-radii cutoff values agree best in the thickness design relationship,

$$t \rightarrow (0.23 \log C + 0.15)\sqrt{\frac{ESWL}{8.1\ CBR} - \frac{A}{\pi}} \tag{23}$$

as shown in the following tabulation.

Item	CBR	Coverage	ESWL lb	A sq in	Thickness, in. Calculated (Approx)	Actual
1	3.7	8	44,000	285	13.3	15
2	4.4	104	51,500	285	22.6	24
3	3.8	1500	59,400	285	37.7	33
4	4.0	1500	59,400	285	36.7	33
5*	4.0	>3850	67,250	285	43.4	41

* Nonfailure.

The calculated t is approximate, since the ESWL is dependent on the calculated t , and the value is shown only for first-order accuracy.

A similar type of approach was then directed toward the data from traffic by the twin-tandem gear spaced 44 by 58 in. on test items of lane 3B. A plot of ESWL (percent of assembly load) versus depth from computations using elastic theory, different modifications of elastic theory, and instrumentation deflection values is shown in figure 23. It is noteworthy that the instrumentation ESWL curve for the twin-tandem gear loading more closely approximates the values derived from the elastic theory than those derived from the modified elastic theory. However, the 12-wheel-gear-loading ESWL curve is best approximated by the modified elastic theory 20-radii cutoff.

Analysis of traffic test data with the two gear configurations did not

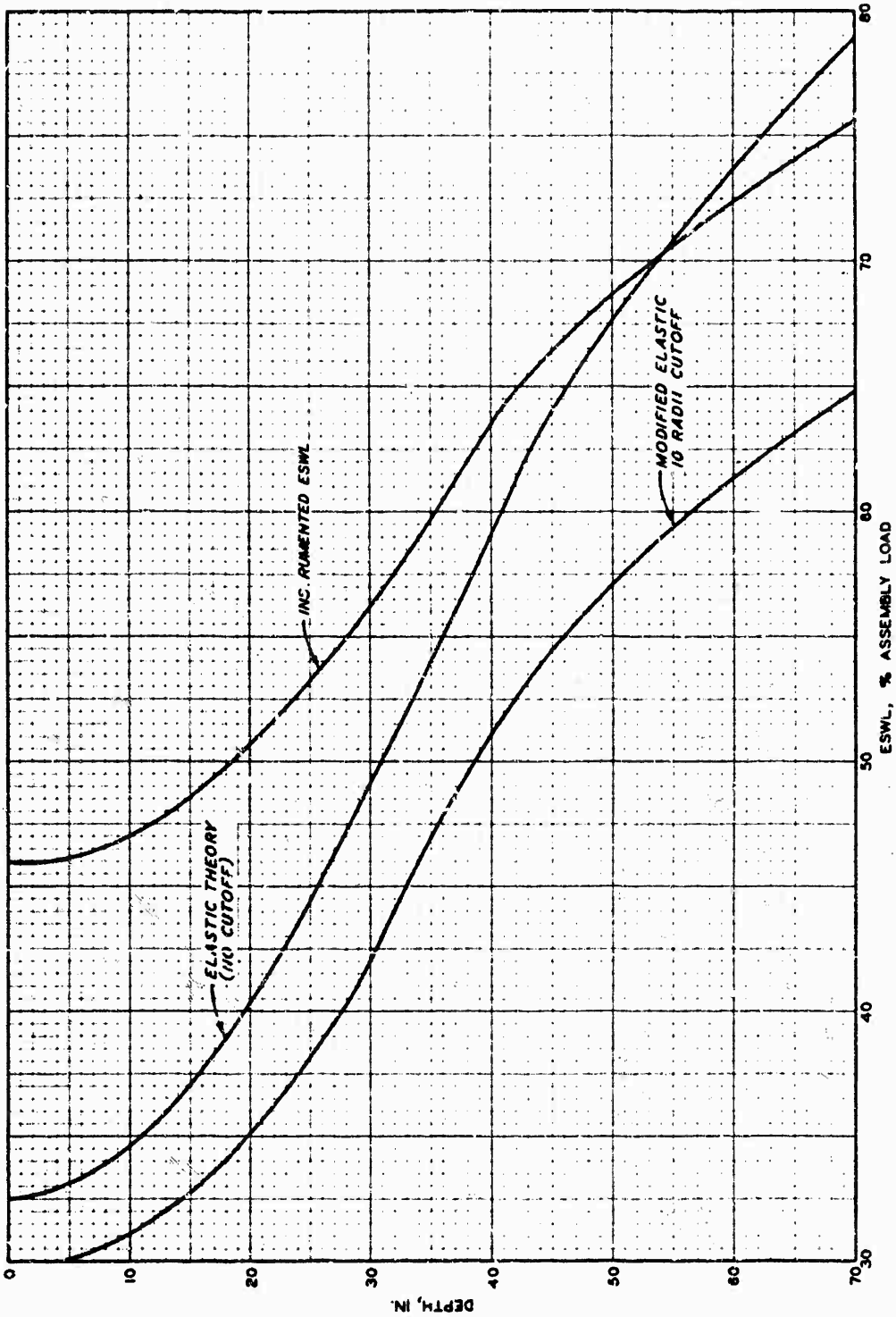

Figure 23. Comparison of Measured (Static Load, Item 3, Volume III) and Computed Equivalent Single-Wheel Load for Twin-Tandem Assembly

yield values of ESWL consistent with the elastic theory or any one modification thereof. To prevent the necessity of assigning different methods of computing the ESWL values for different gear configurations, the elastic theory without modification was selected as best representing the relationship of ESWL for all multiple-wheel assemblies. This decision was also supported by related work (reference 29). The difference in the behavior of the nonmoving single-wheel, twin-tandem, and 12-wheel assemblies can be related to their different configurations, spacing, and consequently, different load distributing characteristics. However, the effects of total number of wheels, method of application of traffic, and load repetitions must also be considered.

c. Traffic Study

(1) Repetitions effect. The factor f , which equals (0.23 log C + 0.15), employed in the current design of flexible pavements accounts for the known effect of traffic repetitions. This factor was developed from previous studies (reference 38). Using the MWHGL test section data and the elastic theory for ESWL determination, the following analysis was made. The flexible pavement equation was rewritten as

$$t_a \rightarrow \alpha \sqrt{\frac{ESWL}{8.1(CBR)} - \frac{A}{\pi}} \tag{27}$$

then

$$\alpha \rightarrow \frac{t_a}{\sqrt{\frac{ESWL}{8.1(CBR)} - \frac{A}{\pi}}} \tag{28}$$

where

α = load repetitions factor
t_a = actual test section thickness, in.
ESWL = ESWL, lb, at the depth t_a
CBR = strength value of supporting layer
A = measured tire contact area, sq in.

The α factors or the effect of repetitions on the total thickness requirements were computed and are shown in table 5.

Figure 24 shows a semilog plot of the α values versus coverages. For comparison, the existing relationship of f versus coverages is also shown in figure 24. The existing criteria for low-intensity traffic seems

Table 5

Comparison of α and f with Coverages

Identification	Failure Coverages	Actual Thickness t in.	ESWL,* lb	CBR	A sq in.	α	f
Lane 1, item 1	8	15	62,280	3.7	285	0.336	0.357
item 2	104	24	77,760	4.4	285	0.525	0.614
item 3	1500	33	94,320	3.8	285	0.605	0.880
item 4	1500	33	94,320	4.0	285	0.621	0.880
item 5	3850**	41	108,360	4.0	285	0.719	0.975
Lane 2, item 1	6	15	50,000	3.7	285	0.378	0.329
item 2	200	24	50,000	4.4	285	0.662	0.679
Lane 3A, item 1	120	15	30,000	3.7	285	0.497	0.628
item 2	450**	24	30,000	4.4	285	0.875	0.760
Lane 3B, item 3	40	33	124,800	3.8	290	0.524	0.518
item 4	40	33	124,800	4.0	290	0.538	0.518
item 5	280	41	144,000	4.0	290	0.621	0.713

* Obtained from figure 18 or 23, as appropriate. All computed using elastic theory without modification.

** Nonfailure.

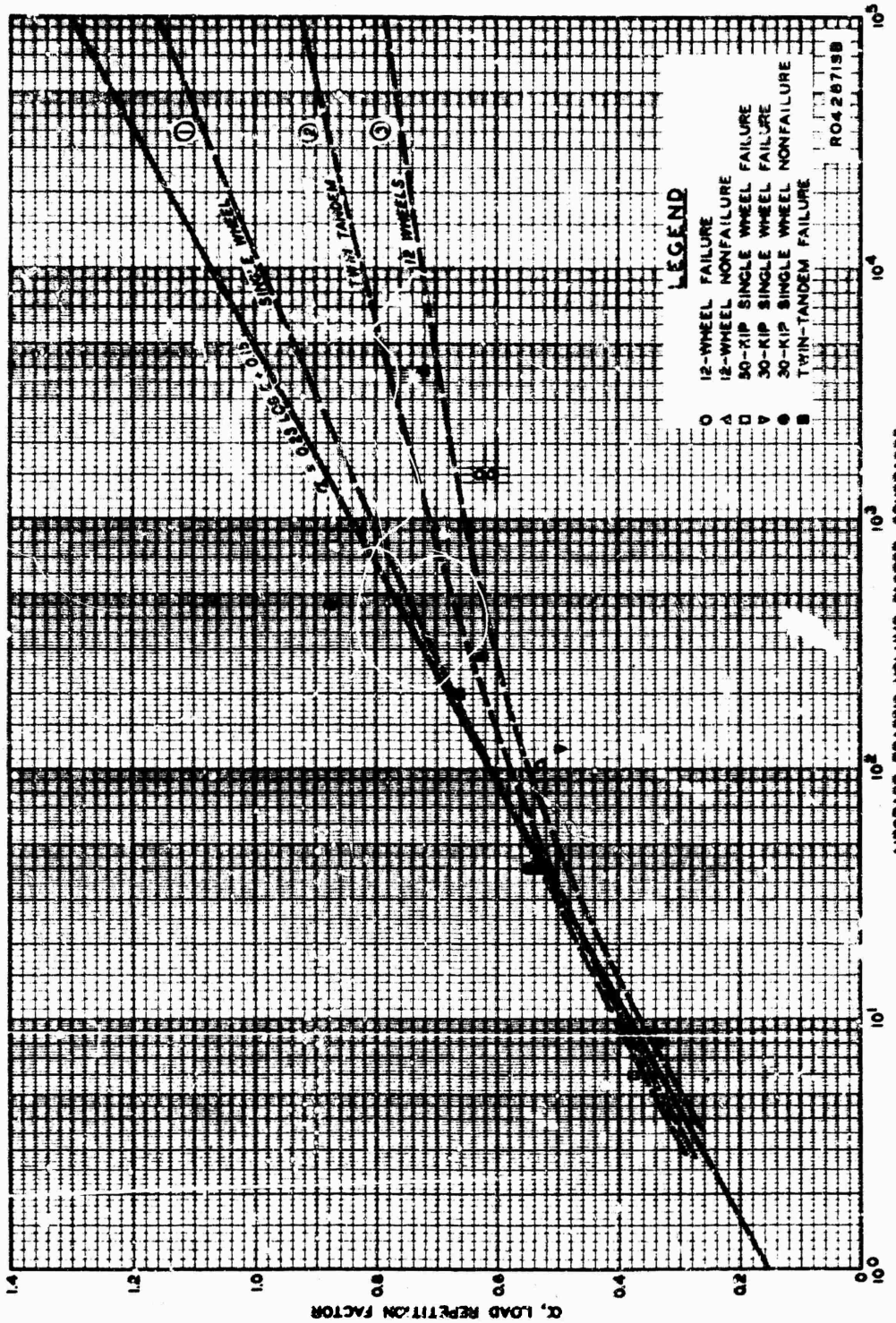

Figure 24. Load Repetition Factors Versus Coverages

adequate for all wheel gears shown (reference 52). However, as noted, with an increase in coverages, the present load repetition factor is too large and hence yields too great a thickness. Curves 1, 2, and 3 in figure 24 represent failure envelopes for the single-wheel, twin-tandem, and 12-wheel gears, respectively. An additional point was obtained for curve 3 for the 12-wheel assembly. This was obtained by extrapolating the nonfailure of item 5 to failure at 15,000 coverages as shown in curve A, figure 19.

A statistically weighted curvilinear regression (references 53 and 54) was performed on the MWHGL failures, given in table 5, to determine the best-fit curve for coverages and α. The results are shown in figure 25 and table 6. The results showing standard deviations and comparison of estimates with prediction equations and actual data are shown in table 6. The quadratic equation, curve B, represents the best-fit curve. Curve A is the existing design curve. Curve B is a good estimate for the twin-tandem assembly but requires too much thickness for the 12-wheel gear. If the curve B were shifted downward a constant amount to include 12-wheel data, it would not require enough thickness for the twin-tandem assembly. This would indicate a need for a separate α versus traffic volume factor plots for each of the assemblies used.

Using the relationships for α_i shown in figure 24 and earlier conclusions, the following design pattern was developed for thickness requirements to protect supporting layers.

$$t \rightarrow \alpha_{SW} \sqrt{\frac{ESWL}{8.1\ CBR} - \frac{A}{\pi}} \qquad \alpha_{SW} = \text{equation of curve 1, figure 24} \tag{23a}$$

$$t \rightarrow \alpha_{TT} \sqrt{\frac{ESWL}{8.1\ CBR} - \frac{A}{\pi}} \qquad \alpha_{TT} = \text{equation of curve 2, figure 24} \tag{23b}$$

$$t \rightarrow \alpha_{12WH} \sqrt{\frac{ESWL}{8.1\ CBR} - \frac{A}{\pi}} \qquad \alpha_{12WH} = \text{equation of curve 3, figure 24} \tag{23c}$$

Using the above relationships, computations were made to check predictions of the pattern with performance of the test section (table 7). As shown in table 7, this method of predicting required thickness is in agreement with the performance of the test pavements.

(2) Traffic distribution studies. During the early stages of development of criteria for the design and evaluation of pavements, it became apparent that a method was needed to account for repetitions of traffic. To simply

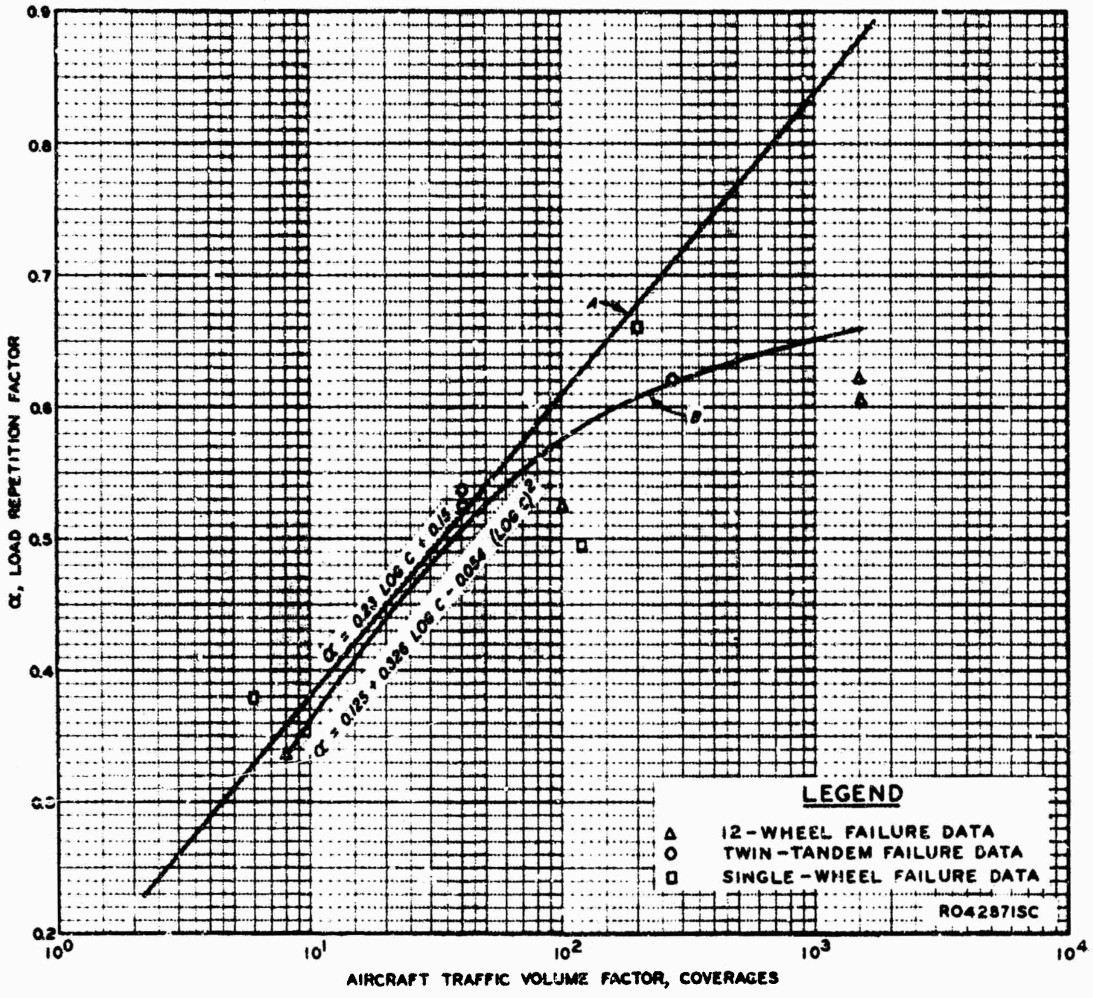

Figure 25. Comparison of Existing Design Curve (A) and Best-Fit Curve (B)

Table 6

Res[illegible] Curvi[illegible]ear Multi-Regression

I. First-Order Equation

Term	Coefficient	Standard Deviation
0	.409047	5.12733E-2
1	.110479	.023802

Standard Deviation = 5.86692E-2

X Value	α Value	Y Estimate	Residual
.90309	.336	.408719	-7.27194E-2
2.01703	.525	.531676	-6.67561E-3
3.17609	.605	.659612	-5.46115E-2
3.17609	.621	.659612	-3.86115E-2
.778151	.378	.504929	-1.69287E-2
2.30103	.662	.568023	9.09771E-2
2.07918	.497	.538535	-4.15354E-2
1.60206	.524	.485871	3.81288E-2
1.60206	.538	.485871	5.21288E-2
2.44716	.621	.579152	4.18476E-2

II. Quadratic Equation

Term	Coefficient	Standard Deviation
0	.125569	9.30489E-2
1	.326092	9.95199E-2
2	-5.38154E-2	2.43453E-2

Standard Deviation = 4.81318E-2

X Value	Y Value	Y Estimate	Residual
.90309	.336	.376169	-4.01695E-2
2.01703	.525	.564364	-3.93641E-2
3.17609	.605	.618402	-1.34018E-2
3.17609	.621	.618402	2.59821E-3
.778151	.378	.346732	.031268
2.30103	.662	.590978	7.10215E-2
2.07918	.497	.57093	-7.39302E-2
1.60206	.524	.509866	.014134
1.60206	.538	.509866	.028134
2.44716	.621	.601229	1.97098E-2

III. Cubic Equation

Term	Coefficient	Standard Deviation
0	.257267	.320773
1	6.96445E-2	.603499
2	8.88475E-2	.331537
3	-.023712	5.49364E-2

Standard Deviation = 5.11994E-2

X Value	Y Value	Y Estimate	Residual
.90309	.336	.375159	-3.91594E-2
2.01703	.525	.564628	-3.96277E-2
3.17609	.605	.61501	-1.000962E-2
3.17609	.621	.61501	5.99043E-3
.778151	.378	.354087	2.39126E-2
2.30103	.662	.599054	.062946
2.07918	.497	.573028	-7.60278E-2
1.60206	.524	.499378	2.46223E-2
1.60206	.538	.499378	3.86223E-2
2.44716	.621	.612269	8.73069E-3

Note: X = aircraft volume traffic factor, coverages.
Y = load repetition factor, α .

Table 7

Comparison of Predicted Thicknesses Versus Test Section Thicknesses

Identification	α_i Factor	$\sqrt{\frac{ESWL}{8.1\ CBR}} - \frac{A^*}{\pi}$	Thickness t, in. Predicted	Actual
Lane 1, item 1	0.340	44.5	15.1	15
item 2	0.550	45.7	25.1	24
item 3	0.661	54.5	36.0	33
item 4	0.661	53.1	35.1	33
item 5**	0.692	57.0	39.4	41
Lane 2, item 1	0.360	39.7	14.3	15
item 2	0.670	36.2	24.2	24
Lane 3A, item 1	0.625	30.2	18.9	15
item 2**	0.740	27.4	20.3	24
Lane 3B, item 3	0.510	62.9	32.1	33
item 4	0.510	61.3	31.3	33
item 5	0.640	66.0	42.2	41

* ESWL determined using elastic theory without modifications.
** Nonfailure.

count the number of aircraft using an airfield is not adequate. The incremental detriment to a pavement resulting from a particular aircraft wheel at a specified location on pavements is influenced by many factors. Some of the more important factors are: (a) number of wheels, (b) wheel configuration, (c) tire contact area, (d) tire inflation pressure, and (e) location of wheel on pavement.

In an attempt to normalize these factors so that one number could be obtained to reflect their collective influence on the total system of design and evaluation, the concept of coverage was introduced where coverage is defined as sufficient contiguous wheel passes so that every point in a traffic lane has been touched one time by a moving wheel.

In the past, traffic on test sections was programmed so that successive wheel paths were not overlapping, and an accurate value of coverages resulted. It was assumed that coverages on a test section could be related directly to coverages on airfield facilities (runways, taxiways). However, the random traffic on runways and/or taxiways can only be conveniently counted as aircraft passes. The general equation currently used for determining pass per coverage ratios (sometimes called operation per coverage ratios), given as equation 7 in reference 55, is:

$$\frac{p}{c} = \frac{W_t + S + W_w}{0.75\ N\ W_t} \tag{29}$$

where

p/c = pass per coverage ratio

W_t = tire width, in.

S = wheel spacing, in.

W_w = wander width (40 in. assumed for channelized traffic of military aircraft on a taxiway)

N = number of wheels in traffic lane

In accordance with the traffic pattern used on the C-5A test sections (Volume II) where the traffic was programmed in such a manner that 22 passes of the load cart generated 32 coverages, p/c equaled 22/32 or 0.68. In comparison, when the dimensions for the C-5A gear are substituted in equation 29 (W_t = 14.3 in., S = 121 in., and N = 12), then p/c equals 1.36. Thus the pass per coverage ratio determined from the current method for aircraft operating on runways and/or taxiways does not agree with the

actual pass per coverage ratio for the test section. In addition, there has been considerable confusion and some misunderstanding relative to the use of coverage as a means of accounting for traffic repetitions and some indication that the current method of converting coverages into passes (or vice versa) may contribute to some of the difficulty encountered in analysis of test section data. For these reasons, a revised method, based on statistical analysis, for determining pass per coverage ratios has been developed. The revised method and its application are described in the following paragraphs. The background and details of the development and application of the method are given in reference 55.

(3) Development of revised traffic distribution concepts. Statistical analysis combined with actual traffic distribution data has been used to develop a new method for determining pass per coverage ratios. A fundamental assumption is made that airfield traffic is normally distributed instead of uniformly distributed as was assumed in development of equation 29. For a large number of aircraft passes, the lateral placement of the center line (of the aircraft) will be, statistically, as shown in figure 26. The general shape is assumed to be normal, while the specific shape depends on the standard deviation σ. The specific shape may also be described by prescribing the wander width W_w, which is defined as that width over which the center line of the aircraft traffic is distributed 75 percent of the time. It has been determined, on the basis of an analysis of a small amount of actual military aircraft traffic distribution, that wander widths of 40 and 80 in. should

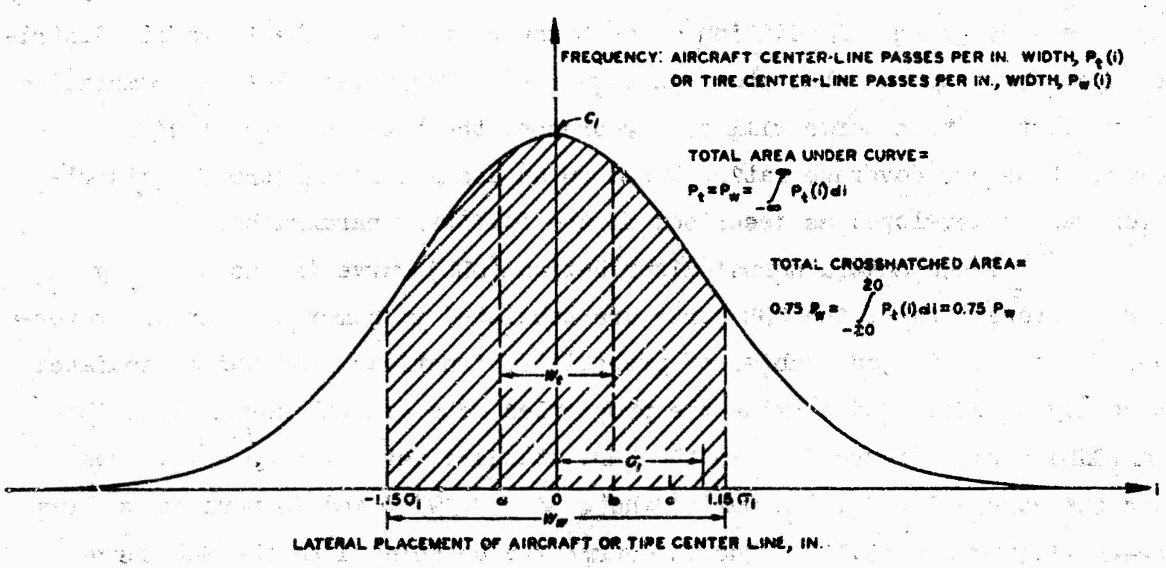

Figure 26. Theoretical Normal Distribution of Aircraft Traffic

be used in determining pass per coverage ratios for taxiways and runways, respectively. These values represent the best values obtainable from existing data and are subject to change if and when additional actual traffic distribution data are obtained.

The definition for coverage was revised for the traffic distribution study. It was considered that coverage represents the maximum number of tire prints or partial tire prints applied to the pavement surface at that point where maximum accumulation occurs. In figure 26, the distribution curve also represents the distribution of the center line of one wheel on the aircraft. When the wheel center line is at $a = -(W_t/2)$, wheel passes accumulate at 0. Similarly when the wheel center line is between $a = -(W_t/2)$ and $b = W_t/2$, there will be accumulations at 0 equal to:

$$\int_{-\frac{W_t}{2}}^{\frac{W_t}{2}} P_t(i)di \tag{30}$$

As can be seen, this is approximately equal to $(C_i)(W_t)$. It is assumed in equation 30 that the effect of the edge of a tire at 0 is as detrimental as the effect of the tire center line at 0. This is not necessarily true and a further refinement could be made through use of a location weighting factor as discussed in detail in reference 55. However, for the present this refinement will not be used and the simplified definition for coverage, $C = (C_i)(W_t)$, will be used. This method can be extended to aircraft having many wheels by graphical addition of any number of single-wheel traffic distribution curves, such as that shown in figure 26. The area under the cumulative traffic distribution curve will then represent the total number of wheel passes. Pass per coverage ratios based on an assumed normal traffic distribution can be developed as described in the following paragraphs.

The standard normal distribution (SND) curve is shown in figure 27. Properties of the SND curve are tabulated in numerous standard references for statistics and tables of probability functions, and these tabulated values may be used to determine the properties of a general normal distribution (GND) curve, figure 28. In the SND, standard deviation $\sigma = 1$, area under the curve $A = 1$, maximum ordinate $C = 0.399$, and 75 percent A lies between $-1.15 < z < +1.15$. The GND curve may be related to the SND curve

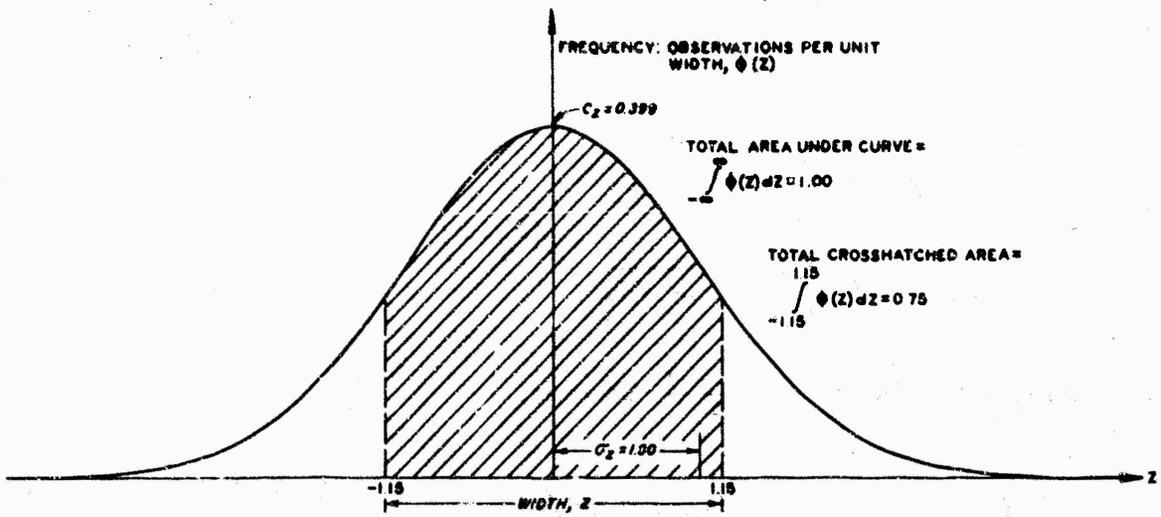

Figure 27. Standard Normal Distribution (SND) Curve

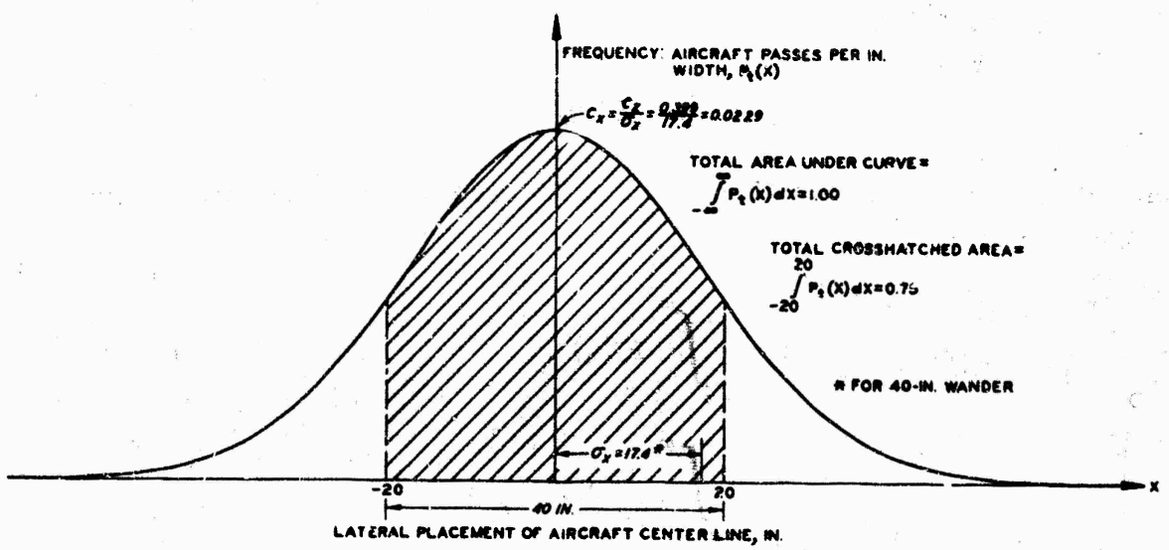

Figure 28. General Normal Distribution (GND) Curve for Aircraft Traffic

using the following substitution.

$$z = \frac{x - u}{\sigma_x} \tag{31}$$

where

z = a variable in SND

x = a variable in GND

u = mean value in GND

σ_x = standard deviation in GND

Then where the wander width W_w equals 40 in. or 2x, X = 20 in., and u = 0, by substitution, $1.15 = \frac{20 - 0}{\sigma_x}$, or σ_x for the GND = 17.4. Now the SND curve has the equation:

$$\phi z = \frac{1}{\sqrt{2\pi}} e^{-\frac{z^2}{2}} \tag{32}$$

and the GND equation has the equation:

$$P_t(x) = \frac{1}{\sigma_x \sqrt{2\pi}} e^{\frac{1}{2}\left(\frac{x - u}{\sigma_x}\right)} \tag{33}$$

where in substitution of $z = \frac{x - u}{\sigma_x}$ becomes:

$$P_t(x) = \frac{1}{\sigma_x}(\phi z) \tag{34}$$

and

$$C_x = \frac{1}{\sigma_x} C_z \tag{35}$$

where C_x is the maximum ordinate on the GND curve. Also, the area under the GND curve A is equal to:

$$\begin{aligned} A &= \int_{-\infty}^{\infty} P_t(x)dx \\ &= \int_{-\infty}^{\infty} \frac{1}{\sigma_x}(\phi(z))\sigma_x dz \\ &= \int_{-\infty}^{\infty} \phi(z)dz = 1.00 \end{aligned} \tag{36}$$

Note, however, that as wander width W_w is changed, σ_x must be recalculated as indicated above.

The GND curve can now be applied to the study of real aircraft traffic distribution. For example, using an aircraft with a single-wheel tricycle landing gear (figure 29) and neglecting the nose gear, plot the general normal distribution of each wheel, both on the same plot, as shown in figure 29. Graphically adding these curves results in a cumulative curve identical (for all practical considerations) with the GND curve. The total area under the cumulative curve is equal to two wheel passes (wp) or one

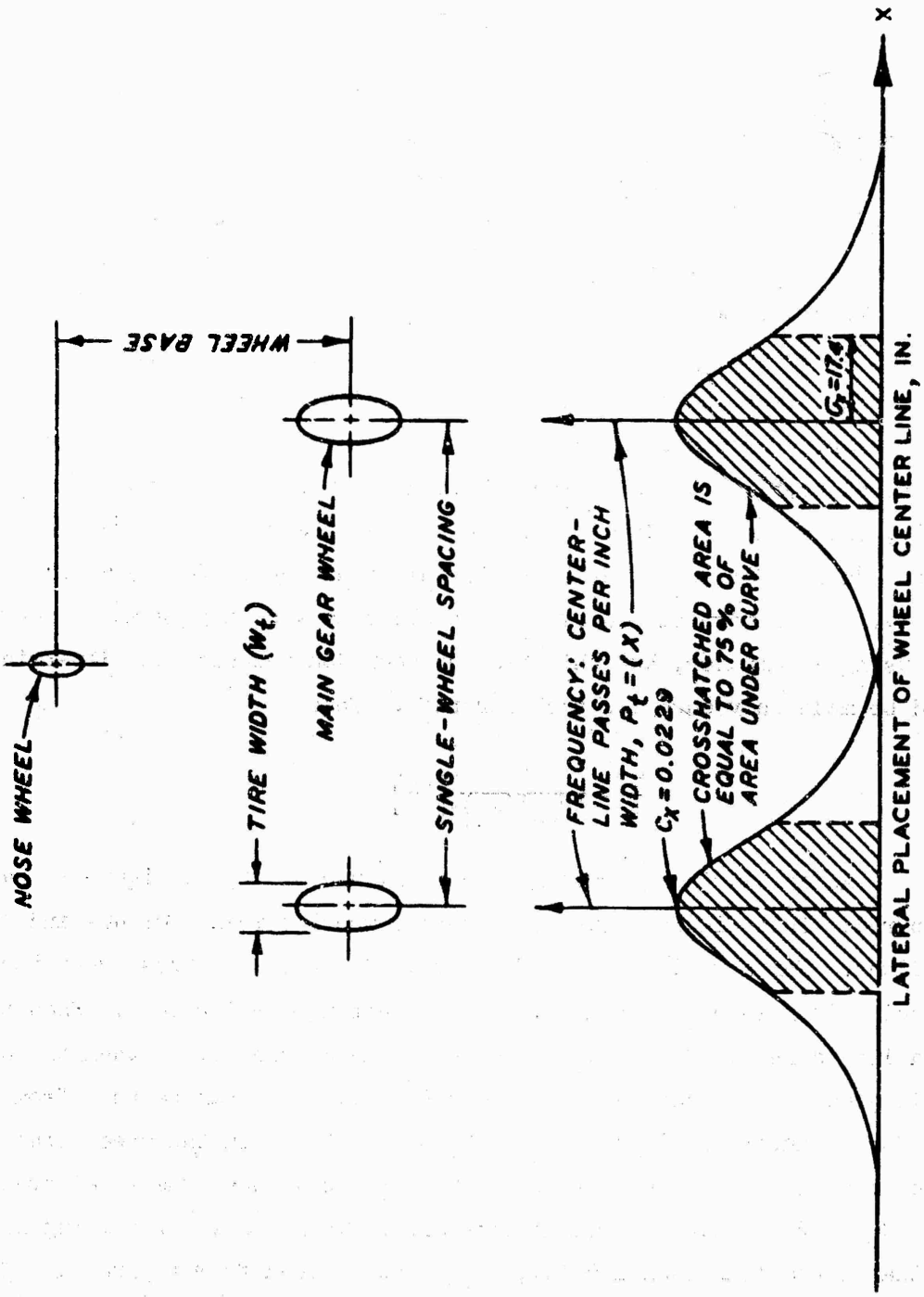

Figure 29. General Normal Distribution for Nonoverlapping Wheels for the Typical Single-Wheel Tricycle Landing Gear Shown Above

aircraft pass (ap), and the maximum number of coverages C is: $C = (C_x)(W_t)$ and

$$\frac{p}{c} = \frac{1}{(C_x)(W_t)} \left[\frac{ap}{wp}\right] \tag{37}$$

As the wheel spacing S becomes smaller, the GND curve for each single-wheel overlap and the distribution pattern shown in figure 30 are obtained. In this case, graphical addition of the individual single-wheel curves results in a cumulative distribution curve with a maximum ordinate greater than that of either single-wheel curve. The area under the cumulative curve is still 2.00. Now, however, the maximum number of coverages is the maximum area under the cumulative curve with a width of W_t. This value may not necessarily occur under one wheel and its location must be determined by trial and error. For example, the maximum area may be as shown in figure 30 (cross-hatched area). Such a refinement is not considered warranted, and for simplicity, the value $(C_{xc})(W_t)$ will be used as the maximum value for coverages. Values for C_{xc} developed in this study have been obtained graphically. The determination of C_{xc} could easily be a programmed determination using a computer, but this has not been done because the determination need be made only once for each aircraft. Thus

$$\frac{p}{c} = \frac{1}{(C_{xc})(W_t)} \left[\frac{ap}{wp}\right] \tag{38}$$

As an aid in determining the magnitude of C_{xc}, figure 31 has been prepared. This figure shows C_{xc} versus wheel spacing for 40- and 80-in. wander widths. For a wander width of 40 in., $C_{xc} = C_x = 0.0229$ when the wheel spacing is greater than 60 in. (nonoverlapping wheel paths). When the wheel spacing is zero, $C_{xc} = 2C_x = 0.0458$ (tandem assembly). When the wheel spacing is greater than zero and less than 60 in., C_{xc} can be read from figure 31. For a wander of 80 in., $C_{xc} = C_x = 0.01145$ when the wheel spacing is greater than 156 in. (nonoverlapping wheel paths). When the wheel spacing is zero, $C_{xc} = 2C_x = 0.0229$ (tandem assembly). When the wheel spacing is greater than 0 and less than 156 in., C_{xc} can be read from figure 31. The values read from figure 31 are applicable to the following landing gear configurations without exception: single conventional, single tricycle,

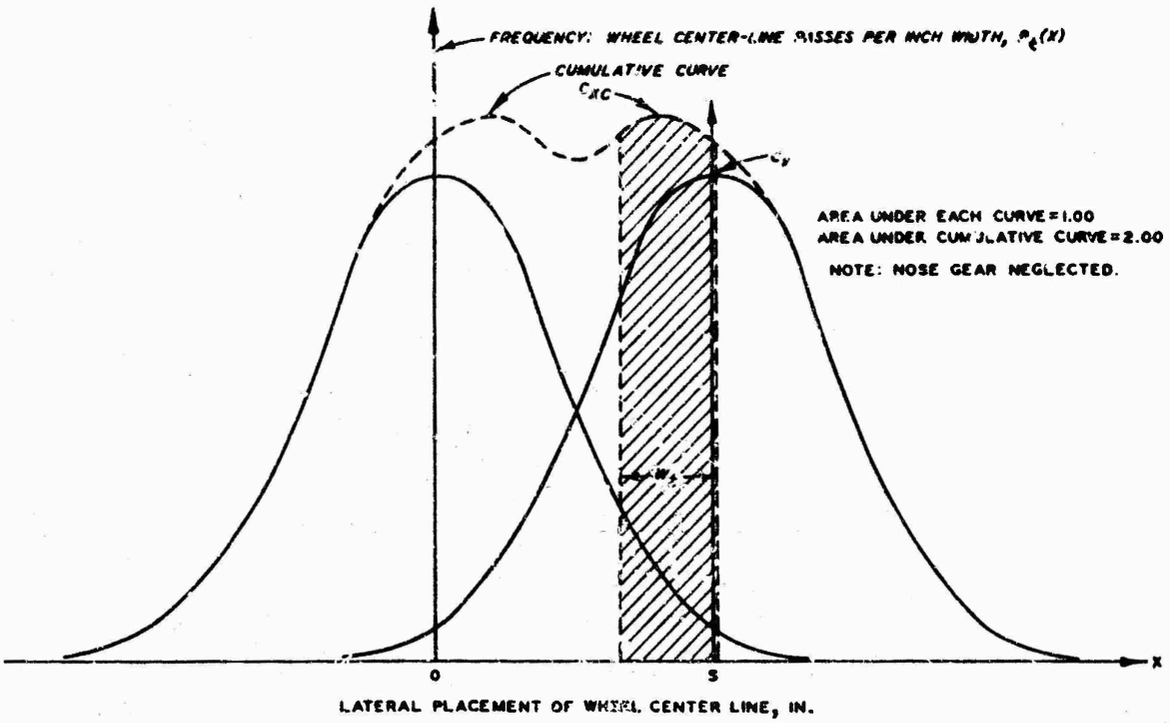

Figure 30. General Normal Distribution Curve for Overlapping Single Wheels

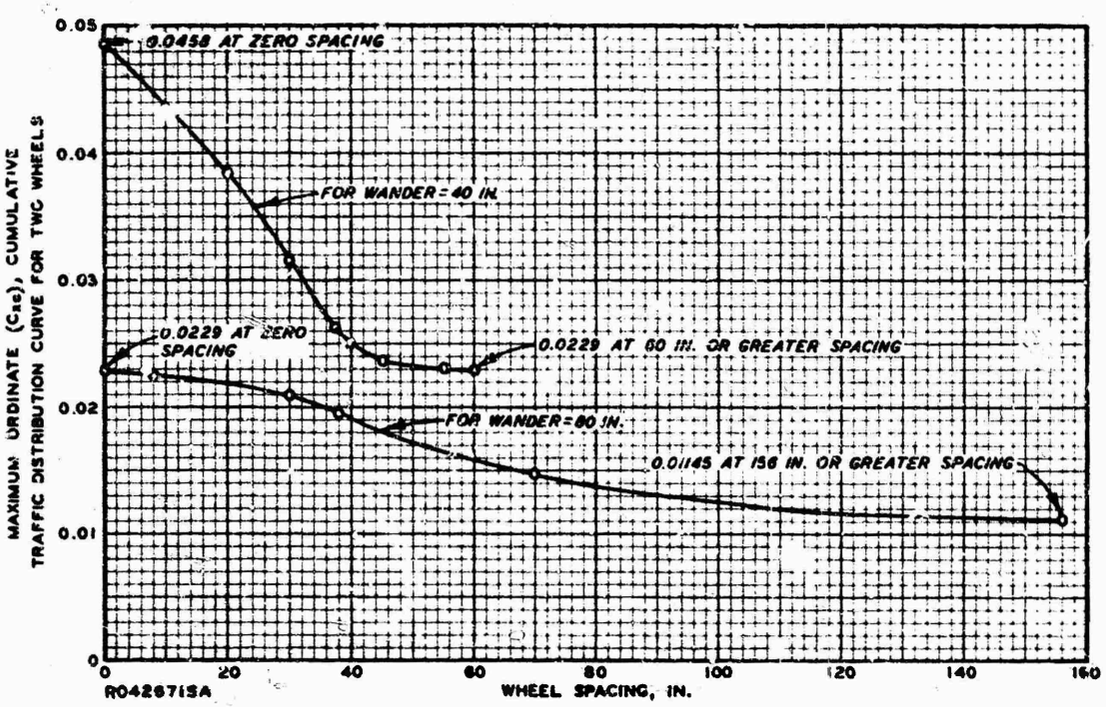

Figure 31. Maximum Ordinate on Cumulative Traffic Distribution Curve for Two Wheels Versus Wheel Spacing

single-tandem tricycle,[2] and twin bicycle[2] and to the following landing gear configurations when the tread is greater than 60 in. (for W_w = 60 in.) or 156 in. (for W_w = 80 in.): twin conventional, twin tricycle, twin-tandem tricycle,[2] and twin-twin bicycle.[2] For other landing gear configurations, C_{xc} can be determined by plotting the individual wheel distribution and determining the cumulative distribution curve by graphical addition as demonstrated in figure 32.

The versatility of this method is demonstrated with the determination of p/c ratios for the C-5A and Boeing 747 landing gear wheel configurations and a wander of 40 in. as shown in the following paragraphs.

(a) p/c ratio for the C-5A. The C-5A wheel configuration is shown in figure 33. The normal distribution curves for wheel groups A, B, and E are shown in figure 32 where the cumulative distribution curve was obtained by graphical addition of individual wheel distribution curves. By inspection, it can be seen that the maximum ordinate for Group A plus Group C (or Group B plus Group D), on the cumulative curve, is the maximum ordinate for the assembly. Thus $C_{xc} = 2(0.0500) = 0.1000$. For the entire assembly, total number of wheel passes = 24. However, 24 wheel passes = 1 aircraft pass. Thus,

$$\frac{p}{c} = \frac{1}{24}\left[\frac{ap}{wp}\right]\frac{24}{1}\left[\frac{wp}{}\right]\frac{1}{(0.1000)(W_t)}\left[\frac{in.}{wp}\right]\left[\frac{1}{in.}\right] = \frac{1}{(0.1000)(W_t)}\left[\frac{ap}{wp}\right]$$

Or as before (equation 19), $p/c = \frac{1}{(C_{xc})(W_t)}\left[\frac{ap}{wp}\right]$. Therefore, for the C-5A where W_t = 15.1 in., $p/c = \frac{1}{(0.1000)(15.1)} = 0.662$, which is in general agreement with the operations per coverage ratio determined from actual test traffic.

(b) p/c ratio for the 747. The Boeing 747 wheel configuration is shown in figure 34. The pass per coverage ratio for the Boeing 747 can be determined by the graphical procedure used for the C-5A aircraft. However, since the individual twin-tandem gear assemblies are spaced far enough apart to prevent any overlap between twin-tandem assemblies for a 40-in. wander, the value of C_{xc} can be determined through use of figure 31. For a 44-in. twin-wheel spacing, the maximum ordinate for a 44-in. spacing is 0.024 and $C_{xc} = (2)(0.024) = 0.048$. Therefore, for the Boeing 747, where

---

[2]Note that for these configurations, C_{xc} will be twice the value read from figure 31 because there are two wheels in line in the direction of travel.

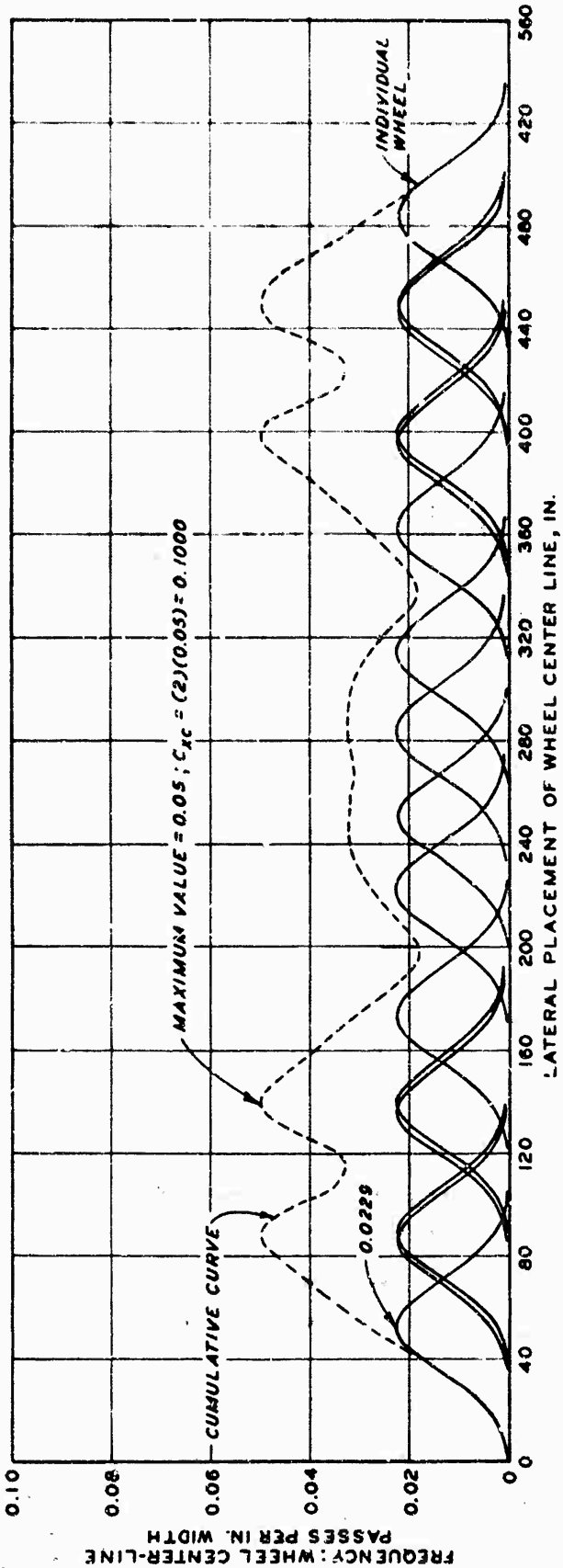

Figure 32. Theoretical Normal Distribution for C-5A Gear (Partial). Note: The Distribution Curve Shown Is for Wheel Groups A, E, and B as Shown in Figure 33

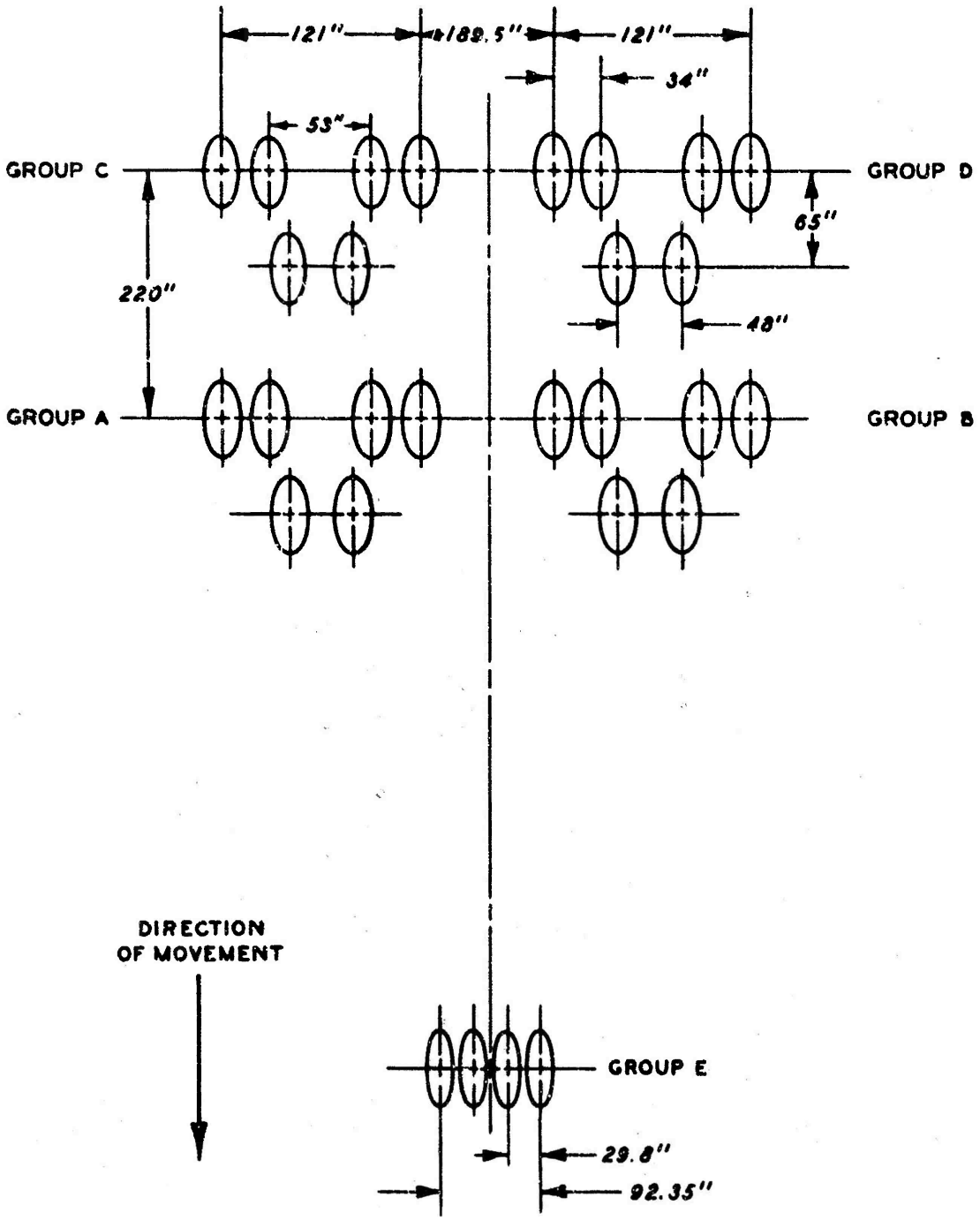

Figure 33. C-5A Landing Gear Configuration

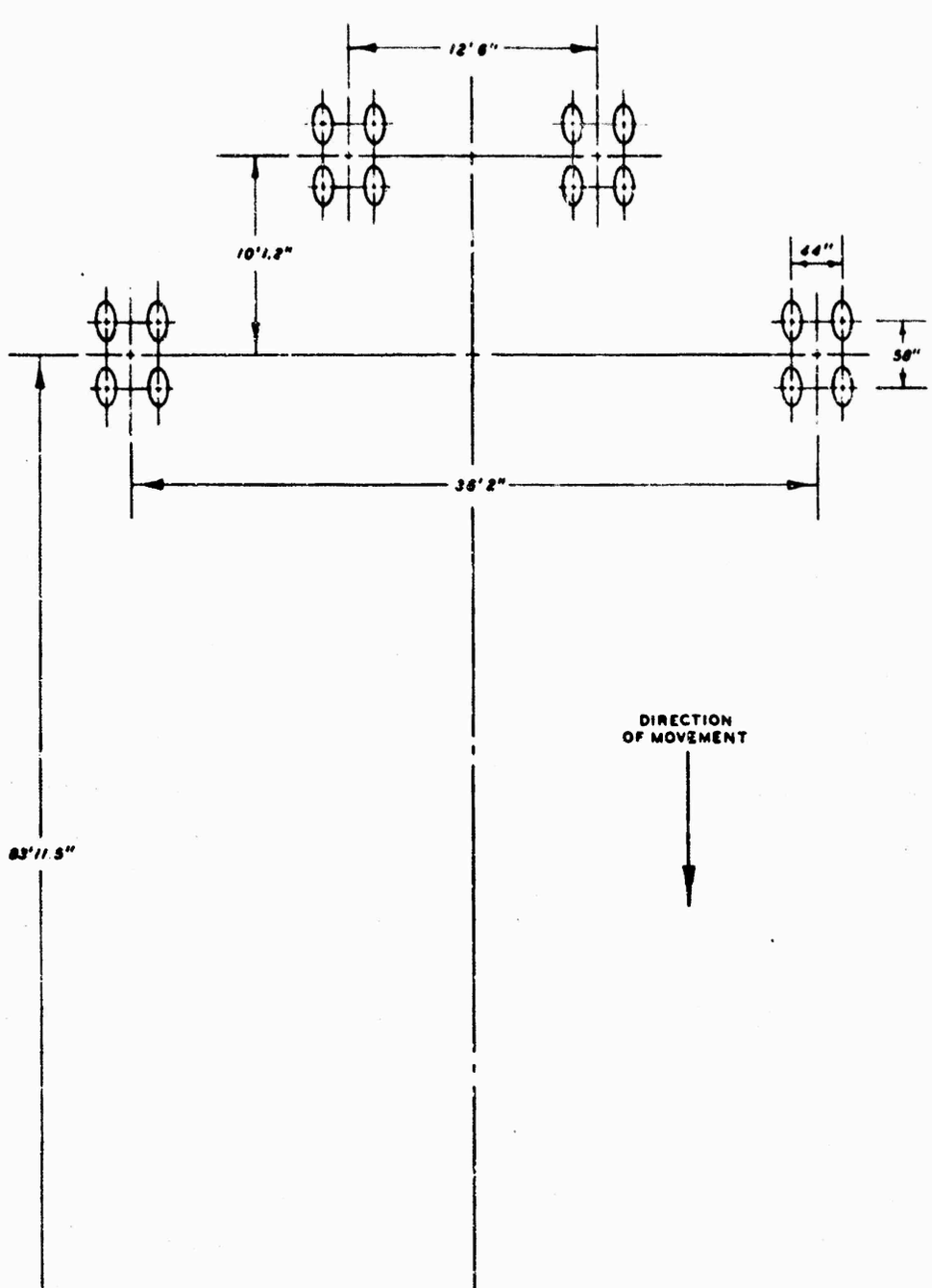

Figure 34. Boeing 747 Landing Gear Configuration

$W_t = 12.9$ in. , $p/c = \frac{1}{(0.048)(12.9)} = 1.62$.

Pass per coverage ratios for the various landing gear wheel configurations used in the MWHGL investigations reported herein and for other similar data obtained from related studies have been determined through use of equation 36 or 37 and are shown in tables 8 and 9. Values for C_x and C_{xc} were read from figure 31 or were determined by the graphical procedure just demonstrated.

Using these p/c factors, the test section failure coverages were converted to actual field facility failure passes. This conversion is shown in table 8. The α_i factors versus passes were plotted, as shown in figure 35, and limiting failure envelopes were drawn for the 12-wheel, twin-tandem, and single-wheel gear configurations.

(4) Related studies. Previous flexible pavement failures (references 39-46) in which insufficient thickness could be determined as having an effect on pavement behavior are listed in table 9. These previous failures were plotted as α_i versus passes to form a plot as shown in figure 36. Differences in test objectives, failure criteria, methods of rating strength, rate of field measurements and observations, construction techniques and materials, and methods of applying traffic account for some of the variations shown in figure 36. These variables were minimized in testing the MWHGL test section; therefore, the data shown in figure 35 are more consistent and will be used with weighted emphasis in this analysis.

(5) Summary. The results of the investigations discussed previously indicate that load repetition factors α_i decrease at a reduced rate with repetitions for the single-wheel, twin-tandem, and 12-wheel configurations. A better performance dependent on a larger number of wheels may be explained in part by the interior soil confinement afforded by a larger number of perimeter wheels. An additional advantage may be that the partial stress reversals imposed within the elastic domain are actually of benefit to the performance of the pavement structure. The decrease in the rate of thickness increase with repetitions reflects the past and recent testing experience in protecting supporting layers from shear deformation. Figure 37 shows a plot similar to that in figure 35, with a logarithm extension of the test pattern shown to encompass different numbers of wheels.

The design curves to be used to obtain α_i have been developed using the load on one landing-gear assembly of an aircraft. In actual

Table 8

Conversion of MWHGL Test Section Coverages

to Actual Airfield Facility Passes

Identification	Assembly	A sq in.	Failure Coverages	α_i Factor	p/c Factor	Failure Passes
Lane 1, item 1	12 wheel	285	8	0.340	0.66	5
item 2	12 wheel	285	104	0.550	0.66	69
item 3	12 wheel	285	1500	0.661	0.66	990
item 4	12 wheel	285	1500	0.661	0.66	990
item 5	12 wheel	285	3850*	0.692	0.66	2541
Lane 2, item 1	Single wheel	285	6	0.360	2.9	17
item 2	Single wheel	285	200	0.670	2.9	580
Lane 3A, item 1	Single wheel	285	120	0.625	2.9	348
item 2	Single wheel	285	450*	0.740	2.9	1305
Lane 3B, item 3	Twin tandem	290	40	0.510	1.62	65
item 4	Twin tandem	290	40	0.510	1.62	65
item 5	Twin tandem	290	280	0.640	1.62	454

* Nonfailure.

Table 9

Previous Related Studies

Reference No.	Assembly	A sq in.	Failure Passes	α_i Factor
38	Single wheel	1501	190	0.646
	Single wheel	1501	2,140	0.924
	Single wheel	1501	13	0.550
	Single wheel	1501	76	0.686
	Single wheel	1501	455	0.704
	Single wheel	1501	1,890	0.980
	Single wheel	1501	1,640	0.959
	Single wheel	250	11,650	0.813
	Single wheel	250	11,650	0.893
41	Twin wheels	330	5,250	0.787
45	Twin tandem	150	410	0.758
		150	135	0.475
		150	2,250	0.870
41	Twin tandem	262	1,310	0.693

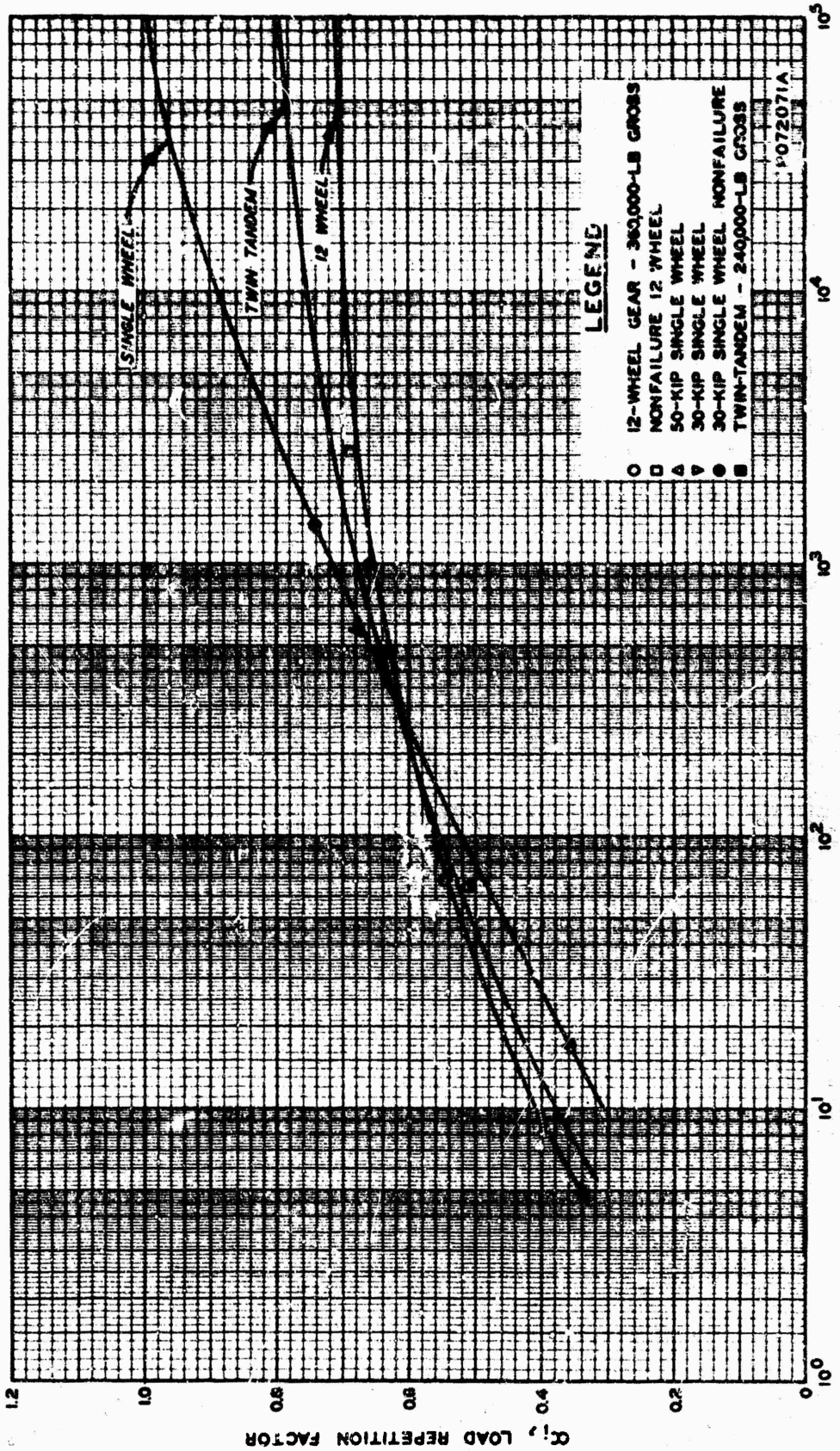

Figure 35. Load Repetition Factor Versus Passes for MWHGL Study

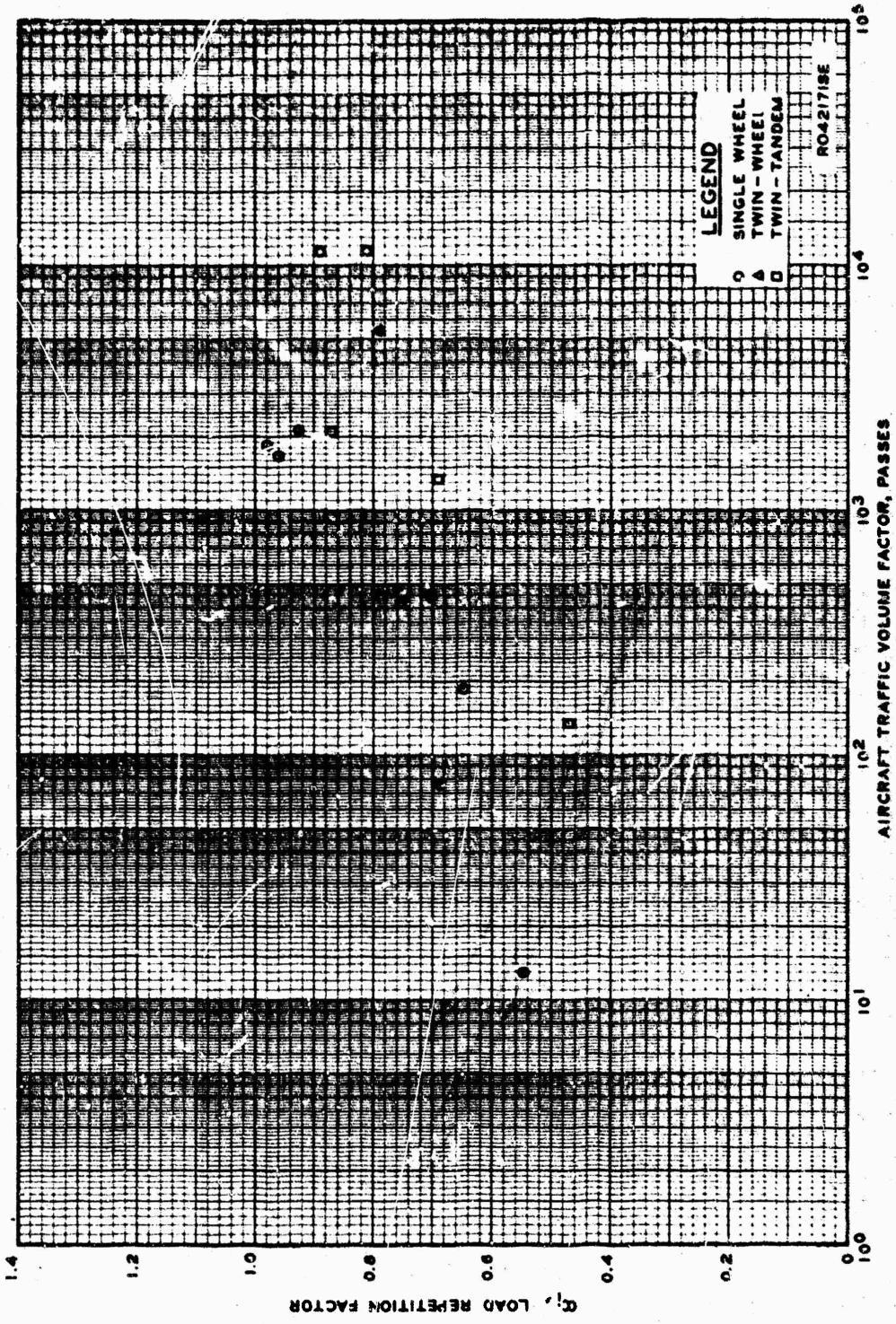

Figure 36. Load Repetition Factors Versus Passes for Related Studies

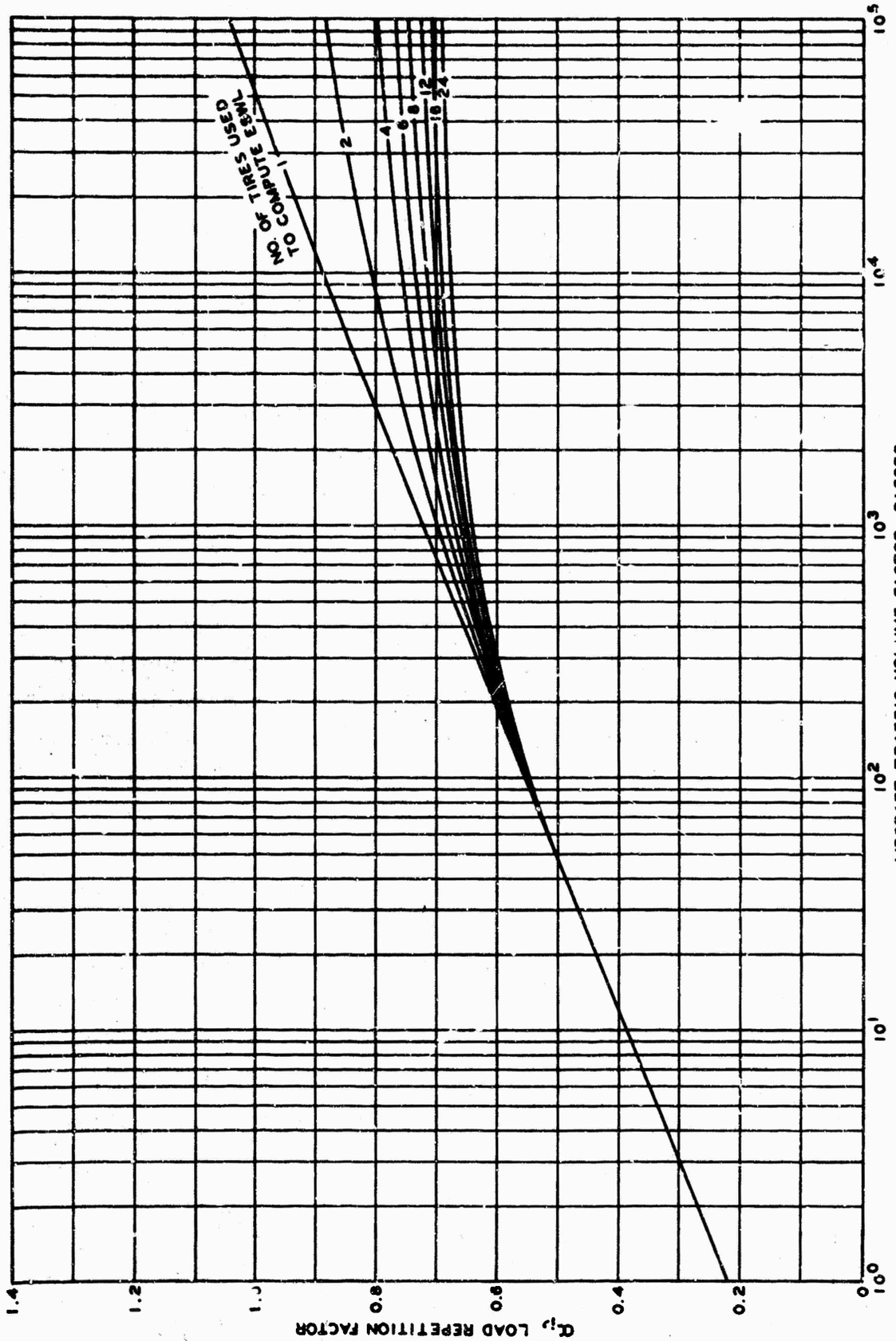

Figure 37. Composite Plot of Load Repetition Factors Versus Passes

practice, however, designs are to be based upon the load on all main-gear tires. Therefore, the α_i versus passes curves (figure 37) show not only the landing gear type used to develop the curves but also the total number of aircraft main-gear tires represented by the gear type. Use of the criteria, therefore, is accomplished by determining the ESWL and the α_i for all main-gear tires. However, where it is shown that some combination or grouping of tires other than all main-gear tires will produce a greater thickness requirement than the main tires, then the other combination or group will be used. Use of the criteria for aircraft having a number of wheels other than shown requires interpolation between the curves. The unique limiting curve shown from 1 to 100 passes represents a composite of the single, twin-tandem, and 12-wheel curves shown in figure 35. Actually, the composite curve for the very low operational level is used for convenience because there is such a small difference in repetitions effect and because it is difficult to differentiate failure at a low operational level.

d. Stationary Requirements

The static requirements, other than due to repetitions, may be well defined by the two basic parameters $t/\sqrt{A}$ and CBR/p_e. These parameters may be reduced to a single plotted curve that separates service-behavior data with regard to failures and nonfailures. Such a representation is shown in figure 11. Results from the MWHGL test section and those from earlier related test sections are separated by this curve in figure 11, with the failure located above this curve and nonfailures below. In the region of higher CBR/p_e and lower $t/\sqrt{A}$ values, certain minimum requirements (i.e. drainage and mix design requirements) are considered in the total thickness requirements. To incorporate these parameters of design and extreme cases of high tire pressure, light loads and low tire pressure, or heavy loads, the curve shown in figure 38 was developed. This curve represents an average of these extremes in this upper region of CBR/p_e and approximately the same as figure 11 in the lower regions of $\frac{CBR}{p_e}\left(\frac{CBR}{p_e} < 0.05\right)$. The statistical equation of the best-fit cubic curve is

$$t \rightarrow \left[\sqrt{A}\left(-0.0481 - 1.1562\left(\log\frac{CBR}{p_e}\right) - 0.6414\left(\log\frac{CBR}{p_e}\right)^2 - 0.4730\left(\log\frac{CBR}{p_e}\right)^3\right)\right] \qquad (39)$$

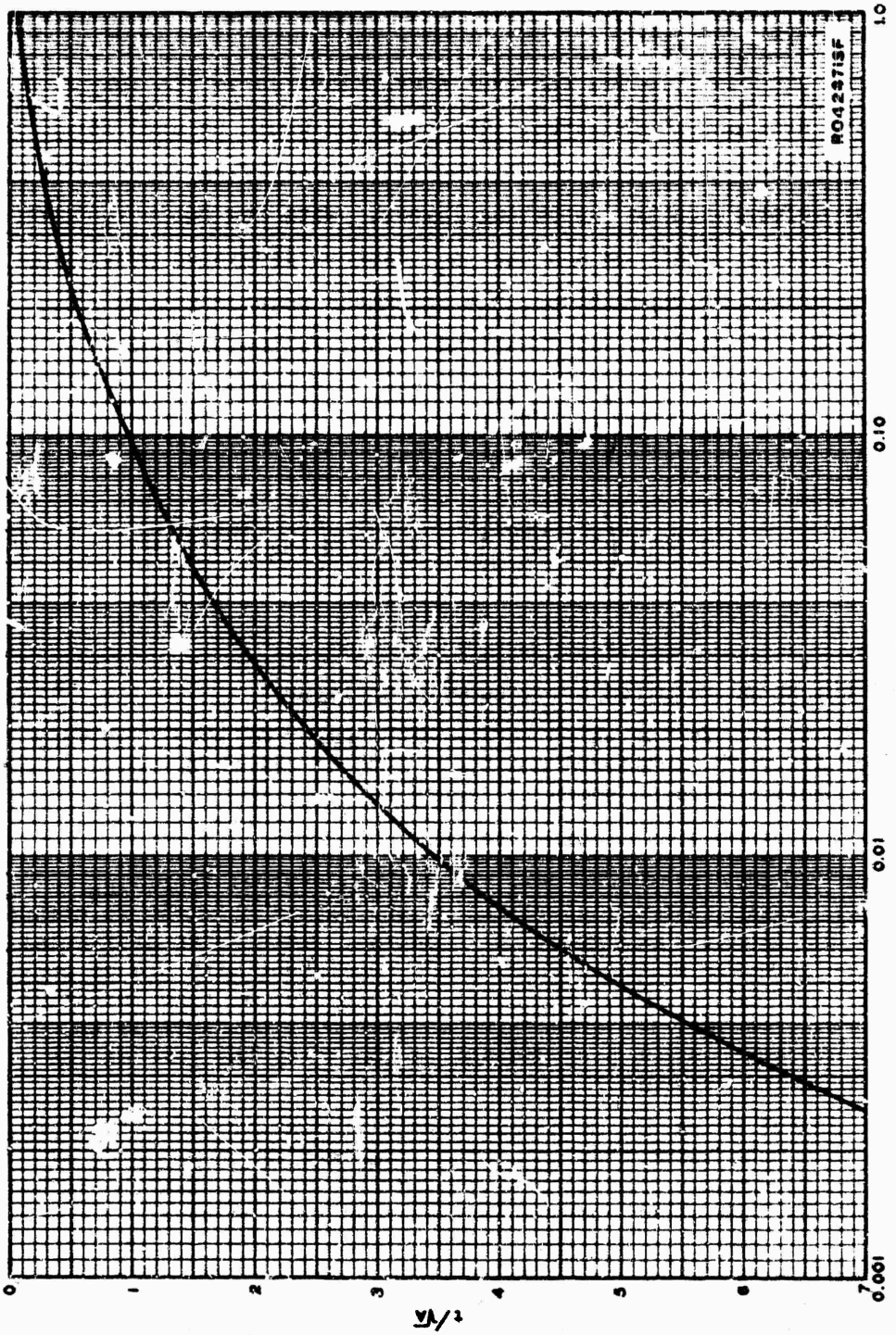

Figure 38. Complete $\frac{t}{\sqrt[3]{A}}$ versus $\frac{CRR}{\rho_e}$

This cubic equation was the best-fit curve of the $n = 1.5$ order polynomials attempted. The standard deviation and comparison of predicted $t/\sqrt{A}$ are shown in table 10.

e. Design Method

The cubic equation yielded the best statistical curve fit for the separation of failures and nonfailures. The equation would be used for a computer solution for the computation of thicknesses of overlying layers required to prevent shear deformation in supporting layers. With the cubic equation representing the static condition and the α_i factors developed previously representing the effect of repetitions, the thickness requirement equation based on the MWHGL test section was finalized in the following form:

$$t \rightarrow \alpha_i \left[\sqrt{A}\left(-0.0481 - 1.1562\left(\log \frac{CBR}{p_e}\right) - 0.6414\left(\log \frac{CBR}{p_e}\right)^2 - 0.4730\left(\log \frac{CBR}{p_e}\right)^3\right)\right] \quad (40)$$

where

t = total thickness required above supporting layer.

α_i = load-repetition factor which varies with number of wheels on main gear of aircraft considered and the volume of aircraft traffic, in passes, anticipated as shown in figure 37.

A = measured contact area of tire, sq in.

p_e = ESWL or SWL tire pressure, psi. For multiple-wheel gear, p_e = ESWL/A where ESWL is determined by the method shown in reference 33 and for single-wheel gear, p_e = SWL/A . This is an artificial tire pressure for multiple-wheel loads consistent with use of contact area of one tire and has no relation to actual tire inflation pressure. However, for single-wheel loads this pressure is the actual average contact pressure and is nominally the same as the tire inflation pressure.

ESWL = ESWL computed using all main-gear wheels of the aircraft. However, where it can be shown that some other combination or grouping of wheels will produce a greater thickness requirement than the main-gear wheels, the other combination or group will be used.

2. RIGID PAVEMENT

a. Plain Concrete Criteria

(1) 12-wheel assembly. A comparison of pavement performance observed under MWHGL traffic and the predicted performance based on current criteria

Table 10

Comparison of Predicted and Actual $t/\sqrt{A}$ Values Using the Best-Fit Cubic Prediction Equation

Standard Deviation = 0.047782

Log CBR/P	$t/\sqrt{A}$	Equation Estimate of $t/\sqrt{A}$	Residual	Log CBR/P	$t/\sqrt{A}$	Equation Estimate of $t/\sqrt{A}$	Residual
0.0	0.05	-4.81065E-2	9.81065E-2	-1.34579	1.45	1.50105	-5.10489E-2
-4.57575E-2	0.07	3.50007E-3	6.64999E-2	-1.39794	1.665	1.60686	5.81445E-2
-0.09691	0.097	5.83461E-2	3.86539E-2	-1.45593	1.785	1.73533	0.049675
-0.124939	0.11	8.72561E-2	2.27439E-2	-1.52288	1.945	1.89558	4.94172E-2
-0.154902	0.13	0.117356	1.26435E-2	-1.60206	2.135	2.10278	3.22238E-2
-0.187087	0.14	0.148847	-8.84721E-3	-1.69897	2.4	2.38435	1.56485E-2
-0.221859	0.168	0.181988	-1.39877E-2	-1.75696	2.57	2.56858	1.42178E-3
-0.259637	0.183	0.217122	-0.034122	-1.82391	2.785	2.79678	-1.17757E-2
-0.30103	0.204	0.254718	-0.050718	-1.90309	3.07	3.08927	-1.92671E-2
-0.346787	0.245	0.295432	-5.04223E-2	-2.0	3.4	3.48253	-8.25282E-2
-0.39794	0.275	0.340219	-6.52194E-2	-2.04576	3.65	3.68239	-3.23936E-2
-0.455932	0.32	0.390529	-7.05294E-2	-2.09691	3.9	3.91705	-1.70472E-2
-0.522879	0.375	0.44869	-7.36898E-2	-2.12494	4.031	4.05078	-1.97801E-2
-0.60206	0.445	0.518709	-7.37091E-2	-2.1549	4.175	4.19787	-2.28695E-2
-0.69897	0.55	0.608182	-5.81818E-2	-2.18709	4.326	4.3607	-3.46993E-2
-0.756962	0.625	0.664706	-3.97056E-2	-2.22185	4.52	4.5423	-2.23014E-2
-0.823909	0.71	0.733612	-2.36121E-2	-2.25964	4.705	4.7466	-4.16031E-2
-0.90309	0.818	0.821284	-3.28374E-3	-2.30103	4.935	4.9788	-4.38026E-2
-1.0	0.965	0.939651	2.53493E-2	-2.34679	5.2	5.24596	-4.59582E-2
-1.04576	1.035	1.00046	3.45425E-2	-2.45593	5.885	5.92916	-4.41622E-2
-1.09691	1.12	1.07262	4.73773E-2	-2.52288	6.38	6.38151	-1.51034E-3
-1.12494	1.168	1.11417	5.38282E-2	-2.60206	6.99	6.95059	3.94081E-2
-1.1549	1.21	1.16025	4.97507E-2	-2.69897	7.755	7.6993	5.57026E-2
-1.18709	1.268	1.21174	0.05626	-2.75696	8.22	8.17581	4.41935E-2
-1.22185	1.325	1.26978	5.52156E-2	-2.82391	8.82	8.75329	6.67121E-2
-1.25964	1.39	1.33588	5.41191E-2	-2.90309	9.485	9.47531	9.68689E-3
-1.30103	1.47	1.41204	5.79569E-2	-3.0	10.38	10.4185	-0.038496

has been made. Due to the age of the pavement at the time of testing (approximately 1 year), the properties of the pavement structure determined in the after-traffic testing program were considered more applicable than the construction control properties for the comparative analysis. Some increase was noted in the subgrade modulus and concrete flexural strengths from the time of construction to the after-traffic test program completion. An estimate of strength at any given time could have been formulated, but due to the scarcity of available data, a linear relationship would have had to be assumed. Previous experience has shown that the relationship between strength change (subgrade and concrete) and time is a curvilinear relation that tends to become asymptotic to a given strength value as time progresses. Based on this knowledge, the after-traffic test measurements were used for subgrade and concrete strengths in the analysis of the MWHGL traffic test data. The physical properties used for this analysis are given in table 11.

The application of the analysis of an elastic plate supported on a dense liquid by Westergaard is inherent in the existing CE and FAA criteria. The adequacy of the current criteria will be examined by first assessing the applicability of the basic algorithm to the problem at hand. Some comparisons of predicted and measured response are shown in table 12. The comparisons were chosen merely to be representative of the data collected under loading. In table 12, the computed values are at the same point in the slab with respect to the gear geometry as the measured values but not necessarily at the same points from one test item to another. Some measured values had to be discarded because of the noise level in the recording; the criterion used to discard a reading was a signal-to-noise ratio of less than 10:1. These data show that the measured deflection for the single-wheel and twin-tandem-wheel gear loadings were normally slightly less than, but in generally good agreement with, the computed values. This is consistent with similar results from other test tracks. The deflection measurements for the 12-wheel static load were very erratic and inconsistent; therefore, the measured values shown in table 12 are those taken during the dynamic load (slowly moving load cart[3]) instrumentation tests. From a comparison of the few reliable static load measurements available, there is little difference between those obtained from the static and dynamic load tests. There is, in general, a fairly good agreement of measured and computed deflections; however, there is a strong

[3]Load cart traveled at a rate of speed of approximately 3 mph.

Table 11

Summary of Physical Properties Used for Analysis of MWHGL Test Results

Test Item	Slab	Concrete Thickness in.	Overlay Thickness in.	Modulus of Rupture psi	Modulus of Elasticity 10^{-6} psi	Subgrade Modulus lb/in.^{3}
			12-Wheel Assembly			
1	SW	10.4	3.9	725	6.6	140
	SE	10.0	4.5	725	6.6	140
2	SW	12.0	N/A	800	7.2	78
	SE	12.1	N/A	800	7.2	78
3	SW	14.1	N/A	700	6.7	65
	SE	13.9	N/A	700	6.7	65
4	SW	8.1	5.3	775	6.3	125
	SE	8.1	5.6	775	6.3	125
			Twin-Tandem Assembly			
1	NW	9.7	3.9	695	6.5	169
	NE	9.6	3.8	695	6.5	169
2	NW	11.5	N/A	700	6.5	111
	NE	11.3	N/A	700	6.5	111
3	NW	13.6	N/A	660	6.4	115
	NE	13.9	N/A	660	6.4	115
4	NW	7.5	5.4	605	6.1	128
	NE	7.4	5.6	605	6.1	128

Table 12

Selected Comparisons of Predicted and Measured Pavement Response

Test Item	Location on Slab	Strain and Deflection Under Indicated Loading: 15,000-lb Single Wheel Load — Strain μ in. Measured	15,000-lb Single Wheel Load — Strain μ in. Computed	15,000-lb Single Wheel Load — Deflection in. Measured	15,000-lb Single Wheel Load — Deflection in. Computed	22,500-lb Single Wheel Load — Strain μ in. Measured	22,500-lb Single Wheel Load — Strain μ in. Computed	22,500-lb Single Wheel Load — Deflection in. Measured	22,500-lb Single Wheel Load — Deflection in. Computed	15,000-lb-per-Wheel Twin-Tandem Load — Strain μ in. Measured	15,000-lb-per-Wheel Twin-Tandem Load — Strain μ in. Computed	15,000-lb-per-Wheel Twin-Tandem Load — Deflection in. Measured	15,000-lb-per-Wheel Twin-Tandem Load — Deflection in. Computed	22,500-lb-per-Wheel Twin-Tandem Load — Strain μ in. Measured	22,500-lb-per-Wheel Twin-Tandem Load — Strain μ in. Computed	22,500-lb-per-Wheel Twin-Tandem Load — Deflection in. Measured	22,500-lb-per-Wheel Twin-Tandem Load — Deflection in. Computed
1	Longitudinal joint	2	45	0.009	0	1	68	*	0.026	*	28	0.030	0.037	*	42	0.051	0.055
	Transverse joint	12	51	0.013	0.021	22	77	*	0.032	17	28	0.042	0.027	38	42	0.062	0.041
	Center	*	51	0.013	0.013	29	77	*	0.019	21	32	**	0.038	34	48	**	0.057
2	Longitudinal joint	0	33	0.009	0.012	4	50	0.012	0.018	14	22	0.029	0.033	30	33	0.042	0.049
	Transverse joint	1	37	0.016	0.016	1	56	*	0.023	0	17	*	0.030	2	26	*	0.050
	Center	16	38	0.010	0.009	25	57	0.013	0.014	25	21	**	0.029	32	32	0.019	0.043
3	Longitudinal joint	4	24	0.009	0.009	10	36	0.011	0.013	15	19	0.017	0.027	13	29	0.019	0.041
	Transverse joint	*	28	0.008	0.012	11	42	0.010	0.018	**	--	0.021	0.020	**	--	0.024	0.041
	Center	11	29	0.007	0.007	12	44	0.009	0.011	8	27	0.022	0.025	5	41	0.027	0.036
4	Longitudinal joint	†	†	0.051	0.028	†	†	††	--	†	†	0.146	0.074	†	†	††	--
	Transverse joint	†	†	**	--	†	†	††	--	†	†	**	--	†	†	††	--
	Center	†	†	0.043	0.017	†	†	††	--	†	†	*	0.040	†	†	††	--

Test Item	Location on Slab	15,000-lb-Per-Wheel 12-Wheel-Gear Load — Strain μ in. Measured	15,000-lb-Per-Wheel 12-Wheel-Gear Load — Strain μ in. Computed	15,000-lb-Per-Wheel 12-Wheel-Gear Load — Deflection in. Measured	15,000-lb-Per-Wheel 12-Wheel-Gear Load — Deflection in. Computed	22,500-lb-Per-Wheel 12-Wheel-Gear Load — Strain μ in. Measured	22,500-lb-Per-Wheel 12-Wheel-Gear Load — Strain μ in. Computed	22,500-lb-Per-Wheel 12-Wheel-Gear Load — Deflection in. Measured	22,500-lb-Per-Wheel 12-Wheel-Gear Load — Deflection in. Computed	30,000-lb-Per-Wheel 12-Wheel-Gear Load — Strain μ in. Measured	30,000-lb-Per-Wheel 12-Wheel-Gear Load — Strain μ in. Computed	30,000-lb-Per-Wheel 12-Wheel-Gear Load — Deflection in. Measured	30,000-lb-Per-Wheel 12-Wheel-Gear Load — Deflection in. Computed
1	Longitudinal joint	83	27	0.030	0.048	2	40	0.013	0.072	41	60	**	--
	Transverse joint	40	29	0.068	0.028	**	44	0.049	0.041	**	--	**	--
	Center	65	59	0.074	0.036	**	89	0.002	0.054	62	98	0.076	0.086
2	Longitudinal joint	8	24	0.045	0.028	51	36	0.029	0.042	69	46	0.048	0.056
	Transverse joint	**	20	0.010	0.046	15	30	0.052	0.069	96	47	**	--
	Center	23	44	0.033	0.030	16	66	0.024	0.044	36	48	0.044	0.060
3	Longitudinal joint	117	14	0.028	0.025	64	30	0.024	0.037	50	37	0.036	0.050
	Transverse joint	**	15	0.033	0.040	**	23	0.044	0.060	86	40	0.049	0.080
	Center	78	20	0.055	0.025	34	20	0.019	0.037	42	40	**	--
4	Longitudinal joint	†	†	0.017	0.036	†	†	††	--	†	†	**	--
	Transverse joint	†	†	**	--	†	†	††	--	†	†	**	--
	Center	†	†	0.123	0.039	†	†	††	--	†	†	**	--

* Noise-to-signal ratio excessive.
** Gage inoperable.
† Strain gages not installed in item. No computations made.
†† Load not applied to item because of possible overload.
‡ Magnetic tape saturated.

tendency for the measured deflection to be greater than the computed deflection. This is opposite to that which was experienced with the single-wheel and twin-tandem-wheel gear tests on this and other test tracks. A rather poor agreement was obtained between the measured and predicted strains; however, the responses of the strain gages were of doubtful validity considering the erratic nature of the output signal and the high loss of gages due to malfunctioning. A few of the strain gages responded well and gave good results. A comparison of the measurements from these gages with computed values indicated that the measured strains were generally less than the computed strains for the single-wheel and twin-tandem-wheel gear loadings; however, for the 12-wheel gear loadings, the reverse was generally true. Therefore, the comparisons of the measured and computed deflection and strain values seem to raise a question regarding the applicability of the Westergaard algorithm for the multiple-wheel heavy gear loadings. This should not be surprising, since the original algorithm was for single wheels, later was extended for multiple-wheel gears (twin and twin-tandem), and is now being further extended to account for deflections and strains under 8- and 12-wheel gears.

The Westergaard algorithm yields the concrete stress and deflection under static load conditions. Airfield pavements are subjected to rolling loads, impact loads, and vibrations, as well as static loads. Inasmuch as these dynamic and repetitive loadings may result in loadings excessive of the static load and may result in fatigue of the pavement materials, these loadings must be taken into consideration in the design and evaluation procedures. The current CE design method makes use of a DF to account for the effects of rolling repetitive-type loadings. The DF is the ratio of the concrete flexural strength to the computed flexural stress, and from the full-scale accelerated traffic testing, the relationship between the DF and traffic volume has been established for three separate and distinct levels of slab distress: initial crack, shattered slab, and complete failure. The curves presented in Section III of this report represent an upper bound for these tests.

Although each test item was composed of four slabs, the traffic area was laid out so that the 100 percent traffic was all in the south slabs and tangent and parallel to the longitudinal joint between the north and south slabs. Thus, for the analysis of the 12-wheel gear results, only the two south slabs in each test item are considered. Inasmuch as there are slight variations in the physical properties of the slabs, each slab in each test

item has been analyzed separately. This results in two data points for each test item. For computational convenience, use was made of the graphical solution of the Westergaard algorithm from reference 51. Using the edge-loading influence charts, a relationship between N, the number of blocks covered by the tire contact areas on the influence charts, and ℓ, the radius of relative stiffness, which was previously defined in equation 21, was developed and is shown in figure 39 for the C-5A gear configuration. As illustrated in figure 39, only one of the two 6-wheel arrays of the 12-wheel main gear was used for the N versus ℓ relationship, since the other 6-wheel array does not change the N count from the influence chart. An example comparative analysis for item 2 is shown below.

	SW Slab	SE Slab
Slab thickness, h	12.0 in.	12.1 in.
Subgrade modulus, k	78 lb/in.^{3}	78 lb/in.^{3}
Concrete flexural strength, R	800 psi	800 psi
Tire contact area, A	285 sq in.	285 sq in.
Load per wheel, P	30,000 lb	30,000 lb
Modulus of elasticity of concrete, E	7.2×10^6 psi	7.2×10^6 psi
Poisson's ratio of concrete, μ	0.20 (assumed)	0.20 (assumed)

Using the above-listed properties, the ℓ value is computed for each slab and the N value for each slab is determined from figure 39. According to reference 51, the flexural stress σ is computed from the following equation:

$$\sigma = \frac{6q\ell^2 N}{10{,}000h^2} \tag{41}$$

where

q = contact pressure per tire, psi, obtained by dividing the wheel load, P by the tire contact area, A

ℓ = radius of relative stiffness, in.

N = number of blocks from influence chart (dimensionless)

h = slab thickness, in.

6 and 10,000 = constants associated with the unit width moment of inertia (6) and a scaling factor associated with the graphical solution (10,000) (dimensionless)

The current criteria are based on the flexural stress developed at a jointed edge by a landing gear oriented parallel and tangent to the jointed edge. The

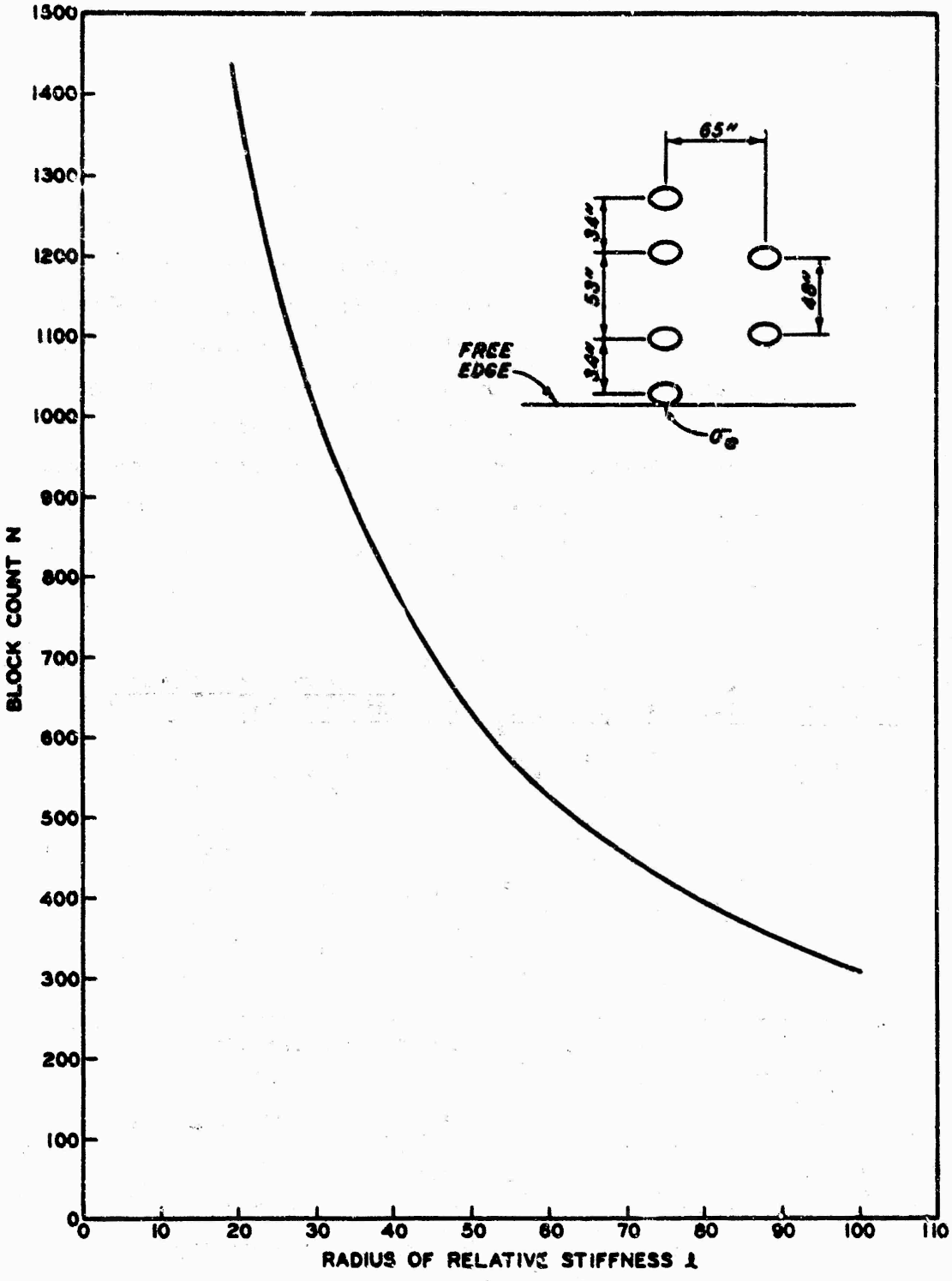

Figure 39. Number of Blocks Versus Radius of Relative Stiffness for 12-Wheel Assembly at a Free Edge (One 6-Wheel Bogie Used for Analysis)

load-transfer device in the joint is assumed to transfer a minimum of 25 percent of the load from the loaded side of the joint to the unloaded slab; therefore, this load transfer must be reflected in equation 41 above. This is accomplished in the computation of q as follows:

$$q = \frac{0.75P}{A} = \frac{0.75 \times 30{,}000}{285} = 79 \text{ psi}$$

The flexural stress computed using equation 41 yields the stress at the edge of the slab when the N is determined from the influence chart for edge loading and the 25 percent load transfer is reflected in the computation of q as shown above. The computed edge stress divided into the concrete flexural strength gives the DF for the test slab. The DF is then plotted versus the number of 12-wheel gear coverages required to produce the initial-crack and shattered-slab conditions on the current CE DFS versus coverage relationships presented in Section III (figures 12-14) to determine the adequacy of the current CE design method. The following tabulation shows the development of the DF for each slab of each test item.

Test Item	Slab	ℓ in.	N	σ_e psi	R psi	DF	Coverages for Failure: Initial	Coverages for Failure: Shattered-Slab
1	SW	46.2	680	635	725	1.14	251	592*
	SE	44.9	727	694	725	1.04	192	592
2	SW	61.0	520	637	800	1.25	4496	5008*
	SE	61.4	512	625	800	1.28	3963	5008*
3	SW	70.5	455	540	700	1.30	2208	5008*
	SE	69.5	460	553	700	1.27	592	5008*
4	SW	39.0	812	893	775	0.87	180	240
	SE	39.0	812	893	775	0.87	181	240

* Slab did not reach failure condition at maximum coverage level applied.

A comparison of the predicted versus actual performance for each slab is shown in figure 40 for the initial failure condition and in figure 41 for the shattered-slab failure condition. An examination of figure 40 shows that there is some scatter of data points for the initial failure condition; however, with the exception of item 4, the data agree fairly well with the relationship currently used by the CE criteria for jointed-edge loading. Item 3, especially the SE slab, failed prematurely, which is attributable to the excessive pumping that occurred with the resultant loss of subgrade

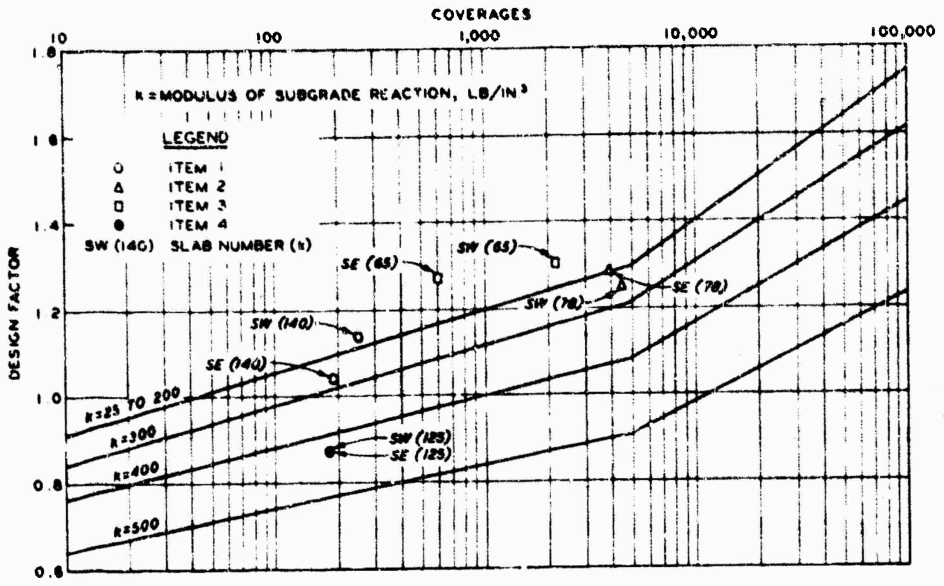

Figure 40. Comparison of Actual Performance Data with Current CE Design Methodology for 12-Wheel Assembly Initial Failure Condition. Pass per Coverage Ratio = 1.34

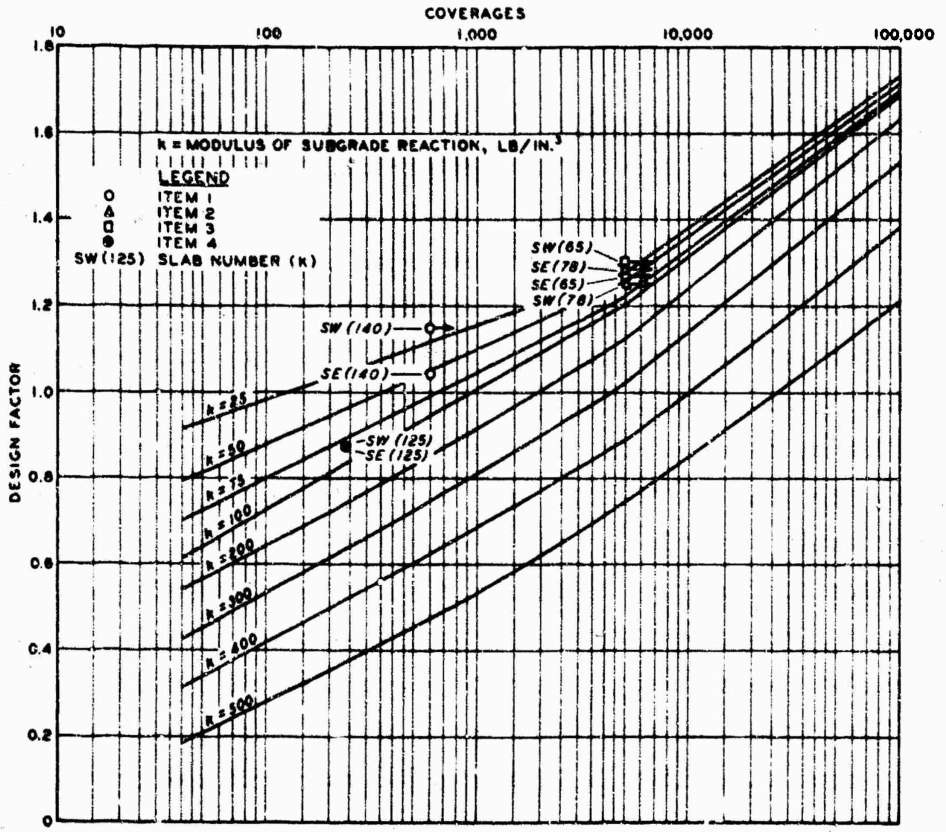

Figure 41. Comparison of Actual Performance Data with Current CE Design Methodology for 12-Wheel Assembly Shattered-Slab Failure Condition. Pass per Coverage Ratio = 1.34

support. Both slabs of item 4 performed identically, and, based upon the data available, there is no explanation for the better-than-predicted performance. It is possible that the strengths of the concrete and subgrade were higher than the measured values indicate; however, it is more probable that for such a low coverage level this magnitude of data scatter is not unreasonable. Items 1 and 2 performed almost as predicted, and overall the performance data indicate that use of the CE DF versus coverage relation with the Westergaard algorithm is reasonable for the 12-wheel assembly loading.

Only three slabs were trafficked to the shattered-slab failure condition and the comparison of the performance of these slabs with current CE DF versus coverage relationship is shown in figure 41. All three slabs reached the shattered-slab condition in the low-coverage range and at a slightly lower coverage level than the existing relationship predicted. Items 2 and 3, which according to the existing DF versus coverage relation should have been approaching the shattered-slab condition, had not reached that condition at the conclusion of traffic. Based upon their condition at the conclusion of traffic, it is probable that they would have exceeded the predicted values.

(2) Twin-tandem assembly. The twin-tandem assembly traffic was performed in the north paving lane of the test track. Both the Westergaard algorithm and past test track experience with twin-tandem assemblies indicate that maximum stresses occur in the concrete when the tandem wheels are oriented parallel and tangent to the longitudinal joint. However, since the 12-wheel gear had trafficked along the longitudinal joint in the south lane with some traffic across the joint in the north lane, the effects of this 12-wheel traffic on the analysis of results of tests with the twin-tandem assembly along the same joint would have been indeterminable. Therefore, it was decided to apply the twin-tandem assembly traffic in the center of the north paving lane to avoid any influence of the prior 12-wheel traffic. This meant that the maximum stress from this traffic should, according to theory, occur when the twin wheels were tangent to the transverse joints. In addition, theory indicates that this orientation of the twin-tandem assembly results in stresses only slightly less than the more critical orientation with the tandem wheels tangent to a joint. The analysis of the twin-tandem assembly traffic results was accomplished in the same manner as for the 12-wheel traffic results, i.e. determination of a DF for each slab of each test item, which,

along with coverages required to produce the initial crack and shattered slab in the test item, were compared with the current CE DF versus coverage relationship. The physical properties of the test pavements were again assumed to be those measured after the traffic program had been completed for the same reasons as explained before. These properties are summarized in table 11. Only test items 2 and 3 could be analyzed as plain rigid pavements, since items 1 and 4 were nonrigid overlay pavements throughout the twin-tandem assembly traffic testing.

An example of the analysis of pavement behavior under twin-tandem assembly traffic is discussed below. A curve of N, the number of blocks covered on the influence chart for edge loading, versus ℓ, the radius of relative stiffness, was prepared for the twin-tandem assembly oriented perpendicular and tangent to a jointed edge (transverse joint). This relationship is shown in figure 40. Utilizing this relationship and equation 41, the flexural stress caused by the twin-tandem assembly can be computed for each test item. A DF is then determined which, when plotted versus the traffic causing failure on the current CE DF versus traffic volume relationship, shows the comparison of current criteria to actual performance. A comparative analysis for item 2 is shown below:

	NW Slab	NE Slab
Slab thickness, h	11.5 in.	11.3 in.
Subgrade modulus, k	111 lb/in.^{3}	111 lb/in.^{3}
Concrete flexural strength, R	700 psi	700 psi
Modulus of elasticity of concrete, E	6.5×10^6 psi	6.5×10^6 psi
Tire contact area, A	207 sq in.	207 sq in.
Load per wheel, P	41,500 lb	41,500 lb
Poisson's ratio for concrete, μ	0.20 (assumed)	0.20 (assumed)
Tire contact pressure, $\frac{0.75P}{A}$	150.4 psi	150.4 psi

Using the above listed properties, the ℓ value is computed for each slab and the N value for each slab is determined from figure 42. The edge stress is then computed using equation 41, again assuming that 25 percent of the load is transferred from the loaded to the unloaded slab through the aggregate interlock of the transverse joint. A DF is then computed for each slab by dividing the computed edge stress into the concrete strength and is plotted versus the number of coverages of the twin-tandem assembly that produced the initial-crack and shattered-slab conditions on the current CE

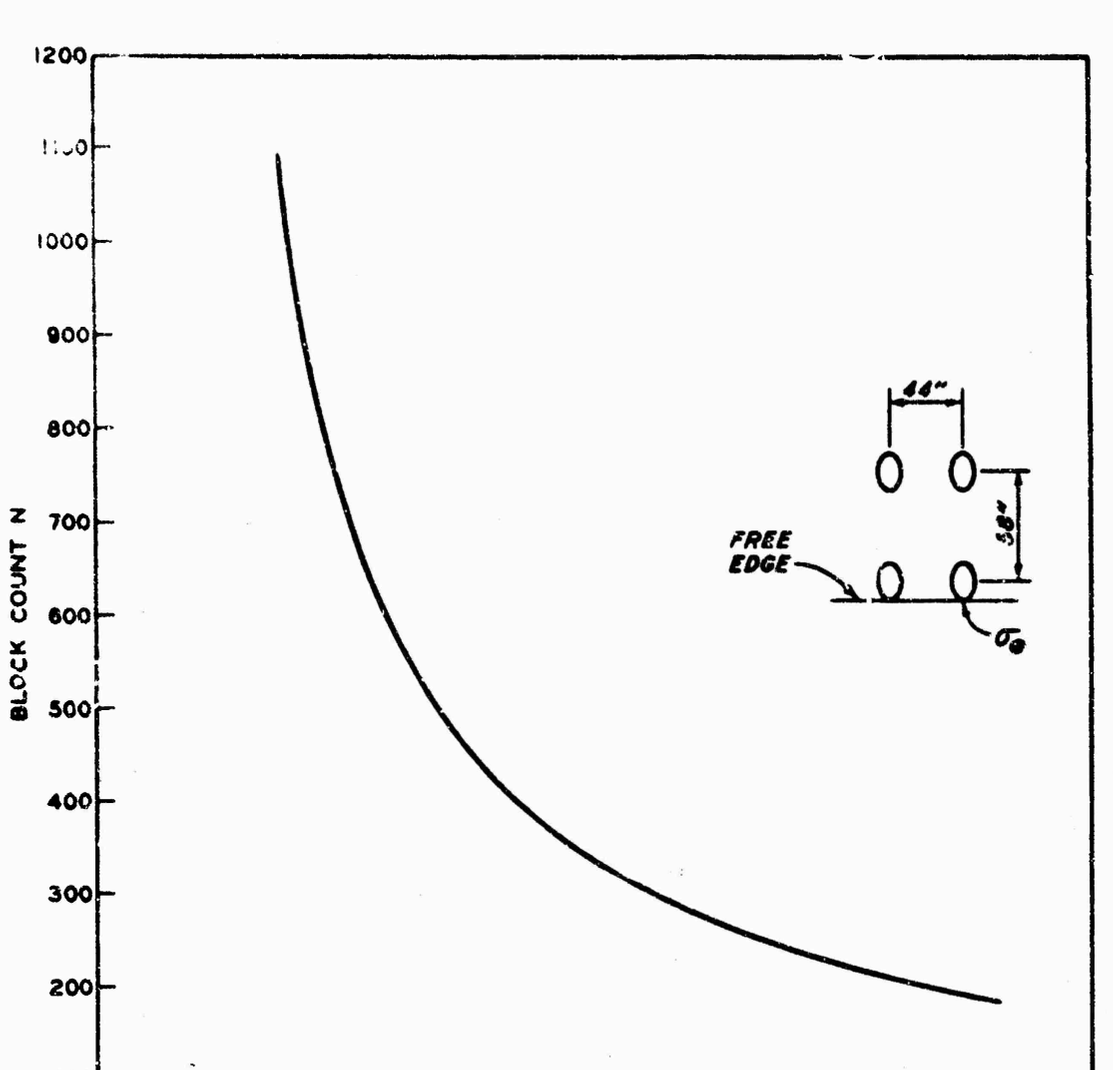

Figure 42. Number of blocks versus radius of relative stiffness for twin-tandem assembly at a free edge

DF versus coverage relationship. The following tabulation shows the development of the DF for each slab of each test item:

Test Item	Slab	ℓ in.	N	σ_e psi	R psi	DF	Coverages for Failure: Initial	Coverages for Failure: Shattered Slab
2	NW	53.0	347	664	700	1.05	40	680
	NE	52.0	358	686	700	1.03	150	680
3	NW	59.0	320	542	660	1.22	260	680*
	NE	60.0	310	520	660	1.27	150	680*

* Slab did not reach failure condition at maximum coverage level applied.

A comparison of the predicted versus actual performance for each slab is shown in figure 43 for the initial failure condition and in figure 44 for the shattered-slab failure condition.

As shown in figure 43, item 2 performed about as predicted for the initial failure conditions; however, item 3 failed prematurely. There is no evident explanation for this premature failure. Unlike item 3 under the 12-wheel-assembly traffic, which pumped excessively and undoubtedly contributed to its premature failure, item 3 under twin-tandem traffic did not pump excessively. As reported in Volume II of this report, there was some pumping in item 3 that was not believed to be of such severity as to affect the performance of the slab. In fact, from all observations the performance of item 3 was entirely normal. This suggests that the slope of the DF versus coverage relation may be different for the twin-tandem assembly than for the 12-wheel assembly; however, to make such a conclusion from the limited data available is not warranted.

As mentioned earlier, the twin-tandem assembly traffic was applied in the middle of the north paving lane, and the critical stress was selected as being with the gear tangent to the transverse joint. This meant that the maximum stress would be parallel to the transverse joint and the resulting crack would be longitudinal. A review of the crack development and progression described in Volume II shows that the initial crack in both items 2 and 3 was in the longitudinal direction and originated at the tranverse joint. Thus, the crack development validates the assumption regarding location of critical stress.

Both slabs of item 2 had reached the shattered-slab failure condition at the conclusion of the twin-tandem assembly traffic, whereas both

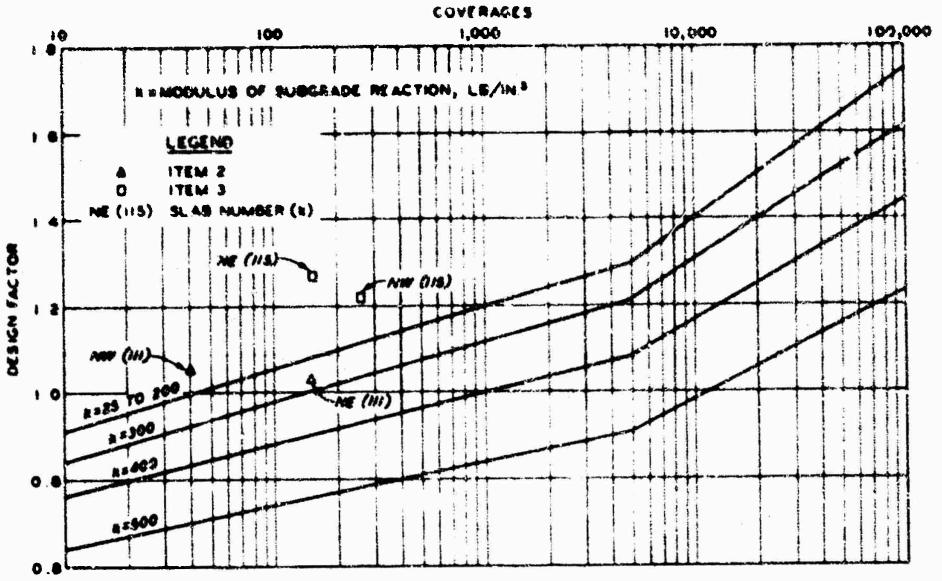

Figure 43. Comparison of Actual Performance Data with Current CE Design Methodology for Twin-Tandem Assembly Initial Failure Condition. Pass per Coverage Ratio = 3.30

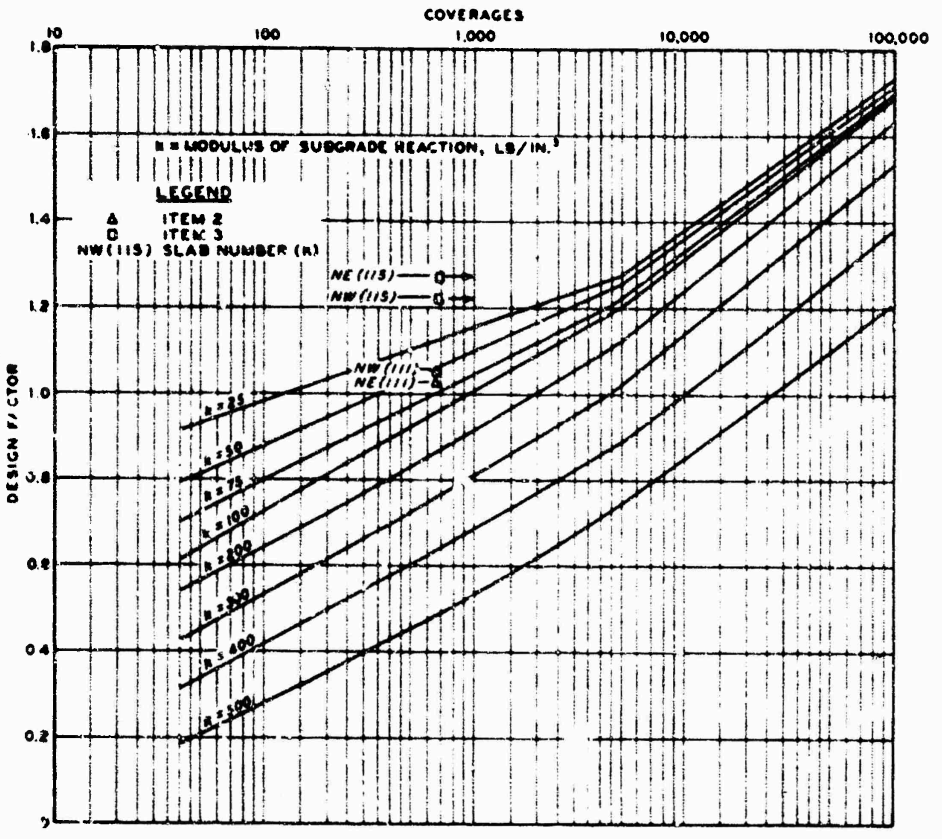

Figure 44. Comparison of Actual Performance Data with Current CE Design Methodology for Twin-Tandem Assembly Shattered-Slab Failure Condition. Pass per Coverage Ratio = 3.30

slabs of item 3 contained only one crack (longitudinal). A comparison of the predicted with the actual performance for the shattered-slab failure condition is shown in figure 44. Both slabs of item 2 reached the shattered-slab condition at a coverage level slightly less than the existing DF versus coverage relation would have predicted. These two slabs, with their k value of 111 lb/in.^{3}, performed as the DF versus coverage relation would have predicted for a k value of about 65 to 70 lb/in.^{3}. As shown, both slabs of item 3 according to the DF versus coverage relation should have carried about 7000 to 8000 coverages before reaching the shattered-slab condition, and at the conclusion of traffic, each contained only one crack. It is probable that both slabs would have reached the shattered-slab condition before the predicted coverage level.

b. Nonrigid Overlay Criteria

The MWHGL test sections were utilized to provide information as to the adequacy of criteria for the strengthening of existing rigid pavements with nonrigid overlay.

Items 1 and 4 were overlaid with asphaltic concrete after some structural damage had occurred from the 12-wheel assembly traffic. This was done to simulate an existing pavement that had received traffic, was beginning to show distress, and was to be strengthened with a nonrigid overlay. The nonrigid overlays were designed using the properties of the subgrade and concrete determined from the construction control tests. The design was for 4000 to 4500 coverages of the 12-wheel assembly. A condition factor C of 1.0 was assigned to the slabs in item 1, since these slabs showed only initial cracking, and a C of 0.75 was assigned to the slabs in item 4 inasmuch as each slab was cracked into 6 pieces. The same thickness of nonrigid overlay was applied to both the north and south slabs of items 1 and 4, and, when evaluating the performance of the north slabs under twin-tandem assembly traffic, condition factors C of 1.0 were assigned, since the north slabs were not trafficked prior to the overlay and did not contain structural cracking.

In retrospect, the thickness of the nonrigid overlay used was excessive for the 12-wheel assembly traffic that was programmed because both the modulus of subgrade reaction and concrete flexural strength were considerably higher than the values selected for design from the construction control testing. As a result, neither item 1 nor 4 nonrigid overlay was failed with the programmed 12-wheel assembly traffic. The evaluation of item 1 nonrigid

overlay was excessive for the programmed twin-tandem assembly traffic and a failure was not experienced; however, item 4 nonrigid overlay was considered failed at the conclusion of the programmed twin-tandem assembly traffic.

The nonrigid overlay test items were analyzed by relating the combined plain concrete and asphaltic concrete thickness to an equivalent thickness of plain concrete pavement as follows:

$$h_e = \frac{1}{F}\left(Ch_b + \frac{t}{2.5}\right) \tag{42}$$

where

h_e = equivalent plain concrete thickness, in.

A table of equivalent thickness computations for all applicable slabs is shown below.

Gear	Test Item	Slab	h_b in.	C	F	k lb/in.^{3}	t in.	h_e in.
12-wheel	1	SW	10.4	1.0	0.86	140	3.9	13.9
		SE	10.0	1.0	0.86	140	4.5	13.7
	4	SW	8.1	0.75	0.87	125	5.3	9.4
		SE	8.1	0.75	0.87	125	5.6	9.6
Twin-tandem	1	NW	9.7	1.0	0.69	169	3.9	16.3
		NE	9.6	1.0	0.69	169	3.8	16.1
	4	NW	7.5	1.0	0.71	128	5.4	13.6
		NE	7.4	1.0	0.71	128	5.6	13.6

Using the equivalent thickness h_e, the test items were analyzed in the same manner as for the plain concrete test items. The N versus ℓ values shown in figures 39 and 42 are used for the 12-wheel and twin-tandem assembly traffic, respectively. The flexural stress was computed using equation 41 and was used to obtain a DF by dividing it into the concrete flexural strength. The following tabulation shows the determination of the DF for each test item:

Gear	Item	Test Slab	E 10^6 psi	ℓ in.	N	σ_e psi	R psi	DF	Coverages to Fail
12-wheel	1	SW	6.5	57.5	550	408	725	1.78	4416*
		SE	6.6	56.8	551	402	725	1.81	4416*
	4	SW	6.3	43.5	725	737	775	1.05	4416*
		SE	6.3	44.3	715	720	775	1.08	4416*
Twin-tandem	1	NW	6.5	61.4	300	383	699	1.82	680*
		NE	6.5	60.9	302	389	699	1.79	680*
	4	NW	6.1	56.6	330	515	699	1.17	680
		NE	6.1	56.6	330	515	699	1.17	680

* Traffic was halted before failure occurred.

A comparison of existing criteria with actual performance is made by plotting the above values of DF and the coverages to failure in the existing CE relationship of DF and aircraft coverages as shown by figure 45.

As stated earlier, the thicknesses of nonrigid overlay used were excessive for the 12-wheel-traffic volume anticipated because of a greater-than-normal gain in concrete strength and subgrade modulus. This is evident for item 1 when the DF for each slab is plotted on the CE relationship. Based upon this relationship, coverages of up to 100,000 would have been required to produce failure. Based upon the CE DF versus coverage relationship, item 4 should have been approaching failure when traffic was halted. According to Volume II, item 4 at the conclusion of traffic was approaching failure, but it is probable that the item would have exceeded the predicted coverage level. Item 1 for the twin-tandem traffic was also overdesigned because of the high strength gain in concrete and subgrade and, as shown in figure 45, probably would not have failed at any reasonable coverage level. Item 4 was considered failed at the conclusion of the twin-tandem traffic and according to the current CE relationship of DF versus coverages failed prior to its predicted coverage level.

A polypropylene membrane was placed on the surface of the southwest slab of test item 1 prior to placement of the nonrigid overlay to assess the effects of the membrane on the retardation of reflection cracking. At the time of the nonrigid overlay, the southwest slab had both a longitudinal and transverse crack which subdivided the slab into four pieces. The transverse crack had occurred prior to the beginning of traffic, and during the traffic, the crack spalled and raveled badly. Prior to placement of the polypropylene, the crack was cleaned of spalled concrete and then primed and filled with asphaltic concrete. The membrane did seem to retard the reflection cracking to some degree; however this cannot be supported by data, for both slabs began to show reflection cracks from the joints in the base pavement even prior to traffic on the overlay. During traffic, reflection cracks from both joints and structured cracks in the jointing systems occurred with little difference between the sections where the polypropylene was and was not used.

c. Performance of Keyed Joints

The keyed longitudinal joints failed early in all test items under the MWHGL traffic. The exact time of failure is not known for the first evidence was faulting of the longitudinal joint. Faulting was noted in most test items

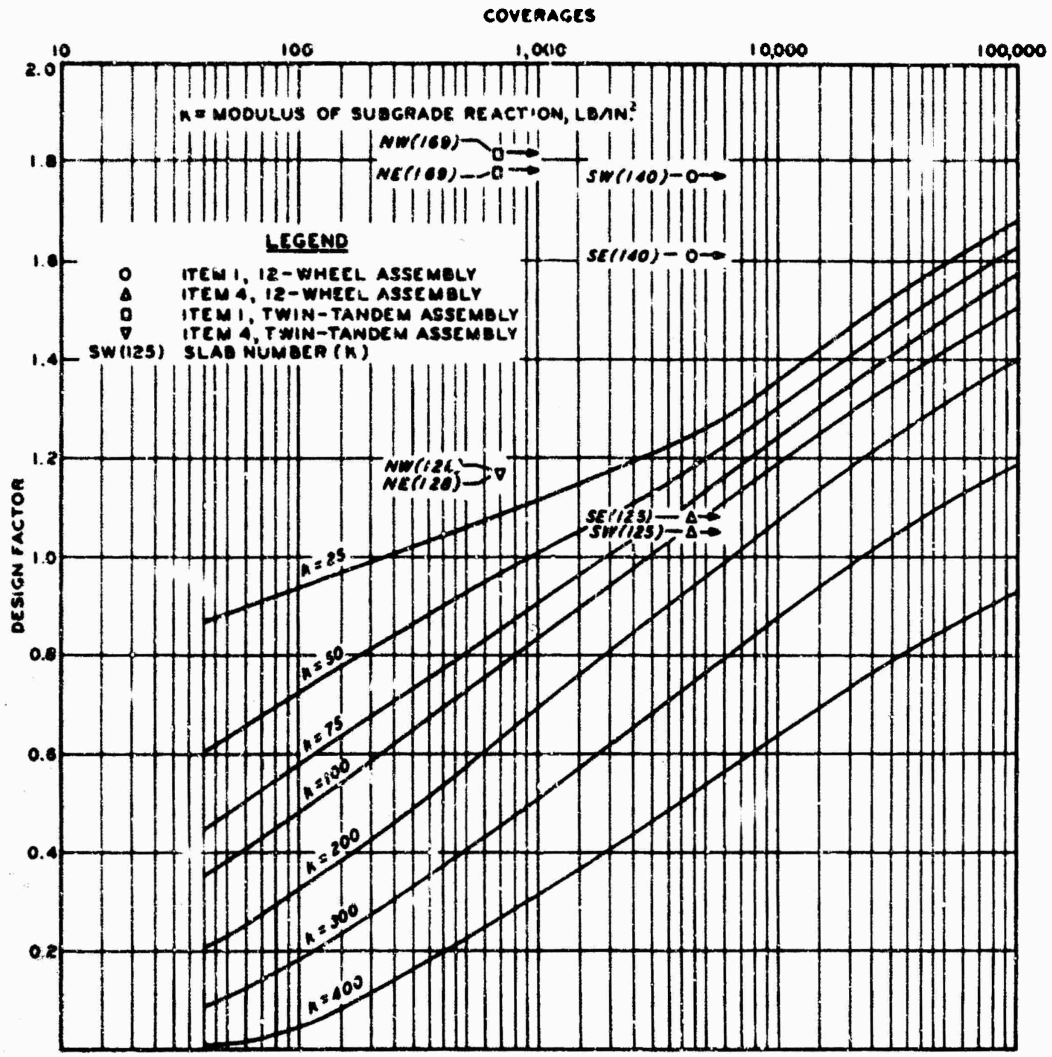

Figure 45. Comparison of Actual Performance Data with Current CE Design Methodology for 12-Wheel and Twin-Tandem Assemblies Complete Failure Condition. Pass per Coverage Ratios for 12-Wheel and Twin-Tandem Assemblies = 1.34 and 3.30, respectively.

after only a few hundred coverages, and it is highly probable that the faulting was the result of the keyed joint failure; thus, the keyed joint failed at an even lower coverage level. Past experience indicated that a keyed joint would yield satisfactory performance if the pavement slabs were adequate for the flexural stresses generated by the load. Keyed joint design is based on the results of model tests and observations from previous test tracks and operational pavements containing keyed joints.

The failure of the keyed joint did not appear to be associated with the flexural stress due to the load. For example, in item 4, the flexural stress was high, and in item 3, the flexural stress was low, with items 1 and 2 falling between; however, insofar as can be determined, the keyed joint failed at almost the same coverage level in each item. Ordinarily a keyed joint is not used in pavements less than 9 in. thick because of the difficulty in construction and because of past poor performance in thin pavements; however, the keyed joint was used in item 4 (8 in.) to reduce the number of test variables. Nevertheless, the performance of the keyed joint in the 8-in.-thick item was as good as for the thicker pavements insofar as could be determined. The performance of the keyed joint in item 3 may have been influenced by the pumping that occurred; however, it is the opinion of the personnel involved that the keyed joint failed before pumping became severe enough to influence the joint performance. As a matter of fact, it is probable that the keyed joint failure accentuated the pumping that occurred.

Because both the keys and keyways failed without a significant pattern, the optimal key and keyway dimensions adopted by the CE are valid. The optimal keyed joint dimensions are those that will produce an equal number of key and keyway failures. No purpose would be served by constructing a large, very strong key as the keyway will fail prematurely, and conversely, if the keyway is overdesigned, the key will fail prematurely. It is possible that a thickened-edge keyed joint would be satisfactory. Transverse contraction joints of this aggregate-interlock type (weakened plane) seemed to pose no problems under multiple-wheel loadings. No abnormal behavior or premature failures (except where pumping was severe) were experienced. In the test track, the transverse contraction joints were always normal to the longitudinal axis of the 12-wheel and twin-tandem assemblies and therefore probably had to transfer less shear than did the longitudinal joint.

d. Subgrade Behavior

Changes in subgrade material under rigid pavements occur due to environmental conditions, mainly water content, and to inherent soil properties such as thixotropy. In rigid pavement design and analysis, the subgrade materials are described by the subgrade modulus or k value. The subgrade modulus is, in essence, a spring constant that represents the pressure required to produce a unit deflection and is determined by a plate bearing test. Changes in the subgrade support value are reflected as changes in the subgrade modulus. The plate bearing test consists of loading a nest of bearing plates up to 30 in. in diameter and observing the load-deflection curve of the plates for various pressures. The k value is defined as the ratio of the 10-psi load to the deflection that occurred under the 10-psi load. Some technique is involved in the interpretation of the load-deflection curves as the curves are seldom linear. When the load-deflection curve is nonlinear, a straight line is drawn through the portion of the curve with the least curvature and corrected for seating, and a value of deflection is established for the 10-psi load. The determination of the portion of least curvature is a judgment decision and can drastically affect the results of the plate bearing test.

Changes in subgrade moduli were noted on the rigid test section. The load-deflection curves observed on the test section were nonlinear and of nearly constant curvature (see Volume II), making interpretation of the data somewhat difficult. The changes in subgrade moduli seemed to follow the drainage pattern for the site. A low spot was formed under item 3 and was probably the cause of the rather severe pumping that occurred under the test item. The pumping was undoubtedly aggravated by the ponding of water in the low area. In the after-traffic test program, no major variations were found in water content, but the similarity between the changes in subgrade moduli and the drainage pattern seem too close to be coincidence.

The changes in subgrade moduli from the time of completion of the embankment until the posttraffic testing were more uniform in the north lane than in the south lane. The changes follow the drainage pattern for the site; however, no apparent changes in water content of sufficient magnitude to affect the subgrade moduli to the extent measured were found. Densification of the subgrade material due to traffic was ruled out as a possibility, as marked increases in subgrade densities were not found and the water

co. ent was near saturation, making undrained compaction nearly impossible. The pumping in item 3 may be associated with this drainage process.

The permanent deformations experienced under many applications of the MWHGL assembly were larger than those encountered previously under more conventional wheel arrangements on other test tracks and operational pavements. Large permanent deflections should be anticipated on rigid pavements subjected to operations of MWHGL aircraft and some loss of crown will probably result, particularly on low-strength subgrades. Thus, if various soil types are present, some differential settlements may occur. No evidence of deep-seated shear failures was found. However, the deflection measurements indicated appreciable magnitudes of both transient and permanent deflections at a considerable depth. Apparently, the multiple-wheel assemblies are quite efficient in distributing flexural stresses in the pavement slab, but require more work from the supporting materials than, for example, conventional twin-tandem assemblies.

e. Pavement Requirements

(1) Pavements for C-5A aircraft. Pavements to accommodate the C-5A aircraft are discussed in two categories: (a) existing pavements (evaluation) and (b) new pavements (design). The existing evaluation method for determination of allowable loadings at various operational levels is adequate insofar as the pavement thickness and physical properties of materials are concerned. The major problem in evaluation lies with the jointing and load-transfer systems of existing pavements. Most existing pavements having the thickness required for operation of the C-5A aircraft will have been constructed using the keyed construction joint on part of the pavement system. Based on the results of the MWHGL traffic tests, such pavements constructed on low-strength subgrades will experience rapid joint deterioration with a subsequent increase in edge stress and shortened pavement life. Although not demonstrated in the test track, pavements with keyed construction joints on medium- to high-strength subgrades may also experience rapid joint deterioration under the C-5A aircraft traffic. Existing pavements resting directly on pumpable foundations can be expected to experience pumping, depending on soil type, moisture conditions, drainage, and traffic volume, which will result in loss of subgrade support to the pavement slabs and shortened pavement life.

For new construction, use of the Westergaard equations for computation of stresses in the slab due to edge loading (equation 21) is considered

valid. The DF versus traffic volume (figures 12-14) relationships are considered valid for determination of the effects of load repetitions and environment. Therefore, from the results of the MWHGL tests, no changes in the CE basic methods for determination of required rigid pavement thickness are indicated for the C-5A aircraft. Use of the standard keyed construction joint is discouraged, and use of doweled or thickened-edge construction joints regardless of subgrade strength is recommended. Adequately designed filter courses or stabilized layers between the rigid pavement and pumpable subgrade materials should be used, and the compaction requirements for the foundation materials should be increased. Recommendations concerning these factors are presented in Section V.

(2) Pavements for Boeing 747 aircraft. The existing CE method of evaluating pavements for the Boeing 747 aircraft is considered adequate insofar as pavement thickness is concerned. While traffic was applied with only a twin-tandem bogie of the aircraft, inferences can be drawn from these and from the 12-wheel-assembly traffic that would be applicable to the Boeing 747. The keyed construction joints in existing pavements are suspect, and rapid joint deterioration with subsequently increased pavement stresses and shortened pavement life should be anticipated under Boeing 747 aircraft traffic. The above is especially true of pavements constructed on low-strength subgrades and, while not demonstrated by the MWHGL tests, is probably true for pavements on medium- to high-strength subgrades. Pavements on pumpable foundations will probably experience some degree of pumping, depending on soil type, moisture conditions, and traffic volumes, with a long subgrade support and shortened pavement life.

For new construction to serve the Boeing 747 aircraft, the use of the Westergaard equations for computation of pavement stresses and the existing CE relationships of DF versus traffic volume (figures 12-14) is considered valid for development of rigid pavement thickness requirements. Doweled or thickened-edge construction joints in lieu of the keyed construction joints, adequately designed filter or base courses or stabilized layers to prevent pumping, and increased compaction requirements for the foundation materials similar to that discussed for the C-5A aircraft are also recommended for the Boeing 747 aircraft.

SECTION V

CONCLUSIONS AND RECOMMENDATIONS

1. CONCLUSIONS

a. Flexible Pavements

Conclusions based on the findings of this study are given below.

(1) The flexible pavement design procedure described in this report is recommended for use in the development of C-5A and Boeing 747 aircraft flexible pavement design and evaluation curves. The procedure reflects a reduction of thickness requirements of existing multiple-wheel criteria, especially significant in the higher operational level. Using these concepts and procedures, the following behavioral pattern for thicknesses of pavement layers to properly design underlying layers to resist shear deformation was derived:

$$t \rightarrow \alpha_i \left[\sqrt{A} \left(- 0.0481 - 1.1562 \left(\log \frac{CBR}{p_e} \right) - 0.6414 \left(\log \frac{CBR}{p_e} \right)^2 - 0.4730 \left(\log \frac{CBR}{p_e} \right)^3 \right) \right] \qquad (40)$$

(2) The pass concept is presented as being representative of current aircraft volume of traffic and related to actual lateral load applications at airfield facilities. Also, gross aircraft loadings are used to better reflect the total effect of the aircraft and to eliminate the necessity of assembly determination on aircraft similar to the Boeing 747 aircraft.

b. Rigid Pavements

The following is a list of conclusions based on analysis of the data collected during the testing with the 12-wheel assembly. Conclusions are based on the results of static load and traffic tests.

(1) The Westergaard algorithm for determination of pavement deflection and stress under static loading conditions appears to yield reasonable results for the MWHGL assemblies; however, it appears to become more questionable as the number and spacing of wheels increase.

(2) The existing relationship for DF versus traffic volume (coverages) developed by the CE for edge loading is considered to be valid for the

initial-crack failure condition but slightly unconservative for the shattered-slab failure condition. Based on the few test points, the DF versus coverage relation for nonrigid overlays appears to be reasonable.

(3) Keyed longitudinal construction joints for pavements on low-strength subgrades are inadequate for the MWHGL assemblies.

(4) Filter courses or other positive protection devices are required to prevent detrimental effects of pumping when rigid pavements are constructed for MWHGL assemblies on subgrades composed of fine-grained material.

2. RECOMMENDATIONS

a. Flexible Pavements

Based on the findings of the flexible pavement MWHGL study, the following recommendations are made:

(1) The procedures presented in this report should be used for the development of flexible pavement design and evaluation criteria, and all existing criteria should be modified to reflect the results of this study.

(2) Further theoretical studies should be accomplished using the MWHGL traffic and instrumentation data.

b. Rigid Pavements

Based on the results of the tests conducted on the rigid pavement portion of the MWHGL study, the following recommendations are made:

(1) For the construction of new pavements that will be subjected to MWHGL assemblies, the use of keyed construction joints is not recommended. Either thickened-edge or doweled construction joints are recommended.

(2) Further work to determine the adequacy of keyed construction joints on medium and strong foundations should be performed.

(3) When pumpable materials are encountered, the use of a base course or stabilized material is recommended, as pumping will be quite severe where traffic volumes are high.

(4) Current evaluation and design criteria for rigid pavement slab thickness should not be changed.

(5) Consideration should be given to the establishment of a maximum allowable permanent deflection that can be tolerated in a rigid pavement structure.

(6) Consideration should be given to increasing compaction requirements for subgrades.

(7) Studies should be undertaken to examine possible methods of strengthening keyed construction joints in existing airfield pavements.

(8) Studies should be undertaken to establish allowable soil stresses in rigid pavement structures by expanding the work already done in flexible pavements and in repetitive triaxial soils testing.

REFERENCES

1. Peutz, M. G. F.; Jones, A.; van Kempten, H. P.; Layered Systems Under Normal Surface Loads, Computer Program, Koninklijke/Shell Laboratorium, Amsterdam, Holland.

2. Harr, M. E.; Foundations of Theoretical Soil Mechanics, p 19, McGraw-Hill, New York, 1966.

3. Michelow, J.; Analysis of Stresses and Displacements in an N-Layered Elastic System Under a Load Uniformly Distributed on a Circular Area, Computer Program, California Research Corporation, Richmond, Calif., September 1963.

4. Pletta, F.; Engineering Mechanics, pp 265-271, Ronald Press, New York, 1964.

5. Timoshenko, S.; Young, D. H.; Advanced Dynamics, pp 153-181, McGraw-Hill, New York, 1948.

6. Boresi, A. P.; Elasticity in Engineering Mechanics, pp 103-112, Prentice-Hall, 1965.

7. Smith, G. L.; Smith, G. M.; Advanced Dynamics, pp 117-153, International Textbook Co., Scranton, Pa., 1960.

8. Kristnamurthy, N.; Short Course Matrix Operations - Finite Elements as Applied to Structural Analysis, Auburn University, Auburn, Ala., February 1970.

9. Wang, C. K.; Matrix Methods of Structural Analysis, International Textbook Co., Scranton, Pa., 1966.

10. Kristnamurthy, N.; Short Course in Finite Elements, Auburn University, Auburn, Ala., March 1970.

11. Scheid, Francis; Theory and Problems of Numerical Analysis, pp 15-21, McGraw-Hill, New York, 1968.

12. Banks, D. C.; Palmerton, J. B.; Application of Finite Element Method in Determining Stability of Crater Slopes, Preliminary Report, Miscellaneous Paper S-68-3, U. S. Army Engineer Waterways Experiment Station, CE, Vicksburg, Miss., May 1968.

13. Timoshenko, S. P.; Goodier, J. N.; Theory of Elasticity, pp 235-244, McGraw-Hill, New York, 1970.

14. Duncan, J. M.; Monismith, C. L.; Wilson, E. L.; "Finite Element Analysis of Pavements," 47th Annual Meeting of Highway Research Board, January 1968.

15. U. S. Naval Civil Engineering Laboratory; Rational Pavement Evaluation-Review of Present Technology, AFWL-TR-69-9, prepared for Air Force Weapons Laboratory, Kirtland Air Force Base, N. Mex., October 1969.

16. Wilson, E. L.; A Digital Computer Program for the Finite Element Analysis of Solids with Nonlinear Material Properties, Department of Civil Engineering, University of California, Berkeley, Calif., July 1965.

17. Harr, M. E.; Rosner, J. C.; Theoretical Study of Landing Mat Behavior, Contract Report S-69-7, prepared by Purdue Research Foundation, Purdue University, for the U. S. Army Engineer Waterways Experiment Station, CE, Vicksburg, Miss., June 1970.

18. Vlasov, V. Z.; Leont'ev, N. M.; Beams, Plates, and Shells on an Elastic Foundation, Israel Program for Scientific Translations, Jerusalem, 1966.

19. Freudenthal, A. M.; Lorsch, H. G.; "The Infinite Elastic Beam on a Linear Viscoelastic Foundation," Proceedings of the ASCE, Journal of Engineering Mechanics Division, Vol 83, No. EM 1, January 1957, pp 1158; 1-1158; 22.

20. Barksdale, R. D.; Elastic and Viscoelastic Analysis of Layered Pavement Systems, Ph.D. Thesis, Purdue University, Lafayette, Ind., 1966.

21. Chou, Y. T.; "A General Theory of Stresses and Displacements in Elastic and Viscoelastic Layered Systems," Transactions of the Fifteenth Conference of Army Mathematicians, ARL-D Report 70-1, pp 141-168, June 1969.

22. Hudson, R. N.; Discontinuous Orthotropic Plates and Pavement Slabs, Computer Program No. 56-9, Center for Highway Research, University of Texas, Austin, Tex., October 1967.

23. Odemark, N.; Investigations as to Elastic Properties of Soils and Design of Pavements According to Theory of Elasticity, Statens Vaginstitute, Meddelande No. 77, Stockholm, Sweden, 1949.

24. Westergaard, H. M., "A Problem of Elasticity Suggested by a Problem in Soil Mechanics" and "Soft Material Reinforced by Numerous Strong Horizontal Sheets," Contributions to the Mechanics of Solids, Timoshenko Sixtieth Anniversary Volume, Macmillan, New York, 1938.

25. Hogg, A. H. A.; "Equilibrium of a Thin Plate, Symmetrically Loaded, Resting on an Elastic Subgrade of Infinite Depth," Philosophical Magazine, Series 7, Vol 25, March 1938.

26. Holl, D. L.; "Thin Plates on Elastic Foundations," Proceedings, Fifth International Congress of Applied Mechanics, Cambridge, Mass., 1938.

27. Barenberg, E. J.; A Structural Design Classification of Pavements Based on an Analysis of Pavement Behavior, Material Properties, and Modes of Failure, Ph.D Thesis, University of Illinois, Urbana, Ill., 1965.

28. Peattie, K. R.; "A Fundamental Approach to the Design of Flexible Pavements," Proceedings, International Conference on Structural Design of Asphalt Pavements, pp 403-411, 1962.

29. Vesic, A. S.; Domaschuk, L.; Theoretical Analysis of Structural Behavior of Road Test Flexible Pavements, Georgia Institute of Technology, Atlanta, Ga. 1964, p 29.

30. Brandt, E. W.; Concentration Factors for Stress Distribution in Soils, Sols Soils No. 21, pp 11-20, 1968.

31. Shockley, W. G.; Theory and Experimentation Paper, unpublished, U. S. Army Engineer Waterways Experiment Station, CE, Vicksburg, Miss.

32. Westergaard, H. M.; "New Formulas for Stress in Concrete Pavements of Airfields," ASCE Transactions, Paper No. 2340, May 1947.

33. "Development of CBR Flexible Pavement Design Method for Airfields," Transactions of an ASCE Symposium, Vol 115, pp 453-589, 1950.

34. Department of Defense; Military Standard for Test Methods for Pavement, Subgrade, Subbase, and Base-Course Materials, MIL-STD-621A, Washington, D. C., December 1964.

35. Porter, O. J.; "Development of Original Method of Highway Design," ASCE Transactions, Vol 115, p 461, 1950.

36. Jurgenson, Leo; "Application of Elastic Theory and Plasticity of Foundation Problems," Journal, Boston Society of Civil Engineers, July 1934, p 249.

37. Middlebrooks, T. A.; Bertram, G. E.; "Adaptation to the Design of Airfield Pavements," ASCE Transactions, Vol 115, p 468, 1950.

38. U. S. Army Engineer Waterways Experiment Station, CE; Collection of Letter Reports on Flexible Pavement Design Curves, Miscellaneous Paper No. 4-61, Vicksburg, Miss., June 1951.

39. O. J. Porter and Co.; Accelerated Traffic Tests at Stockton Airfield, Stockton, Calif., Stockton Test No. 2, 7 Vols, prepared for U. S. Engineer Office, Sacramento, Calif., May 1948.

40. U. S. Army Engineer Waterways Experiment Station, CE; Rigid Pavement Tests, Marietta, Georgia, Construction, Testing, and Data Report, Vicksburg, Miss., August 1945.

41. U. S. Army Engineer Waterways Experiment Station, CE; Effects of Traffic with Small High-Pressure Tires on Asphalt Pavements, Technical Memorandum No. 3-314, Vicksburg, Miss., June 1950.

42. U. S. Army Engineer Waterways Experiment Station, CE; Design of Flexible Airfield Pavements for Multiple-Wheel Landing Gear Assemblies, Report No. 1, Technical Memorandum No. 3-349, Vicksburg, Miss., September 1952.

43. U. S. Army Engineer Waterways Experiment Station, CE; Design of Upper Base Courses for High-Pressure Tires, Report No. 1, Technical Memorandum No. 3-373, Vicksburg, Miss., December 1953.

44. U. S. Army Engineer Waterways Experiment Station, CE; Proof-Test Section, Columbus Air Force Base, Technical Report No. 3-490, Vicksburg, Miss., December 1958.

45. U. S. Army Engineer Waterways Experiment Station, CE; Investigation of the Design and Control of Asphalt Paving Mixtures, Technical Memorandum No. 3-254, Vol 3, App D, Vicksburg, Miss., May 1948.

46. U. S. Army Engineer Waterways Experiment Station, CE; Investigation of Effects of Traffic with High-Pressure Tires on Asphalt Pavements, Technical Memorandum No. 3-312, Vicksburg, Miss., May 1950.

47. Ahlvin, R. G.; "Consolidated CBR Criteria," Journal of Soil Mechanics and Foundations Division, ASCE, Vol 84, No. SM4, Paper 1825, pp 1825; 1-1825; 16, October 1958.

48. U. S. Army Engineer Waterways Experiment Station, CE; Developing a Set of CBR Design Curves, Instruction Report No. 4, Vicksburg, Miss., November 1959.

49. U. S. Army Engineer Waterways Experiment Station, CE; Compaction Requirements for Soil Components of Flexible Airfield Pavements, Technical Report No. 3-529, Vicksburg, Miss., November 1959.

50. Headquarters, Department of the Army; Standard Practices for Bituminous Pavements, Technical Manual No. 5-822-8, in process of publication, Washington, D. C.

51. Pickett, G.; Ray, G. K.; "Influence Charts for Concrete Pavements," ASCE Transactions, Paper No. 2425, April 1950.

52. Cooksey, D. L.; Ladd, D. M.; Pavement Design for Various Levels of Traffic Volume, AFWL-TR-70-133, Prepared by U. S. Army Engineer Waterways Experiment Station, CE, for U. S. Air Force Weapons Laboratory, Kirtland Air Force Base, N. Mex., July 1970.

53. Bryant, E. C.; Statistical Analysis, pp 113-135 and 198-224, McGraw-Hill, New York, 1960.

54. Snedeior, G. W.; Cochran, W. G.; Statistical Methods, Iowa State University Press, 1967.

55. Brown, D. N.; Thompson, O. O.; Lateral Distribution of Aircraft Traffic, Miscellaneous Paper in preparation, U. S. Army Engineer Waterways Experiment Station, CE, Vicksburg, Miss.

UNCLASSIFIED
Security Classification

DOCUMENT CONTROL DATA - R & D

(Security classification of title, body of abstract and indexing annotation must be entered when the overall report is classified)

1. ORIGINATING ACTIVITY (Corporate author)
U. S. Army Engineer Waterways Experiment Station
Vicksburg, Mississippi 39181

2a. REPORT SECURITY CLASSIFICATION
UNCLASSIFIED

2b. GROUP

3. REPORT TITLE
MULTIPLE-WHEEL HEAVY GEAR LOAD PAVEMENT TESTS: Volume IV, Analysis of Behavior Under Traffic

4. DESCRIPTIVE NOTES (Type of report and inclusive dates)
1 January 1968 through 1 August 1971

5. AUTHOR(S) (First name, middle initial, last name)
George M. Hammitt II
Ronald L. Hutchinson
John L. Rice

6. REPORT DATE	7a. TOTAL NO. OF PAGES	7b. NO. OF REFS
November 1971	134	55

8a. CONTRACT OR GRANT NO. MIPR 68-7	9a. ORIGINATOR'S REPORT NUMBER(S)
b. PROJECT NO. 3224	AFWL-TR-70-113, Vol IV
c.	9b. OTHER REPORT NO(S) (Any other numbers that may be assigned this report)
d.	

10. DISTRIBUTION STATEMENT
Distribution limited to U S Government agencies only because of test and evaluation (1 Nov 1971). Other requests for this document must be referred to AFWL (DEZ), Kirtland AFB, NM 87117.

11. SUPPLEMENTARY NOTES	12. SPONSORING MILITARY ACTIVITY
	AFWL (DEZ) Kirtland AFB, NM 87117

13. ABSTRACT

(Distribution Limitation Statement B)

Flexible and rigid pavement test sections were constructed and tested to obtain data to validate present criteria, to establish modifications to present criteria, or to develop new criteria for the evaluation and design of airfield pavements to be subjected to multiple-wheel heavy gear loads (MWHGL). The basic CBR design method was expanded and modified to obtain a method of design for flexible pavements subject to traffic by MWHGL. The recommended method reflects a reduction of existing U. S. Army Corps of Engineers (CE) thickness requirements that is especially significant for multiple-wheel assemblies in the higher operational level. Current CE evaluation and design methods for rigid pavements are based on stress in the concrete pavement as calculated from the Westergaard analysis; extrapolations to the existing criteria were found to be valid for MWHGL assemblies insofar as pavement thicknesses were concerned. Results of traffic testing of the rigid pavement indicate that current jointing recommendations allowing keyed construction joints may be unconservative when MWHGL assemblies will be trafficking a pavement resting on a low-strength subgrade.

DD FORM 1 NOV 68 1473

UNCLASSIFIED
Security Classification

14 KEY WORDS	LINK A		LINK B		LINK C	
	ROLE	WT	ROLE	WT	ROLE	WT
California bearing ratio						
Flexible pavements						
Multiple-wheel heavy gear loads						
Rigid pavements						
Runways						
Traffic tests						